



A numerical investigation of the irradiation of CNT bundles for enhancement of mechanical properties by improved inter-tube coupling

Nathan P. O'Brien

Publication date

01-01-2014

Licence

This work is made available under the **CC BY-NC-SA 1.0** licence and should only be used in accordance with that licence. For more information on the specific terms, consult the repository record for this item.

Document Version

1

Citation for this work (HarvardUL)

O'Brien, N.P. (2014) 'A numerical investigation of the irradiation of CNT bundles for enhancement of mechanical properties by improved inter-tube coupling', available: <https://hdl.handle.net/10344/4039> [accessed 20 Jan 2023].

This work was downloaded from the University of Limerick research repository.

For more information on this work, the University of Limerick research repository or to report an issue, you can contact the repository administrators at ir@ul.ie. If you feel that this work breaches copyright, please provide details and we will remove access to the work immediately while we investigate your claim.



UNIVERSITY of LIMERICK

O L L S C O I L L U I M N I G H

A numerical investigation of the irradiation of CNT bundles for enhancement of mechanical properties by improved inter-tube coupling

AUTHOR

Nathan P. O' Brien, B.Eng.

A THESIS SUBMITTED FOR THE DEGREE OF DOCTOR OF PHILOSOPHY AT THE
COLLEGE OF SCIENCE AND ENGINEERING, UNIVERSITY OF LIMERICK, IRELAND.

CANDIDATE SUPERVISORS

Prof. Michael A. McCarthy

DEPARTMENT OF MECHANICAL, AERONAUTICAL AND BIOMEDICAL ENGINEERING. IRISH
CENTRE FOR COMPOSITES RESEARCH, MATERIALS AND SURFACE SCIENCE INSTITUTE.
UNIVERSITY OF LIMERICK, IRELAND

Prof. William A. Curtin

INSTITUTE OF MECHANICAL ENGINEERING, ATI-IGM-GE, ÉCOLE POLYTECHNIQUE
FÉDÉRALE DE LAUSANNE, 1015 LAUSANNE, SWITZERLAND

SUBMITTED TO THE UNIVERSITY OF LIMERICK, February 2014



UNIVERSITY of LIMERICK

OLLSCOIL LUIMNIGH

DECLARATION

The substance of this thesis is the original work of the author, due reference and acknowledgement has been made, where necessary, to the work of others. No part of this thesis has already been submitted for any degree and is not being concurrently submitted in candidature for any degree.

Nathan P. O' Brien
(Candidate)

Date

Prof. Michael A. McCarthy
(Supervisor)

Date

University of Limerick. Tel: +353-61-202700 Fax: +353-61-330316
Web: <http://www.ul.ie>

Abstract:

The ultra-high stiffness and strength of carbon nanotubes (CNTs), of the order of 1 TPa and 100 GPa respectively, has stimulated intense interest in CNT-based composites, including the development of super strong fibres from CNT bundles. However, the mechanical properties of such fibres are generally far lower than that of individual CNTs, due to the weak van der Waals shear interactions between neighbouring shells and tubes, which severely limits load transfer. This deficiency affects not just shear and bending properties, but also the tensile strength and toughness when such fibres are used in composite materials, since load is generally introduced by the matrix to the outer tubes in the fibre, and must be transferred through inter-tube shear if the inner tubes are to share the load. Additionally CNTs generally do not run the full length of the fibre so inter-tube shear load transfer is essential if the fibre is to behave as a coherent entity. Without it, sword-in-sheath type fibre failure occurs in which only a few of the CNTs are actually fractured, with the rest pulled out with minimal resistance.

In this thesis, carbon ion irradiation of carbon nanotube (CNT) bundles to enhance mechanical performance is investigated using classical molecular dynamics. Strategies to achieve inter-tube cross-linking for improved shear response without a drastic reduction in tensile strength due to induced defects are considered. Irradiation energies of 50–300 eV/ion, fluences of $4 \times 10^{13} \text{ cm}^{-2}$ to $2 \times 10^{14} \text{ cm}^{-2}$, and dosages of 2–60 MGy on 7-tube bundles are studied. Within 100–200 eV/ion, the level of cross-linking is directly proportional to dosage and therefore controllable. Lower energy irradiation produces smaller-sized defects, so 100 eV/ion is the preferred energy. More than 10 different types of cross-link and a variety of defects are created. The defect level becomes excessive if either the energy or the fluence is set too high. Extension to larger bundles however is significantly more challenging. In 19-tube bundles, 500 eV/ion is required to form cross-links with the centre CNT, and at this energy careful control of fluence is required to avoid excessive damage. Thus ion irradiation for improving mechanical properties is best suited to small bundles. However, a scenario whereby small bundles are irradiated prior to twisting into bundles is suggested as a possible future method for producing macro-scale cross-linked CNT fibres.

The mechanical properties of irradiated CNT bundles are also investigated using molecular dynamics. Bundles irradiated with carbon ions with energy 50–300 eV/ion, and fluence between $4 \times 10^{13} \text{ cm}^{-2}$ and $2 \times 10^{14} \text{ cm}^{-2}$, are mechanically tested. With careful control of irradiation parameters, it is observed that shear and toughness parameters increase by an order of magnitude, while tensile properties reduce by only 30–40%; in real CNT fibres with discontinuous CNT filaments the reduction would be much less. The nano-scale interface response resembles that of micro-scale composites, in which interstitial C atoms play a key role. This makes C ion irradiation an attractive option over irradiation by electrons or other types of ions, since the extra C atoms can provide the required interstitial atoms. Within a certain cross-link density range, the interface shear modulus, shear stress at bonding onset and frictional sliding stress after debonding are all linearly related to cross-link density making controlled design of fibre shear properties feasible. A possible post-treatment with very low energy irradiation is proposed for healing holes and partially restoring tensile strength.

Acknowledgements:

Firstly, I would like to thank my supervisor Prof. Michael McCarthy. Throughout all stages of my PhD, he has guided me, helped me to achieve my goals and assisted me when in times of difficulty. Thank you so much for your guidance, expertise and planning of PhD program. Thanks also to my co-supervisor, Prof. William Curtin who provided me with a chance to spread my wings and visit an international Ivy League University in Brown University. Thanks to all the staff at Brown University's solid mechanics group who made me very welcome at such a prestigious university and included me in projects with collaborating researchers. These researchers included Prof. Huaijin Gao, Dr. Jun Song, Dr. Xinghua Shi and Dr. Fabio Pavia. Thanks to all those involved with providing me with accommodation during my stay at the Brown University.

Thanks to my parents, brothers and extended family for always being there for me when I required help with my studies.

I am very grateful for all the help Dr. Conor McCarthy provided during my transition from FYP to PhD studies, for his support and reference when applying for funding for this PhD under Professor Michael McCarthy.

Thanks to all the academic and administrative staff at the University of Limerick who assisted me during my undergraduate and postgraduate studies.

Finally, thank you to the staff of the MABE department who were always friendly and provided me with a support network when studying at UL.

Table of Contents

Declaration.....	2
Abstract.....	3
Acknowledgements.....	5
Table of Contents.....	6
List of Figures.....	10
List of Tables.....	15
Nomenclature.....	16
1 Introduction.....	17
1.1 Problem Statement.....	17
1.2 Formation of Inter-tube Links via Irradiation.....	19
1.3 Research Aims and Objectives.....	20
1.4 Thesis Structure.....	24
2 Literature Review.....	25
2.1 Introduction.....	25
2.2 Properties of Carbon Nanotubes.....	25
2.2.1 Chemistry of Carbon Nanotubes.....	25
2.2.2 Geometric Properties of Carbon Nanotubes.....	29
2.3 Synthesis of Carbon Nanotubes.....	30
2.3.1 Arc Discharge.....	30
2.3.2 Laser Ablation.....	31

2.3.3	Chemical Vapour Deposition.....	32
2.4	Molecular Dynamics Modelling Techniques for CNTs.....	33
2.5	Load Transfer between SWCNTs in Bundles and Between Walls of MWCNTs.....	34
2.6	Irradiation of SWCNT Bundles and MWCNTs.....	36
2.7	Summary.....	45
3	Simulation Methodology.....	48
3.1	Introduction.....	48
3.2	Interatomic Potential.....	48
3.3	Irradiation Simulations.....	53
3.3.1	Geometry.....	54
3.3.2	Single-atom Irradiation Simulation Parameters.....	55
3.3.3	Multi-atom Irradiation Simulation Parameters.....	56
3.4	Mechanical Test Simulations.....	58
3.4.1	Geometry.....	58
3.4.2	Tensile and Pullout Test Simulation Parameters.....	58
4	Nanostructure Evolution for Single Carbon Atom Irradiation.....	60
4.1	Introduction.....	60
4.2	Direct Impact.....	61
4.2.1	Threshold kinetic energy to displace an atom from the CNT (E_{th}).....	61
4.2.2	Effects on CNT Bundle at energies above E_{th}	62
4.2.3	Energy Analysis for Direct impact.....	67
4.3	Penetrating Impact.....	69
4.3.1	Energy analysis for Penetrating Impact.....	69

4.3.2 Effects on CNT Bundle at Energies of 50-200eV.....	70
4.4 Oblique Impact.....	76
5 Nanostructure Evolution for Multi-Carbon Atom Irradiation of Pristine SWCNT Bundle.....	81
5.1 Introduction.....	81
5.2 Inter-tube Links Formed by Multi-atom Irradiation.....	82
5.3 Defects Formed by Multi-atom Irradiation.....	86
5.4 Effects of Irradiation Parameters on Inter-tube Cross-link And Defect Characteristics.....	87
5.5 Irradiation Strategies to Improve Mechanical Performance in 7-tube Bundles.....	93
5.6 Extension to Larger Bundles.....	94
6 Interface Friction Behaviour and Tensile Strength of Pristine and Irradiated SWCNT Bundles.....	99
6.1 Introduction.....	99
6.2 Irradiation Effects on Inter-tube Shearing.....	99
6.3 Tensile Properties of Irradiated Specimens.....	107
7 Conclusions and Recommendations.....	112
7.1 Conclusions.....	112
7.2 Recommendations for future work.....	114
Bibliography.....	116

Appendix A: Detailed Schematics and Snapshots of Bond Breaking Behaviour for Different Types of Inter-tube Bond.....	124
Appendix B: O’Brien, N.P., M. A., McCarthy, W. A., Curtin, 2013, Improved Inter-tube Coupling in CNT Bundles Through Carbon Ion Irradiation, Carbon, 51, 173-184.....	135
Appendix C: O’Brien, N.P., M. A. McCarthy, W. A. Curtin, 2013, A Theoretical Quantification of the Possible Improvement in the Mechanical Properties of Carbon Nanotube Bundles by Carbon Ion Irradiation, Carbon, 53, 346-356.....	148

LIST OF FIGURES

Figure 1-1:	Experimental (TEM, reproduced from [4]) and computational (MD) visualizations of DWCNT bundles	18
Figure 1-2:	Visualizations and schematics of fibre-spinning process, reproduced from [5] [7], (a) yarn spinning procedure (b) snapshot of 1 cm wide CNT array and (c) SEM image of as-spun coiled CNT yarn.	18
Figure 1-3:	Visualisations of (a) irradiation, (b) pullout and (c) tensile tests for 7 CNT bundles.	23
Figure 2-1:	Diamond, buckyball, graphite and carbon nanotubes; graphitic structures all based on different configurations of carbon atoms (reproduced from Lau and Hui, 2002 [2]). Graphene (single sheets of carbon) and Carbyne (linear chains of carbon) have been isolated since this reference.	26
Figure 2-2:	sp^2 hybridization process for carbon atoms in graphite and CNTs.	27
Figure 2-3:	sp^3 hybridization process for carbon atoms in diamond and sp^3 bonds in CNTs and 4 hybrid orbitals.	27
Figure 2-4:	A multi-walled CNT (MWCNT) consisting of three walls.	28
Figure 2-5:	The tensile strength of the carbon nanotube compared to other engineering materials (reproduced from Lau and Hui, 2002 [2])	28
Figure 2-6:	(a) Armchair and (b) Zig-zag configurations for single wall CNTs (reproduced from Thostenson et al., 2001 [56])	29
Figure 2-7:	The chiral vector and chiral angle for armchair and zig-zag CNTs (Reproduced from Thostenson et al., 2001 [56])	30
Figure 2-8:	Arc discharge technique for producing carbon nanotubes (Reproduced from Thostenson et al., 2001 [56]).	31
Figure 2-9:	Laser ablation technique used for processing carbon nanotubes (reproduced from Thostenson et al., 2001 [56]).	32
Figure 3-1:	The covalent and van der Waals bonds in the CNT lattice which are described by the Brenner and Lennard Jones potential respectively (reproduced from Odegard et al., 2004 [60]).	49
Figure 3-2:	Bond lengths and angles considered for the potential energy in the bonds connected to atom i using the Brenner potential.	52
Figure 3-3:	One of the bond angles considered in calculating the potential energy of (a) bond jk4 (b) bond jk3 which is affected by movement of atom i.	52

Figure 3-4:	(a) Hexagonally arranged 7-tube (26 0) SWCNT bundle model with five “rings” of deposition atoms; the atoms in each ring are distributed randomly in the axial and circumferential directions (b) random deposition atom trajectory parameters and reference area A_{INT} used to determine the number of bonds per area at each interface; the curve segment S is defined to include all atoms in the outer CNT which are within the interaction distance of centre CNT, for the potential function used.	54
Figure 3-5:	Snapshots of incoming atom (black) with incident energy of 14 eV directly colliding with a CNT atom (a) 0° impact (b) oblique impact	55
Figure 3-6:	Diagrams of (a) pullout and (b) tensile tests for 7 CNT bundles.	58
Figure 4-1:	Single C atom impacts, (a) direct impact sequence, (b) penetrating impact sequence, (c) oblique impact sequence for 200 eV case	60
Figure 4-2:	Snapshots in time for direct impact of atom with 50 eV incident energy	63
Figure 4-3:	Snapshots in time for direct impact of atom with 100 eV incident energy	64
Figure 4-4:	Snapshots in time for direct impact of atom with 150 eV incident energy	65
Figure 4-5:	Snapshots in time for direct impact of atom with 200 eV incident energy eV	66
Figure 4-6:	Time versus energy for direct impact of atom with 50 eV incident energy and snapshots of incoming and ejected atom’s trajectory (Incoming atom = Red; Ejected atom = Black)	68
Figure 4-7:	Time versus energy for atom penetrating C6 hexagon for CNT bundle (incoming atom energy = 50 eV) and snapshots of incoming atom’s trajectory (Incoming atom = Red)	70
Figure 4-8:	Snapshots in time for penetrating impact of atom with 50 eV incident energy	72
Figure 4-9:	Snapshots in time for penetrating impact of atom with 100 eV incident energy	73
Figure 4-10:	Snapshots in time for penetrating impact of atom with 150 eV incident energy	74
Figure 4-11:	Snapshots in time for penetrating impact of atom with 200 eV incident energy	75
Figure 4-12:	Snapshots in time of CNT bundle outer surface for oblique impact with incident energy of 50 eV	77

Figure 4-13:	Snapshots in time of CNT bundle outer surface for oblique impact with incident energy of 100 eV	78
Figure 4-14:	Snapshots in time of CNT bundle outer surface for oblique impact with incident energy of 150 eV	79
Figure 4-15:	Snapshots in time of CNT bundle outer surface for oblique impact with incident energy of 200 eV	80
Figure 5-1:	Irradiated SWNT bundles for: (a) 50 eV/ion, fluence = $2 \times 10^{14} \text{ cm}^{-2}$, (b) 100 eV, fluence = $2 \times 10^{14} \text{ cm}^{-2}$, (c) 150 eV, fluence = $2 \times 10^{14} \text{ cm}^{-2}$, (d) 200 eV, fluence = $1.2 \times 10^{14} \text{ cm}^{-2}$, (e) 200 eV, fluence = $2 \times 10^{14} \text{ cm}^{-2}$, (f) 300 eV, fluence = $4 \times 10^{13} \text{ cm}^{-2}$, (g) 300 eV, fluence = $1.2 \times 10^{14} \text{ cm}^{-2}$, (h) 300 eV, fluence = $2 \times 10^{14} \text{ cm}^{-2}$, (Original irradiation atoms = Red; Original CNT bundle atoms = Blue)	83
Figure 5-2:	Inter-tube cross-link types, (a) direct sp^3 - sp^3 bond (b) two sp^3 - sp bonds with one interstitial atom, (c) three sp^3 - sp^2 bonds with one interstitial atom, (d) one sp^3 - sp^2 and two sp^2 - sp^2 bonds with one interstitial atom, (e) four sp^3 - sp^3 bonds with one interstitial atom, (f) one sp - sp and two sp^3 - sp bonds with two interstitial atoms, (g) one sp^2 - sp^2 and four sp^3 - sp^2 bonds with two interstitial atoms, (h) seven sp^3 - sp^3 bonds, and two interstitial atoms, (i) three sp^3 - sp^2 and three sp^2 - sp^2 bonds, and three interstitial atoms, (j) six sp^3 - sp^2 and three sp^3 - sp^3 bonds, and three interstitial atoms. Atoms: Red = interstitial, Green: CNT atom directly involved in cross-link, Blue: CNT atom not involved in cross-link. Bonds: Blue = sp^3 - sp^3 , Pink = sp^3 - sp , Green = sp^3 - sp^2 , Black = sp^2 - sp^2 , Red = sp - sp .	84
Figure 5-3:	Vacancies/defects formed for irradiated CNT bundle models (a) one atom vacancy (symmetric reconstruction), (b) two atom vacancy (symmetric reconstruction), (c) two atom vacancy (asymmetric reconstruction), (d) greater than two atom vacancy, (e) Stone-Wales (5775) defect, (f) pentagon-hexagon (5665) defect	86
Figure 5-4:	Number of irradiation atoms trapped (a) and displaced (b) in the CNT bundle as a function of incident energy, for five rings of 50 incident atoms	88
Figure 5-5:	Number of inter-tube links per area (A_{INT} in Fig. 1(b)), between centre CNT and outer CNTs (“Centre Links”), and between outer CNTs only (“Circumferential Links”) as a function of dosage, with incident beam energies of 50-300 eV; error bars show standard error or σ/\sqrt{N} where N is the number of repeats with different random trajectories	90

Figure 5-6:	Number of defects as a function of incident energy, for five different numbers of incident atoms (a) One-atom vacancies, (b) Two-atom vacancies, (c) Greater-than-2-Atom vacancies, (d) 5665 and 5775 defects and (e) Total number of defects	92
Figure 5-7:	Largest hole size as a function of dosage, with incident beam energies of 50-200 eV; error bars show standard error or σ/\sqrt{N} where N is the number of repeats with different random trajectories	93
Figure 5-8:	Final state and number of inter-tube cross-links at each CNT-CNT interface for various irradiation strategies with same overall dosage, (a) 850 ions at 100 eV/ion, (b) 425 ions at 200 eV/ion, (c) 170 ions at 300 eV/ion, then 170 ions at 150 eV/ion, then 85 ions at 100 eV/ion, (d) 85 ions at 400 eV/ion, then 170 ions at 200 eV/ion, then 170 ions at 100 eV/ion, (e) 85 ions at 500 eV/ion, then 170 ions at 150 eV/ion, then 170 ions at 100 eV/ion, (f) 85 ions at 600 eV/ion, then 340 ions at 100 eV/ion. “M” stands for multiple links in cases where the interface is too amorphous to allow counting of links.	96
Figure 6-1:	Areal inter-tube link density (ITLD or ρ), as a function of dosage, with incident beam energies of 50-300 eV (only links to centre CNT included)	100
Figure 6-2:	Pull-out stress versus pull-out distance for irradiated CNT bundles with incident energies of (a) 50 eV, (b) 100 eV, (c) 150 eV, and (d) 200 eV	101
Figure 6-3:	Bond breaking and re-forming during pull out of centre CNT. Snapshots in time, time increasing from left to right, numbers are to guide eye in following individual atoms over time, (a) direct sp^3 - sp^3 bond, (b) cross-link with one interstitial and two sp^3 - sp bonds, (c) cross-link with two interstitials and seven sp^3 - sp^3 bonds.	102
Figure 6-4:	Pull-out force per inter-tube cross-link with the centre CNT versus pull-out distance for irradiated CNT bundles with incident energies of (a) 50 eV, (b) 100 eV, (c) 150 eV, and (d) 200 eV (ITLD = inter-tube link density or ρ in $1/nm^2$)	104
Figure 6-5:	Elastic and sliding parameters for pull-out versus ITLD (or ρ) for irradiated CNT bundles (a) interface shear modulus, (b) interface shear strength, and (c) interface sliding stress. Lines show linear relationships in the range $\rho = 0.7 - 1.7 nm^2$.	105
Figure 6-6:	Tensile test result on 7-tube bundles, (a) stress versus strain for incident energy of 100 eV, (b) tensile strength,	

	(c) maximum strain, (d) strength vs. maximum hole size	108
Figure 6-7:	Largest hole size for 150 eV, 17.88 MGy, (a) pre-healing, (b) after depositing 3 additional rings of 250 atoms at 1 eV (red dashed ring highlights area where hole healing has taken place), (c) line up of adatoms providing weak point in structure; green bonds are ~ 1.54 Å in length, blue bonds are ~ 1.42 Å in length.	111
Figure 6-8:	Effect of “healing” 1 eV C ion irradiation on (a) tensile strength and (b) pull-out stress	111
Figure A-1:	Schematics and snapshots of bond breaking behaviour for a direct sp^3 - sp^3 inter-tube bond.	125
Figure A-2:	Schematics and snapshots of bond breaking and re-forming behaviour for an inter-tube bond involving two sp^3 -sp bonds and one interstitial atom.	126
Figure A-3:	Schematics and snapshots of bond breaking and re-forming behaviour for an inter-tube bond involving three sp^3 - sp^2 bonds and one interstitial atom	127
Figure A-4:	Schematics and snapshots of bond breaking and re-forming behaviour for an inter-tube bond involving one sp^3 - sp^2 and two sp^2 - sp^2 inter-tube bonds, and one interstitial atom.	128
Figure A-5:	Schematics and snapshots of bond breaking and re-forming behaviour for an inter-tube bond involving four sp^3 - sp^3 inter-tube bonds and one interstitial atom.	129
Figure A-6:	Schematics and snapshots of bond breaking and re-forming behaviour for an inter-tube bond involving one sp-sp and two sp^3 -sp inter-tube bonds, and two interstitial atoms	130
Figure A-7:	Schematics and snapshots of bond breaking and re-forming behaviour for an inter-tube bond involving one sp^2 - sp^2 and four sp^3 - sp^2 inter-tube bonds, and two interstitial atoms	131
Figure A-8:	Schematics and snapshots of bond breaking and re-forming behaviour for an inter-tube bond involving seven sp^3 - sp^3 inter-tube bonds, and two interstitial atoms	132
Figure A-9:	Schematics and snapshots of bond breaking and re-forming behaviour for an inter-tube bond involving three sp^3 - sp^2 and three sp^2 - sp^2 inter-tube bonds, and three interstitial atoms	133
Figure A-10:	Schematics and snapshots of bond breaking and re-forming behaviour for an inter-tube bond involving six sp^3 - sp^2 and three sp^3 - sp^3 inter-tube bonds, and three interstitial atoms	134

LIST OF TABLES

Table 5-1:	Inter-tube cross-link bond lengths and angles	85
------------	-----------------------------------------------	----

Nomenclature:

A_{INT}	Interface area for one CNT-CNT interface for atoms involved in inter-atomic interactions during shear
e	Coefficient of restitution
E_{th}	Threshold kinetic energy of incoming ion required for fully displacing an atom from the CNT lattice
m	Mass
N_I	Number of interstitial atoms
T_d	Kinetic energy that needs to be transferred to a CNT Carbon atom to fully displace it from CNT lattice
α	Angle of trajectory of incoming atoms
γ_{xy}	Interface shear strain
μ	Interface shear modulus
ρ	Areal inter-tube link density (links between centre tube in bundle and surrounding tubes)
τ	Frictional sliding stress after debonding
τ_y	Interface shear stress at onset of debonding

Chapter 1 Introduction

1.1 Problem Statement

Carbon nanotubes (CNTs) consist of graphene sheets rolled into seamless cylindrical forms. They have diameters on the scale of nanometres and lengths up to a few millimetres. The discovery of CNTs is generally attributed to the Japanese physicist Sumio Iijima in 1991 [1], after which interest in them accelerated rapidly; however images of CNTs were published prior to this. Due to strong, covalent, inter-atomic bonds between the constituent carbon atoms, CNTs have outstanding mechanical properties with tensile strengths greater than 100 GPa and a density half that of aluminium. This has spawned much research on using them as reinforcing components in ceramic, metal and polymer matrices to produce CNT-based composites. However, much work remains to be completed in order to enable CNT-based composites to achieve their full potential.

Processing methods currently used to produce CNTs include: (a) Arc discharge, (b) Laser ablation and (c) Chemical vapour deposition (CVD). The arc discharge and laser ablation methods are used to produce single-walled CNTs (SWCNTs), while the CVD method mainly yields multi-walled CNTs (MWCNTs) [2]. MWCNTs consist of multiple, concentric, nested SWCNTs separated by a constant graphitic spacing (approximately 0.335 nm). Both SWCNTs and MWCNTs can be used in CNT-based composites.

One of the forms in which CNTs can be used in composites, is as a multi-CNT bundle. During their production, individual CNTs agglomerate naturally into hexagonally arranged bundles due to attractive van der Waals forces (see Figure 1-1), and it can be difficult to keep them apart. CNTs are often mixed with matrices to provide improved mechanical properties, but this tendency to agglomerate means that they often exist as small bundles rather than isolated tubes within the matrix. A second application of CNT

bundles is when much larger bundles are drawn from aligned CNT “forests” to produce a CNT fibre (a fibre made up mostly or entirely of CNTs as shown in figure 1-2) [3].

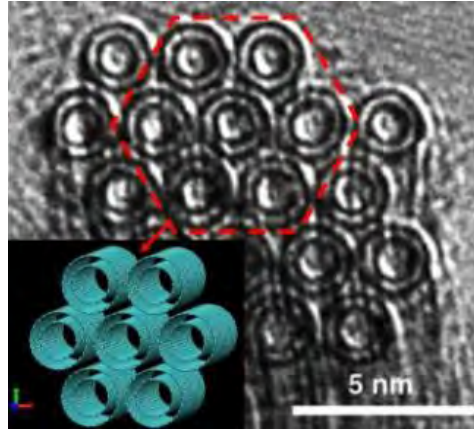


Figure 1-1: Experimental (TEM, reproduced from [4]) and computational (MD) visualizations of DWCNT bundles

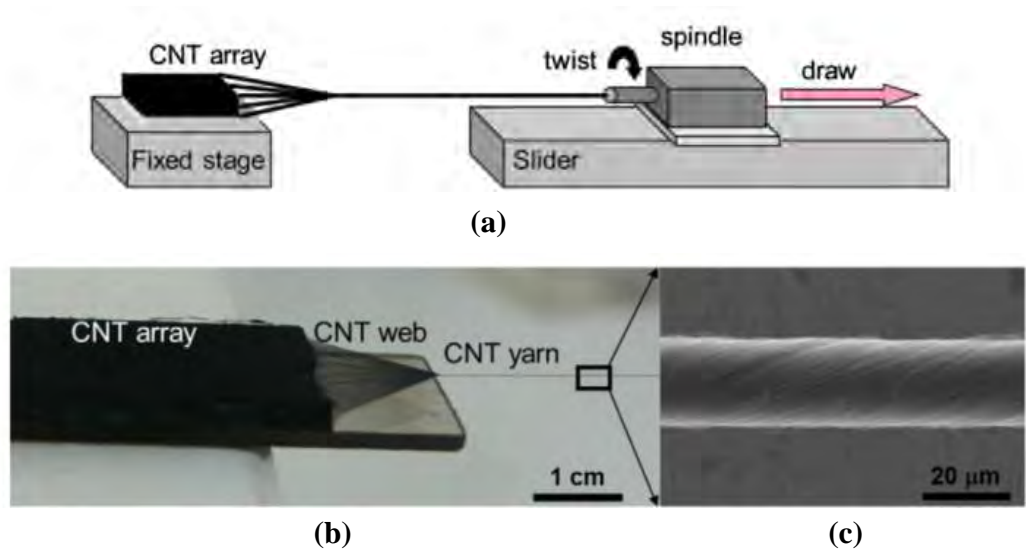


Figure 1-2: Visualizations and schematics of fibre-spinning process, reproduced from [5] [7], (a) yarn spinning procedure (b) snapshot of 1 cm wide CNT array and (c) SEM image of as-spun coiled CNT yarn.

For both applications, a key limiting factor for mechanical properties is poor inter-tube and inter-shell load transfer due to the weak van der Waals shear interactions

between neighbouring shells and tubes. In CNT fibres, this deficiency affects the shear and bending properties of the fibre since individual CNTs can easily slide over each other. Less obviously, it also has a major negative influence on the tensile strength of the fibre. This is because CNTs do not run the full length of the fibre, so inter-tube shear load transfer is essential if the fibre is to behave as a coherent entity. Without it, sword-in-sheath type failure occurs in which only a few of the CNTs are actually fractured, with the rest pulled out with minimal resistance. As a result, the tensile strength of CNT-fibres is generally far lower than that of individual CNTs [3]. Toughness of composites containing small CNT bundles is also compromised, since load is generally introduced by the matrix to the outer tubes in the bundle, and must be transferred through inter-tube shear if the inner tubes are to share the load. With only weak inter-tube load transfer, sword-in-sheath type failure again occurs and very little energy is absorbed in pulling out the unbroken CNTs from the bundle; this is particularly an issue for ceramic composites for which fibre pull-out is a big factor in determining composite toughness [9].

1.2 Formation of Inter-tube Links via Irradiation

One possible way to address the problem of weak inter-tube shear interaction is by introducing controlled levels of bonding between the CNTs by irradiating them with electrons or ions. This process can eject atoms from the CNT lattice and lead to the creation of inter-tube bonding. However, the downside of irradiation is that it also introduces CNT defects which reduce tensile strength. Thus the interplay between enhanced inter-tube shear strength and decreased tensile strength must be examined to see if the benefits outweigh the drawbacks, and to identify what irradiation energy and dosage are optimal.

A number of researchers have investigated the use of irradiation, either with electrons or ions, to promote covalent bonds between neighbouring walls in MWCNTs [9-12, 13-15] or tubes [16-18, 31] in CNT bundles. It has been shown computationally that only a small amount of cross-links can dramatically increase inter-wall or inter-tube stiffness [18, 21]. On the other hand, irradiation produces the unwanted side effect of

other kinds of defects, such as vacancies, adatoms, and Stone–Wales defects, which have a detrimental effect on mechanical properties, particularly tensile properties [15, 18, 22]. Thus, a delicate balance has to be struck. The formation of defects (including cross-links) and their effects on mechanical properties is a formidably complex problem, influenced by many factors including CNT size, the number of walls, the number of tubes in the CNT bundle, incident particle mass, energy, dosage and whether or not the particles form chemical bonds with the C atoms in the CNT lattice [23].

1.3 Research Aims and Objectives

The overall objective of this work is to model irradiation of bundles of single-walled CNTs (SWCNTs), in order to induce controlled levels of inter-tube bonding (with the likely side-effect of some intra-wall defects), and to assess the efficacy of using irradiation to produce CNT bundles with load transfer properties suitable for use in nanocomposites. In particular, the focus is on carbon ion irradiation, as opposed to most experimental studies to date, which have been on electron irradiation or argon ion irradiation. Carbon ion irradiation is an interesting option since it introduces no impurities into the system, provides additional carbon interstitial atoms to mediate cross-links (without necessarily having to knock out atoms from the lattice), and enables efficient momentum transfer due to the match between the mass of the irradiation and target atoms. To achieve this objective, the molecular dynamics simulation method has been chosen as it provides the best balance between predictive capability and computational tractability.

A list of specific aims for this work is outlined below:

- To study carbon ion irradiation of small (7-tube) CNT bundles using molecular dynamics simulations and investigate the delicate balance between achieving a desired inter-wall or inter-tube bond density and keeping the generally unwanted side-effect of intra-wall defects such as

vacancies, ad-atoms and Stone-Wales vacancies to a minimum. For this purpose, a recently-developed reactive bond-order potential is used. This potential has an environment-dependent first nearest-neighbour definition [35] which accurately simulates bond-forming and bond breaking processes in carbon-based systems.

- To analyse various factors which influence the formation of defects (including cross-links) including number of tubes in a CNT bundle, and incident particle energy and dosage.
- To examine and characterise the many different types of cross-links and defects formed during the irradiation process.
- To quantify the effects of cross-links and defects on the mechanical properties of CNT bundles, in particular the tensile strength and the pull-out force required to pull a tube out of the bundle (which strongly influences toughness).
- To compare the carbon ion irradiation process with results in the literature obtained from the irradiation of CNTs with noble gases, CH₃, CF₃, potassium, boron and nitrogen.
- To simulate the carbon ion irradiation process for larger, 19 tube bundles and to explore the challenges in terms of controlling cross-link density.
- To investigate different irradiation strategies aimed at improving mechanical properties. The ideal result would be a uniform level of inter-tube covalent bonding between all adjacent tubes with a minimum level of defects in CNT walls. This would allow transfer of load between CNTs, enabling all of them to engage in loading, with the least loss in strength due to intra-wall defects.

To address these aims, an extensive series of simulations is performed for three related problems, shown in figure 1-3:

- The irradiation process itself, the output of which will be the inter-tube bonds and defects formed for varying energy and dosage.
- Tensile testing of the resulting irradiated bundles, to determine the loss in strength due to defects formed.
- Pull-out tests, in which the one tube is pulled from the irradiated bundle, to examine the gains made in inter-tube shear stiffness and strength, and energy absorbed during pullout, which is related to composite toughness.

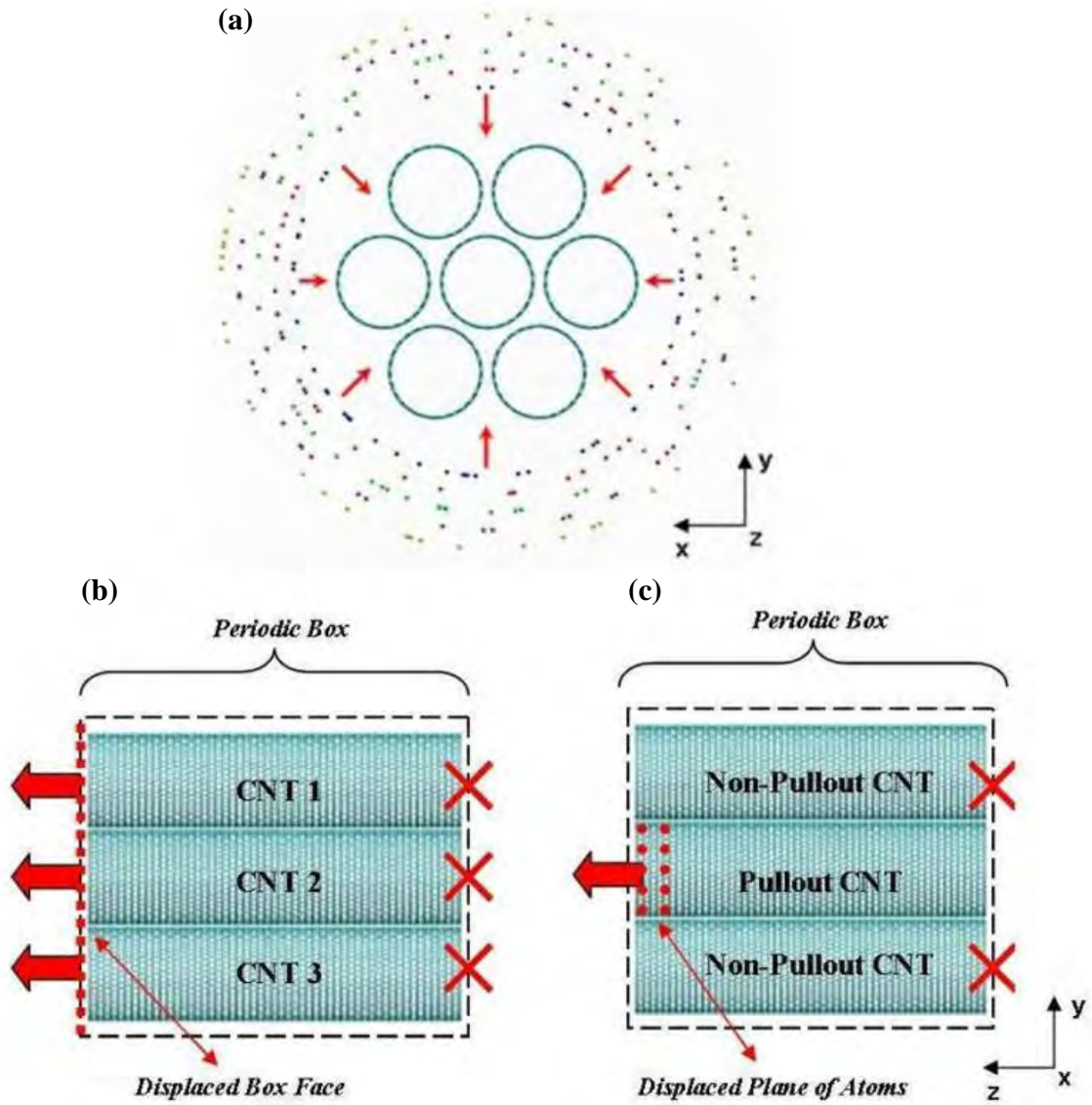


Figure 1-3: Visualisations of (a) irradiation, (b) pullout and (c) tensile tests for 7 CNT bundles.

The start point for the simulations will be the simplest possible hexagonally arranged CNT bundle, namely a 7-tube bundle, illustrated in Figure 1-3, with no defects, and no inter-tube covalent bonds. Later on, larger bundles will be examined. Preliminary work will focus on single-ion impacts, to validate the approach, and examine the effects of a single impact at varying energy and angle.

1.4 Thesis Structure

The thesis is laid out as follows:

Chapter 2 presents a detailed review of the relevant literature, covering the subjects of inter-tube load transfer for pristine CNT bundles and CNT bundle irradiation.

Chapter 3 outlines the simulation methodology. The interatomic potential, system geometry and steps involved in the molecular dynamics simulation are explained in detail.

Chapter 4 presents preliminary results for single ion irradiation, with an analysis of total, kinetic and potential energies for direct, penetrating and oblique impacts, at various energy levels.

In Chapter 5, the inter-tube links and defects formed during irradiation of 7 and 19 tube bundles are examined in detail, for varying irradiation parameters.

Chapter 6 shows how carbon ion CNT bundle irradiation directly affects mechanical properties by examining and comparing tensile and pullout test results for bundles irradiated with variable irradiation parameters.

Chapter 7 summarises the work by drawing conclusions, and making recommendations for future work.

Chapter 2 Literature Review

2.1 Introduction

As stated in Chapter 1, the overall objective of this study is to examine irradiation of CNT bundles as a means of inducing controlled levels of inter-tube bonding, to improve inter-tube load transfer and consequently composite material properties. In this chapter the relevant literature is reviewed, beginning with a brief discussion of the properties of CNTs, followed by a short review of Molecular Dynamics simulation. Next follows a discussion of previous findings on inter-tube load transfer in pristine (non-irradiated) CNT bundles, and finally work to date on irradiation of MWCNT and SWCNT bundles with electrons and various types of ions (e.g. CH_3 , CF_3 , potassium, carbon, argon, boron, nitrogen or hydrogen) is discussed.

2.2 Properties of Carbon Nanotubes

2.2.1 Chemistry of Carbon Nanotubes

Carbon nanotubes were discovered by the Japanese physicist Sumio Iijima in 1991 [1]. The geometrical structure of the carbon nanotube is based on an elongated form of the buckyball. The buckyball is a sphere comprised of 60 carbon atoms with 20 hexagonal and 12 pentagonal faces and was first discovered in 1985 by the Nobel laureate, R. Smalley of Rice University and H. Kroto of the University of Sussex. The carbon nanotube can also be thought of as a graphene sheet rolled into a tubular form. Figure 2-1 illustrates various graphitic structures.

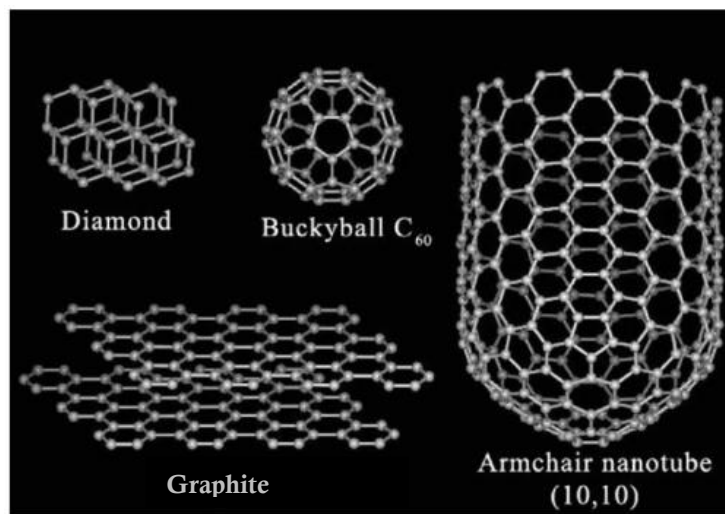


Figure 2-1: Diamond, buckyball, graphite and carbon nanotubes; graphitic structures all based on different configurations of carbon atoms (reproduced from Lau and Hui, 2002 [2]). Graphene (single sheets of carbon) and Carbyne (linear chains of carbon) have been isolated since this reference.

The unique mechanical properties of carbon nanotubes are due to the specific chemical bonds formed. The chemical bonding in carbon nanotubes is similar to that in graphite or graphene, where each carbon atom has three nearest neighbours. This type of bonding is referred to as sp^2 bonding, which is formed by a process called sp^2 hybridization. In the valence shell of atomic carbon, there are two electrons in the 2s orbital and two electrons in the 2p orbitals (two of the three 2p orbitals have one electron each, while the third is empty). When carbon forms bonds with other atoms, one of the 2s electrons is promoted to the empty 2p orbital making it tetravalent (four unfilled orbitals). In doing so, hybrid orbitals form, which are linear combinations of the 2s orbital and one or more of the 2p orbitals. In sp^2 hybridization, three hybrid sp^2 orbitals are formed, replacing two of the 2p orbitals and the 2s orbital (the third 2p orbital is left unchanged). Figure 2-2 illustrates the process. The sp^2 orbitals are in the same plane with angles of 120° between them, while the remaining p orbital is perpendicular to this plane. In graphene and CNTs, all the carbon atoms are sp^2 hybridized and strong sigma bonds of length $\sim 1.42 \text{ \AA}$ are formed via the overlap of the sp^2 orbitals from neighbouring atoms, so the bonding could be called sp^2 - sp^2 bonding or just sp^2 bonding. The remaining p orbitals

also overlap to some extent to form pi bonds, but these are de-localised, so are much weaker. They have some effect on out of plane properties such as wall bending stiffness.

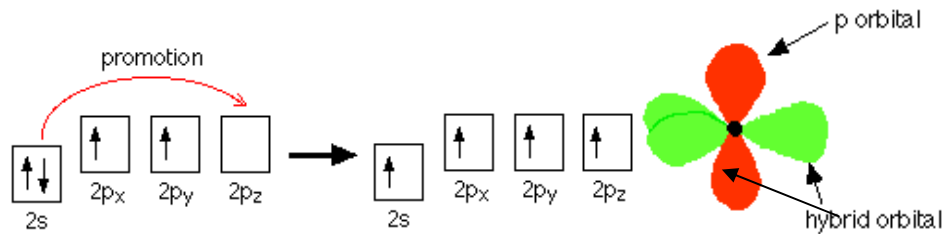


Figure 2-2: sp^2 hybridization process for carbon atoms in graphite and CNTs [64].

The chemical bonding in diamond is referred to as sp^3 bonding. In sp^3 hybridization, the four hybrid orbitals are formed, replacing the 2s orbital and the three 2p orbitals. The angle between the bond centre lines is 109.5° . Figure 2-3 shows the process. Carbon atoms in diamond are thus arranged tetrahedrally. The bond length is $\sim 1.54 \text{ \AA}$ so sp^3 bonding is weaker than sp^2 bonding.

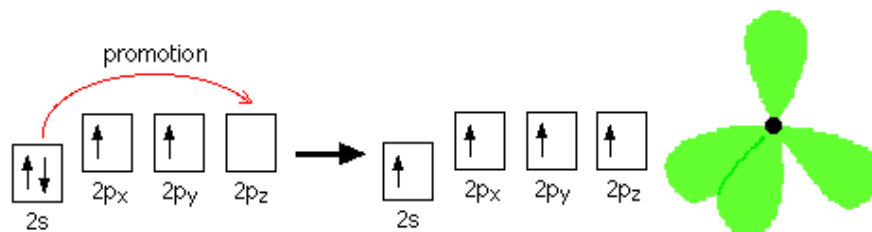


Figure 2-3: sp^3 hybridization process for carbon atoms in diamond and sp^3 bonds in CNTs and 4 hybrid orbitals [65].

CNTs can contain sp^3 bonds, e.g. if adatoms attach to the surface or if direct links form between carbon walls in a multi-wall CNTs (MWCNTs). MWCNTs are made up of concentric single wall tubes separated by a constant graphitic wall thickness of 0.335 nm . Figure 2-4 illustrates the geometric structure of a MWCNT. Such sp^3 bonds, if present, locally weaken the CNT structure.



Figure 2-4: A multi-walled CNT (MWCNT) consisting of three walls.

The strong sp^2 bonds give CNTs their extraordinary mechanical properties, with a reported tensile strength of over 100 GPa. Carbon nanotubes are much stronger than nearly all other engineering materials, including carbon fibre and steel, while having a low density (one sixth the density of steel). It has been hypothesized that these materials could be very useful in extreme engineering conditions where high stresses are common. CNTs would be ideal materials for aerospace or space travel applications, where high strength and low density are a necessity. Figure 2-5 illustrates the strength of carbon nanotubes compared to other commonly used engineering materials.

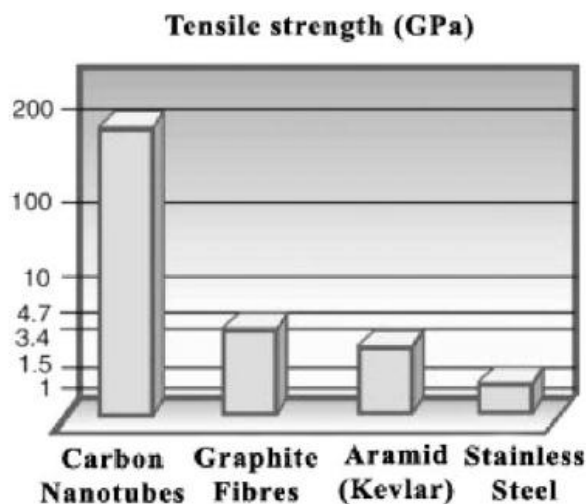


Figure 2-5: The tensile strength of the carbon nanotube compared to other engineering materials (reproduced from Lau and Hui, 2002 [2])

2.2.2 Geometric Properties of Carbon Nanotubes:

There are many geometric definitions for CNTs. The two main geometrical configurations for CNTs are the zig-zag and armchair configurations. Figure 2-6 shows both the zig-zag and armchair configurations for CNTs.

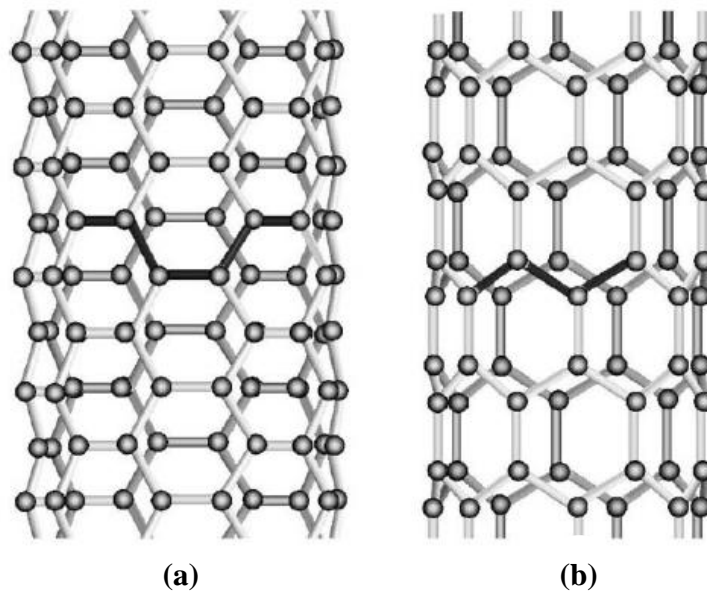


Figure 2-6: (a) Armchair and (b) Zig-zag configurations for single wall CNTs (reproduced from Thostenson et al., 2001 [56])

The main definition used to describe the geometry of a CNT is the chiral vector equation. The chirality or helicity of a carbon nanotube is defined using the chiral vector and chiral angle, as illustrated in Figure 2-7.

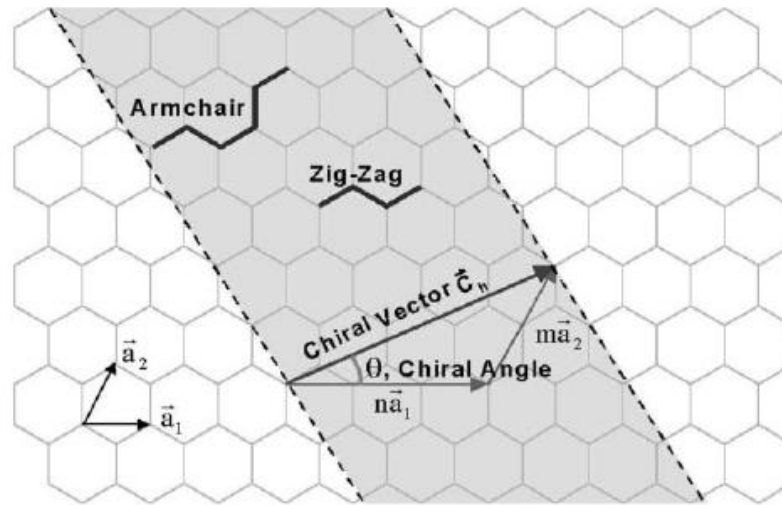


Figure 2-7: The chiral vector and chiral angle for armchair and zig-zag CNTs (Reproduced from Thostenson et al., 2001 [56])

The chiral vector is defined using the following equation:

$$\vec{C}_h = n\vec{a}_1 + m\vec{a}_2 \quad 2-1$$

where n and m are integers which define the number of steps along the zig-zag carbon bonds. The chiral angle is defined using these vectors and describes the amount of twist in the CNT. The zig-zag configuration has a chiral angle of 0 degrees and the armchair configuration has a chiral angle of 30 degrees.

2.3 Synthesis of Carbon Nanotubes

2.3.1 Arc Discharge

The CNTs observed by Sumio Iijima in 1991 were produced using the arc discharge method. This method involves using two high purity graphite rods, one forming

an anode and the other a cathode. These rods are brought close together in a helium atmosphere and a voltage is applied until a stable arc is achieved. A constant distance is maintained, in order to sustain growth of material on the cathode. The black material which forms on the cathode consists of an outer shell and an inner shell. The material in the inner shell contains numerous multi-walled CNTs or MWCNTs. Single-walled CNTs are achieved by doping the electrode with a metal catalyst (Thostenson et al., 2001 [56]). Figure 2-8 shows the arc discharge technique in more detail.

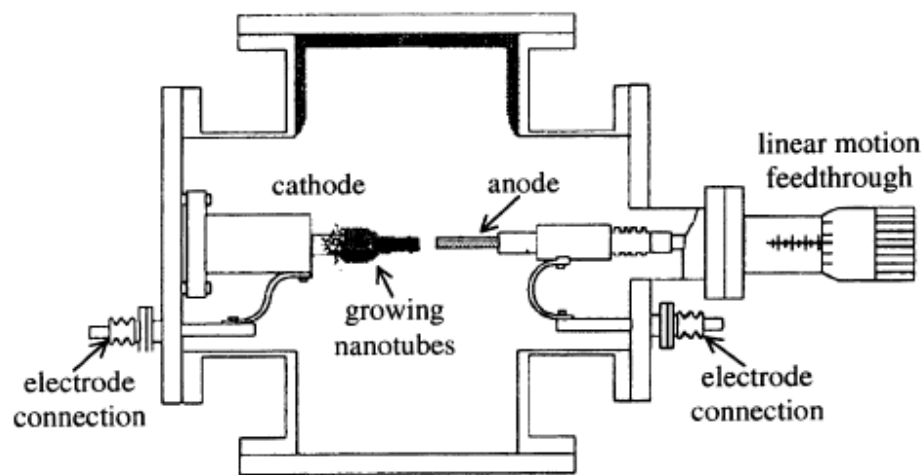


Figure 2-8: Arc discharge technique for producing carbon nanotubes (Reproduced from Thostenson et al., 2001[56]).

2.3.2 Laser Ablation

The laser ablation process was first designed for the production of fullerenes but the process has now been developed for the fabrication of SWCNTs. The basic process involves vaporising a graphitic target in a controlled atmosphere at a temperature near 1200 °C. The graphite target is doped with cobalt and nickel catalysts and after the target has been vaporised, the condensed material is collected on a water cooled target. This condensed material is used to grow SWCNTs (Thostenson et al., 2001 [56]). Figure 2-9 illustrates the laser ablation technique. The two major disadvantages associated with the

laser ablation and arc discharge techniques are: (a) there is a limited volume produced for each sample and (b) subsequent purification steps are necessary to remove impurities (Thostenson et al., 2001 [56]).

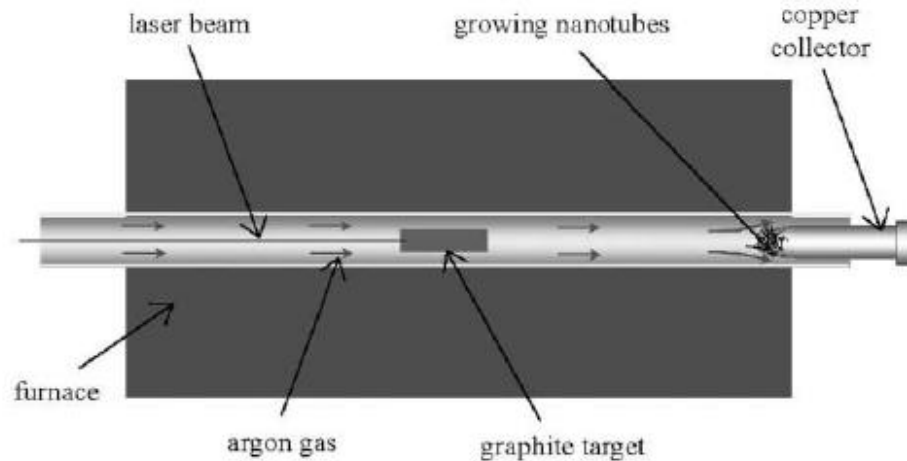


Figure 2-9: Laser ablation technique used for processing carbon nanotubes (reproduced from Thostenson et al., 2001 [56]).

2.3.3 Chemical Vapour Deposition

When using the arc discharge or laser ablation techniques, subsequent purification techniques are necessary to separate CNTs from by-products produced. Therefore, the chemical vapour deposition (CVD) technique is often used to process purified CNTs (Thostenson et al., 2001 [56]). The CNTs are grown in a carbon containing atmosphere such as a hydrocarbon gas. The CVD processing technique is quite cheap compared to other methods but the CNTs often contain many defects. However, counter-intuitively, these CNTs often demonstrate the best mechanical properties (Thostenson et al., 2001 [56]).

2.4 Molecular Dynamics Modelling Techniques for CNTs

Molecular dynamics (MD) is a numerical modelling tool in which a set of mathematical equations are defined for the forces between individual molecules in a system. These equations are then solved in order to compute the acceleration, velocity and position of each molecule in the system for each time step. A system may consist of thousands of molecules, so simulations may take hours or even days to solve.

The equations used to solve molecular dynamics simulations are based on Newton's laws of motion. Haile [57] describes the application of these equations in molecular dynamics thus: *'Molecular dynamics simulation is the modern realization of an old, essentially old-fashioned, idea in science; namely the behaviour of a system can be computed if we have, for the system's parts, a set of initial conditions plus forces of interaction'*, (Haile, 1997 [57] page 1).

MD is primarily used for modelling fluids and solids. It can be used to simulate CNTs under loading conditions. When modelling the behaviour of atoms in CNTs, the simulation is initialized by inputting the initial coordinates for each atom in the system. Variables are then assigned for the simulation. These include the time step (time taken to solve each calculation), the total number of time steps, the simulation temperature, the thermostat type, the applied displacement, the time step at which the load is applied and the number of time steps between each load increment. After applying initial conditions to the system, the simulation can then be run. The system is firstly equilibrated for a certain period of time (equilibration phase) before a velocity, acceleration or load is applied to certain atoms in the CNT system being tested. The simulation then runs until the calculations for the last time step have been solved.

When modelling CNTs using molecular dynamics, equations must be defined for the bonded and non-bonded interactions between the carbon atoms. These equations describe the potential energy for the interaction, the gradient of which gives the forces between the atoms. For this study, the two main potentials used are the Lennard-Jones potential and the Brenner potential. The Lennard-Jones potential is used to model long range van der Waals non-bonded interactions. The short range covalent bonded

interactions are simulated using the Brenner potential. The Brenner potential was first described in Brenner et al., 1990 [8]. This potential was then modified in a subsequent paper by Brenner et al., in 2002 [25] and was named the REBO (Reactive Empirical Bond Order) potential. This REBO potential is referred to as a ‘many body’ potential, because it not only describes the forces between two individual atoms but also allows for the contribution of other bonded atoms. It also takes into account changes in bond-angles. Therefore, it allows for bond-angle bending and bond stretching.

There are many different types of simulation methods used to model materials at the atomic level. Quantum mechanics simulations can be used to model the interaction of electrons as well as nuclei. They are more accurate than MD simulations but are highly computationally intensive, so can only be used to model small systems. Therefore, molecular dynamics is usually used instead of quantum mechanics for modelling the behaviour of CNTs.

2.5 Load Transfer Between SWCNTs in Bundles and Between Walls of MWCNTs

Several authors have examined inter-tube shearing in bundles of "pristine" (defect-free) CNTs and have generally found low shear resistance. Majure et al., 2008 [24] performed molecular dynamics (MD) simulations, utilising the REBO potential [25] within the public domain code LAMMPS, to investigate the sliding behaviour between individual aligned CNTs in a hexagonally arranged bundle. The centre CNT was pulled out from a 7-CNT bundle, and the resisting force was measured. Periodic boundary conditions were used to simulate an infinitely long bundle – the periodic box length was not given but was described as “short”. Several chiralities and diameters were examined. The resulting pullout force was oscillatory in nature, with a maximum value that increased with CNT diameter. Two separate cases were analysed: (a) CNTs free to rotate about their axis and (b) CNTs fixed against rotation about their axes. For the largest

CNTs, which were (75, 75) armchair CNTs, the maximum pull-out force was 1.38 nN and 0.907 nN for freely rotating and frozen boundary conditions respectively. For the smallest CNTs, with a (5, 5) chirality, the maximum force was 0.04 nN and 0.089 nN for free and frozen boundary conditions respectively. These values equate to maximum shear stresses of 0.0525 GPa (free) and 0.0345 GPa (frozen) for the (75, 75) CNTs, while for the (5, 5) CNTs, maximum shear stresses of 0.0205 GPa (free) and 0.047 GPa (frozen) were obtained. These values are consistent with van der Waals interactions. In a separate paper, Majure et al., 2008 [26] examined the effect of CNT length on pullout force. The setup was similar to [24] but periodic boundary conditions were not used, and CNT bundle length was varied up to 2400 Å. Only (5, 5) CNTs were examined. The total force consisted of a capillary force (during entrance and exit of the centre CNT) plus a friction force. For a tube length of 2000 Å, the maximum pullout force (first peak) reached a value of about 8 nN up to a contact length of 1000 Å, and levelled off thereafter. This force equates to a maximum shear stress of 0.021 GPa which compares well with the 0.0205 GPa obtained in [24] for freely rotating (5, 5) CNTs. In an experimental study, Salvétat et al., 1999 [28] tested CNT bundles in bending, and obtained an inter-tube shear modulus from beam theory obtaining a value of 1 GPa.

Both experimental and computational studies on pristine inter-wall MWCNT load transfer exist. The experimental study by Akita and Nakayama, 2003 [61] investigated the pullout forces when the inner shell of a capped MWCNT is pulled out from the outer shell. The MWCNTs were grown using the arc discharge method and the synthesized CNT specimens were found to have an average diameter of 10 nm and lengths ranging from 1 to 5 µm. An experimental apparatus which consisted of a Silicon Platinum cantilever/probe and a razor blade was used to extract the inner CNT from the outer shell of the MWCNT. For a core diameter of 5 nm, pullout force was estimated at 3-5 nN. The main result of this experimental study by Akita and Nakayama, 2003 [61] was confirmed computationally by Curtin et al., 2004 [63]. Molecular dynamics simulations were used to obtain the pullout forces for both fractured end and capped DWCNTs using the original Brenner potential. The inner shell of the DWCNT was pulled from the outer shell in increments of 0.1 Å at a temperature of 0.05 K. Results showed that for a DWCNT

with an inner CNT diameter ranging from 0 – 6 nm, the pullout force varied between 0 and 5 nN. This result is in accordance with that obtained by Akita and Nakayama, 2003 [61]. For an inner CNT diameter of 1 nm, the axial or pullout stress was found to equal 1.5 GPa for both zig-zag and armchair capped DWCNTs according to Curtin et al., 2004 [63].

2.6 Irradiation of SWCNT Bundles and MWCNTs

The process of irradiating CNT bundles or MWCNTs with electrons or ions can be used to eject atoms from the CNT lattice and introduce controlled levels of bonding between the CNTs. However, the downside of irradiation is that it also introduces CNT defects which reduce tensile strength. Both computational and experimental studies have demonstrated that irradiation can be used to improve load transfer between individual SWCNTs in a CNT bundle or between walls in a MWCNT. A solely experimental study by Barber et al., 2005 [6], investigated how synthesized, non-irradiated MWCNTs behaved under tension. An atomic force microscope technique was used to tensile test the MWCNT specimens. The MWCNT samples tested under tension were not irradiated but were processed using two different techniques, CVD and AD. It was shown that the CVD grown MWCNT specimens exhibited a tensile strength of 109.3 GPa which was approximately three times greater than the value of 31.5 GPa observed for AD grown MWCNTs. The authors postulated that this improvement in tensile strength was caused by enhanced interaction between MWCNT walls due to inter-wall bonding in the CVD-grown specimens.

In a computational study by Sinnott et al., 2006 [15], individual triple walled CNTs were bombarded with low energy electrons, argon ions and CF_3 ions. The geometrical configurations for the two MWCNT models tested were, (i) a (15,15) (10,10) (5,5) triple wall CNT (armchair helical structure) and (ii) a (24,4) (15,4) (6,4) triple wall CNT (chiral helical structure). Both of these MWCNTs were irradiated with 50 CF_3 ions, 50 argon ions and 50 electrons. The incident energy for the CF_3 and argon ions was 50 eV. Electron irradiation was simulated using PKA (primary knock on atoms), where random

atoms inside the MWCNT received 10 eV of kinetic energy. After the chiral and armchair MWCNTs were irradiated, the results demonstrated that the number of defects formed depended on the helical structure of the MWCNT. In general, it was found that more defects were formed for the chiral helical structure. It was also found that the MWCNTs bombarded with CF_3 ions experienced less damage and less cross-links compared with the MWCNTs irradiated with argon ions. This was because argon ions are chemically inert while CF_3 ions can chemically bond to carbon atoms on the CNT surface. Therefore, CF_3 ions bonded to the surface of the triple walled CNT, while argon atoms penetrated the CNT walls and formed more cross links within the inner walls of the MWCNT. For the electron irradiation case, the defects were more evenly distributed in the MWCNT compared with the results found for the ion irradiation case. This was because the electron beam was not surface limited for the electron irradiation simulations. In order to test the mechanical properties of the functionalized systems, molecular dynamics pullout simulations were performed for the chiral and armchair MWCNTs bombarded with ions and electrons. For comparison purposes, a pullout simulation of a non-functionalized MWCNT was performed. It was found that the pullout loads for the functionalized MWCNT were approximately 20 times greater than those found for the non-functionalized MWCNT (pullout load for the non-functionalised MWCNTs was around 3-4 nN, while that for functionalized MWCNTs was up to 80 nN). It was also found that for the MWCNTs that were irradiated with electrons, the pullout loads were about twice those for the MWCNTs bombarded with ions. This was because more covalent bonds were formed between the inner walls of the MWCNT for the electron irradiation case.

A computational analysis performed by Curtin et al., 2007 [21] used MD to subject MWCNTs to loading in which the inner wall was pulled out from the outer wall. The results of this study showed that inter-wall bonding could be used to improve load transfer between MWCNT walls. The load transfer mechanism for DWCNTs with and without direct sp^3 inter-wall bonding was analysed. The initial pullout force for a DWCNT with only a few inter-wall bonds was approximately ten times greater than that for a DWCNT without inter-wall bonds. The initial portion of the load-deflection curve

for pullout was found to be linear until slip occurs after which the pullout force was steady. The length of the initial linear range approximately doubled, and the steady pullout force increased 15-fold for the DWCNT with inter-wall bonding, relative to the DWCNT without inter-wall bonding.

In a key study by Peng et al., 2008 [14] electron irradiation was used to induce variable degrees of inter-wall coupling for MWCNTs. This study used experimental and computational approaches to assess the mechanical properties of the non-irradiated and irradiated MWCNTs. In the experimental method, the MWCNT specimens were tensile tested using a MEMS material testing system (electron irradiation and viewing of samples was achieved using a scanning electron microscope (SEM)). For the computational analysis, MWCNT geometries with varying numbers of shells and outer shell chiralities, were analysed using quantum mechanics simulations (the semi-empirical quantum-mechanical PM3 method, density functional theory and self-consistent charge density functional-based tight binding models were employed) and molecular dynamics (using the REBO potential [25]) simulations. It was observed that with increasing dosage, the failure load increased by a factor of 30; it was also shown that the number of walls sharing the load (i.e. the number that fractured) increased with dosage, indicating that the increase in failure load was due to more walls sharing the load, thanks to inter-wall bonding. Irradiation at high doses, though, resulted in an amorphous structure for the outer walls of the MWCNT, therefore poor load transfer was observed for these MWCNT specimens. The main conclusion of this study was that near optimal load transfer can be achieved through introducing only a few inter-wall MWCNT cross-links.

Byrne et al., 2009 [10] demonstrated, using MD, that MWCNTs with sp^3 inter-wall bonds have higher tensile strengths than SWCNTs, when intra-wall cracks are present. This increased tensile strength was due to the inner wall providing a constraint to the opening of the outer wall crack, via stretching of inter-wall bonds. This result is highly relevant when considering CNTs in a composite since after synthesis, CNTs are always defective, containing intra-wall vacancies and defects as stated in Peng et al., 2008 [14]. Byrne et al, 2009 [10] demonstrated through their MD simulations that the fracture mode changes with sp^3 inter-wall bond density. For MWCNTs with low sp^3 bonding, ‘sword

and sheath' fracture was observed. For high sp^3 bond density, stress concentrations developed in neighbouring walls resulted in near-planar fracture.

Turning to CNT *bundle* irradiation, an experimental study performed by Charlier et al., 2000 [32] showed how electron irradiation of SWCNT bundles at a high incident energy of 1.25 MeV can cause CNTs to coalesce. Sun et al., 2005 [33] showed how amorphous carbon nanowires can be formed by irradiating MWCNTs with carbon ions with an incident energy of 40 keV. These two studies show that irradiating CNT bundles with very high incident energies induces structural changes which would not be desirable from the point of view of using CNTs in structural applications.

Carbon ion irradiation is another method used to modify the properties of various materials. Jager et al., 2000 [34] used MD to simulate carbon ion irradiation to grow amorphous carbon layers using incident energies ranging from 30 to 80 eV. Pastewka et al., 2010 [35] also used MD simulations to grow hydrogenated, diamond-like carbon coatings (DLC) and tested these coatings for their mechanical properties using friction tests. In an experimental study by Geohegan et al., 2002 [36], a pulsed laser deposition (PLD) process was used to coat SWCNT bundles with amorphous diamond layers by depositing carbon atoms with incident energies of approximately 100 eV.

Sinnott et al., 2000 [31] used MD to simulate bombardment of SWCNT bundles with CH_3 radicals. The Brenner potential was used for short range forces (forces between carbon atoms) and the Lennard Jones potential was used for long range forces (forces between individual walls of SWCNTs). The CNT system used for this study consisted of a bundle of six (10,10) SWCNTs arranged in a hexagonal pattern, each CNT having a length of 50 Angstrom. The CNT bundle was bombarded with three CH_3 radicals. This was achieved by initially placing the three radicals 10, 12 and 14 Angstrom from the top of the bundle and then giving the radicals initial velocities towards the CNT bundle (initial velocities were calculated from initial kinetic energies). Three initial kinetic energies (10, 45 and 80 eV) and 35 random trajectories were considered, resulting in a total of 105 simulated impacts. The results demonstrated that bombarding a SWCNT bundle with CH_3 radicals resulted in adhesion of radicals or their fragments to the nanotube walls at all incident energies. It was found that for incident energies of 10 eV,

all of the CH_3 radicals either scattered away from or were adsorbed by the CNT walls. For incident energies of 45 or 80 eV, defects and vacancies in CNT walls were formed. It was also found that for this range of incident energies, some 5/7 defects were removed from the CNT walls by carbon atoms from the CH_3 radical bonding to the 5/7 defect. Incident energies of 80 eV induced more cross-linking between individual CNTs in the bundle through sp^3 bonding than for any other energy.

Krashennikov et al., 2002 [30] used MD to simulate argon ion bombardment of a SWCNT bundle with incident energies in the range of 100 – 1000 eV. The Ar-C interactions were modelled using the Ziegler-Biersack-Littmark potential which is implemented in the TRIM (Transport of Ions in Matter) code. The C-C interactions were modelled using the original Brenner potential which is described in Brenner et al., 1990 [8]. The (10, 10) SWCNTs were arranged in a trigonal pattern and consisted of four layers of individual SWCNTs. A four layer arrangement of CNTs was chosen for this study because it was proven that argon ions at energies between 100 and 1000 eV would not penetrate more than four layers of CNTs. The results of this study demonstrated that the most common defects created were vacancies on carbon nanotube walls. The distribution of defects formed was highly non-linear and varied with displacement along the four layers of CNTs. Most defects were generated at the interface regions between layers of CNTs. It was also found that inter-tube covalent bonds were formed by carbon atom recoils (when carbon atoms rebounded off neighbouring atoms belonging to the CNT lattice). The number of inter-tube covalent links increased linearly with increasing incident energy.

Brenner et al., 2002 [25] used MD to perform chemical functionalization and pullout MD simulations for SWCNT-polyethylene composite systems. The REBO potential was used to describe the intermolecular interactions between carbon atoms. The Lennard-Jones 6-12 potential was used to model all non-bonded interactions between the polyethylene matrix and the embedded CNT. Two different CNT-polyethylene systems were irradiated. The first one consisted of a single (10,10) SWCNT embedded in the centre of a crystalline polyethylene matrix while the second system had the (10,10) SWCNT embedded in an amorphous matrix. The two systems were then functionalised

by equilibrating the system to 300°K . Both of the functionalised SWCNT-polyethylene systems exhibited six covalent cross-links with two methylene (CH_2) units for each cross-link. In order to estimate the shear strength for these functionalised systems, MD pullout simulations were performed. It was found that the shear strength of a non-bonded CNT-polyethylene composite can be increased by an order of magnitude by introducing chemical bonds between the CNT and matrix. Both the amorphous and crystalline non-functionalised composites had similar shear strengths, therefore it was concluded that the chemical properties of the matrix did not influence the mechanical properties for the non-bonded case. However, for the cross-linked composites, the shear strength for the composite with the crystalline matrix was much higher than that for the amorphous matrix.

Sinnott et al., 2003 [59] used molecular dynamics to fire an ion beam consisting of twenty C_3F_5^+ ions at different polystyrene-CNT composites. The same Brenner and Lennard Jones potentials that were used by Sinnott et al., 2000 [31] were used in this study, however the Brenner potential for this study was modified in order to take into account carbon-fluorine and hydrogen-fluorine interactions. Ion irradiation was performed on two separate polystyrene-SWCNT composite systems. There was only one difference between the two composite systems tested. One system had the SWCNT positioned one layer beneath the surface of the polystyrene matrix while the other system had the SWCNT positioned three layers beneath the matrix surface. For comparison purposes, a pristine polystyrene matrix without an embedded CNT was also bombarded with twenty C_3F_5^+ ions. The incident energy for each of the twenty C_3F_5^+ ions fired was 50 eV. The results demonstrated that as the number of layers of polystyrene matrix between the CNT and the surface was increased, the number of cross-links between the CNT and polystyrene matrix decreased. It was also observed that for the pristine polystyrene matrix case, there were much fewer trapped atoms compared with the SWCNT- polystyrene composite case.

Kis et al., 2004 [18] used both transmission electron microscopy (TEM) and atomic force microscopy (AFM) to analyse the mechanical properties of CNT bundles after being subjected to high energy electron beam irradiation. Irradiation at 80 keV (just

below the threshold value of 86 keV required to displace an atom from the CNT lattice with electron irradiation) resulted in a thirty-fold increase in bending modulus for low irradiation doses. Note that though the energies involved here were very high, the momentum is still small due to the small mass of electrons. As the irradiation dosage was increased to 200 keV, the bending modulus decreased substantially. This behaviour is in keeping with results obtained by Krashennnikov et al., 2005 [29] who used MD to analyse the effects of bombarding SWCNT bundles with electrons. The second generation Brenner potential [25] was used along with a Berendsen temperature control method. These authors observed that the shear modulus increased linearly with increasing inter-tube covalent bonds. They also found an increase in bending modulus at moderate irradiation doses but a decrease at higher irradiation doses. It was concluded that the bending modulus depends on a trade-off between stiffening due to inter-tube covalent bonds and a drop in stiffness caused by the creation of vacancies. Analytical approximations were also performed to estimate defect production rates. Using theoretical approximations, it was found that the Young's modulus decreased linearly with increasing vacancy concentration.

In the PhD thesis of Shen (2006) [58], molecular dynamics simulations were performed to investigate the effect of irradiation on the mechanical properties of CNT-matrix systems. Both ionic bombardment and pullout simulations were performed on the CNT-composite systems. The Tersoff- Brenner potential was used for carbon-carbon and carbon-hydrogen interactions, while the ZBL (Ziegler-Biersack-Littmark) potential was used for the interaction between argon ions and carbon atoms. A (15,0) SWCNT-polyethylene composite system was bombarded with argon ions with an incident energy of 250 eV. It was shown that ion irradiation is an effective method for forming sp^3 bonds between the matrix and the CNT. It was also shown that as the number of chemical attachments were increased, the interfacial mechanical properties for the composite were enhanced.

In the study by Federizzi et al., 2006 [17], molecular dynamics simulations were performed in which a three-layer CNT bundle was bombarded with low energy atoms (50, 100, 150 and 200 eV). A single carbon atom was fired 460 times, scanning an area of

$2 \times 10 \text{ \AA}$ in order to have good statistics. The Tersoff potential was used for carbon-carbon bonding for near-equilibrium distances and the ZBL potential for small distances. The temperature was kept fixed at 300 K using the Anderson thermostat. The irradiated models were analyzed for adhering atoms and inter-tube cross-links. Seven different types of both internal and external adhering atoms were observed with the single adhering atom (internal or external) being most common. Six types of inter-tube cross-link were analyzed, the most common type being the single interstitial cross-link. All types of adhering atom and cross-link were examined for bond length and angle. It was noted that above a certain energy threshold, damage formation reaches a stable production rate, while cross-link formation increases steadily. Therefore, carbon atom irradiation was confirmed as an advantageous way for creating strong cross-linked CNT bundles, while keeping the number of vacancies to a minimum.

Sinnott et al., 2008 [46] used molecular dynamics to perform ionic bombardment and pullout MD simulations for polymer-CNT composites. The REBO (reactive empirical bond order) potential was used for short range forces and the LJ (Lennard Jones) potential was used for long range forces between atoms as used in the other studies performed by Sinnott et al., [31] [59] [15] [46]. Three different Polystyrene-CNT composite systems were tested: a PS-SWCNT composite, a PS-DWCNT composite and a composite with a bundle of 4 SWCNTs in a PS matrix. The SWCNTs tested had a (10,10) configuration and the DWCNTs tested had a (10,10), (5,5) configuration. Two distinct simulation phases were performed in this study: Firstly ionic bombardment MD simulations and then pullout MD simulations. The MD simulation for ionic bombardment was carried out as follows: the structures were bombarded with argon atoms which were fired at the structures in beams of 100 atoms, with incident velocities equivalent to 80 eV per atom. The first atom was placed 100 nm from the composite surface. Two separate analyses were then carried out on the irradiated structures. Firstly the structures were examined for sp and sp³ chemical bonding. The structures were then analysed for trapped argon atoms. The results of the first analysis showed that after irradiation, the SWCNT had more sp hybridized atoms than the SWCNT bundle and DWCNT composites. It was found that the DWCNT composite displayed more sp³ bonds than both the SWCNT and

SWCNT bundle composites. The results of the second analysis demonstrated that the SWCNT composite had more trapped atoms than both of the other two composites. Pullout MD simulations were then performed in order to test the mechanical properties of the three irradiated composite systems. The results of the simulations showed that ionic bombardment of PS-CNT composite systems resulted in improved mechanical properties. It was also shown that for the DWCNT case, higher pullout loads were observed due to more sp^3 bonds formed between the walls of the DWCNT and the polystyrene matrix.

Comparing Sinnott et al., 2003 [59] and Sinnott et al., 2008 [46], both simulated ionic bombardment of CNT-polystyrene composites. Sinnott et al., 2003 [59] found that, for the irradiated system, as you increase the distance between the polystyrene matrix surface and the CNT, the number of sp^3 bonds formed between the matrix and the CNT decreases. Sinnott et al., 2008 [46] established that an irradiated DWCNT-polystyrene composite contains more sp^3 bonds between the CNT and matrix when compared with both the SWCNT-polystyrene and the SWCNT bundle-polystyrene composite systems. Therefore, based on the results of these two studies, the irradiated CNT-polystyrene composite should have a minimum distance between the polystyrene surface and the CNT, and should contain individual spaced DWCNTs, which are not arranged in bundles for optimum mechanical properties.

Pavia et al., 2011 [13] used molecular dynamics pullout simulations to examine how interstitial bonding between a MWCNT and matrix directly effects interfacial sliding/friction in CNT/diamond matrix composites. MD calculations were processed using the modified REBO potential which was the preferred potential for pullout simulations where interstitial bonding exists since bond forming and breaking are both modelled correctly. Results showed that the total friction force is directly proportional to the number of interstitial carbon atoms along the MWCNT/diamond matrix interface. Frictional stresses for numerous interstitials along the interface reach several GPa, therefore small densities of interstitials (likely to be observed after CVD processes) can increase frictional sliding stresses by a few GPa. In conclusion, control of interstitial carbon density through material processing (atmosphere control during CVD and

tailoring of CNT geometry) will allow for engineering of nanoceramic composites with a high level of strength, hardness, damage tolerance and toughness.

2.7 Summary

In conclusion, this literature review examines studies performed on, (i) the chemistry of interatomic bonding and geometric properties of CNTs, (ii) the synthesis of CNTs, (iii) molecular dynamics modelling techniques for CNTs, (iv) load transfer between SWCNTs in bundles and between walls of MWCNTs and (v) irradiation of SWCNT bundles and MWCNTs.

The main conclusions are:

- i. CNTs (discovered by Iijima et al, 1991 [1]) have unique mechanical properties due to strong sp^2 bonding between carbon atoms which is similar to that found in graphene.
- ii. There are currently three methods used to produce CNTs, (i) Arc discharge, (ii) Laser ablation and (iii) CVD as shown in Thostenson et al., 2001 [56], with CVD being the cheapest method. CNTs produced using CVD generally exhibit more defects but as shown by Peng et al., 2008 [14] can display improved mechanical properties due to cross-linking between walls caused during the CVD process.
- iii. There are numerous methods used to model CNTs. Quantum mechanics simulations are more accurate than MD simulations but are highly computationally intensive. Thus, molecular dynamics is usually employed instead of quantum mechanics for modelling the behaviour of CNTs. The finite element method has been used but requires considerable tuning, being further removed from the reality of the system.
- iv. On the subject of load transfer between SWCNTs in bundles and between walls of MWCNTs, [24, 26] observed a maximum pullout force ranging

between 0.04 nN to 1.4 nN for load transfer between (5, 5) and (75, 75) pristine SWCNT bundles. A maximum shear stress of 0.021 GPa was recorded. Salvetat et al., [28] obtained a SWCNT bundle shear modulus of 1 GPa. For pristine MWCNT load transfer, the experimental study by Akita and Nakayama, 2003 [61] found for a core diameter of 5 nm, the pullout force was estimated at 3-5 nN. This result coincided with that obtained by Curtin et al., 2004 [63] showing that for a DWCNT with an inner CNT diameter ranging from 0 – 6 nm, the pullout force varied between 0 and 5 nN. Thus, we see pullout forces ranging from 0.14 to 5 nN for pullout of pristine (defect-free) CNTs in the literature, though this value obviously depends on the length of the CNTs.

- v. Finally, for SWCNT bundle and MWCNT irradiation, literature was examined for irradiation with different particles. For electron irradiation, the studies by Kis et al., 2004 [18], Charlier et al., 2000 [32], Peng et al., 2008 [14], and Sinnott et al., 2006 [15], showed how inter-tube and inter-wall cross-links for SWCNT bundles and MWCNTs were always evenly distributed for low energies and optimal load transfer was achieved for just a few cross-links. A threshold energy existed above which the CNT structure became amorphous. For the studies performed by Krasheninnikov et al., 2002 [30], Sinnott et al., 2006 [15], Sinnott et al., 2003 [59] and Sinnott et al., 2000 [31], for argon, CF_3 , C_3F_5^+ and CH_3 ion irradiation, it was observed that irradiating with particles resulted in cross-links forming at different layers depending on the irradiation energy. Carbon-carbon bonds formed by carbon atom recoil due to particle irradiation. For carbon ion irradiation, Sun et al., 2005 [33], Jager et al., 2000 [34], Federizzi et al., 2006 [17] and Pavia et al., 2011 [13], found that for high energy irradiation, the CNT structure became amorphous, causing CNTs to coalesce. For low energy irradiation, an amorphous layer formed at the top of the CNT and cross-links were analyzed. Results showed that the total friction force is directly proportional to the number of interstitial carbon atoms along the CNT bundle or MWCNT/diamond matrix interface.

The work performed for the present study builds on research examined in this literature review. The gap in the literature which this study aimed to fill was to provide a more complete and systematic study of the effects of irradiation on CNT bundles than has been performed to date, with a particular focus on potential improvements in mechanical properties of bundles via cross-link formation and the delicate balance to be struck with decreases in properties of individual CNTs through defect formation. The work involved using a new modified potential which models both bond breaking and forming simultaneously, analysing C ion irradiation which only a few authors have considered before, fully characterising the nature of the defects and cross-links formed, studying quite large bundles in comparison to previous work (up to 19 CNT bundles), and quantifying the linkage between energy and dosage of irradiation and final mechanical properties.

Chapter 3 Simulation Methodology

3.1 Introduction

This chapter describes the methodology used to perform the simulations for this thesis. As outlined in chapter 1, the simulations performed were of three types:

- Simulations of the irradiation process itself, the output of which is the inter-tube bonds and defects formed for varying energy and dosage.
- Tensile testing of the resulting irradiated bundles, to determine the loss in strength due to defects formed.
- Pull-out tests, in which the one tube is pulled from the irradiated bundle, to examine the gains made in inter-tube shear stiffness and strength, and energy absorbed during pullout, which is related to composite toughness.

Regarding the irradiation simulations, these can be sub-divided into simulations of single atom impacts, and multi-atom impacts. The single atom impact simulations were performed to investigate the multi-atom irradiation approach, and examine the effects of a single impact at varying energy and angle. The chapter begins by describing the interatomic potential used in all the simulations, and then gives details on the modelling parameters for each of the above types of simulations in turn.

3.2 Interatomic Potential

For realistic molecular dynamics (MD) simulations of the irradiation process and subsequent tensile and pull-out tests, accurate inter-atomic potentials, capable of representing bond breaking and forming, are required. When modelling CNTs using molecular dynamics, equations are defined for the interactions between carbon atoms

within the CNT. These equations describe the potential energy of the interactions, the derivative of which gives the forces between atoms. For this study, the two main potentials used are the Brenner potential [8,25] for short-range covalent bonds and the Lennard Jones potential for long range van der Waals forces. The Brenner potential was first described in Brenner et al., 1990 [8] and then modified in Brenner et al., 2002 [25], where it was named the REBO (Reactive Empirical Bond Order) potential. The Brenner potential is referred to as a ‘many body’ potential, because the force between any two individual atoms depends not only on the positions of those two atoms but also the positions of other neighbouring atoms. It intrinsically takes into account changes in bond-angles as well as bond stretching. Figure 3-1 illustrates the chemical bonds described using the Brenner potential and the Lennard Jones potential.

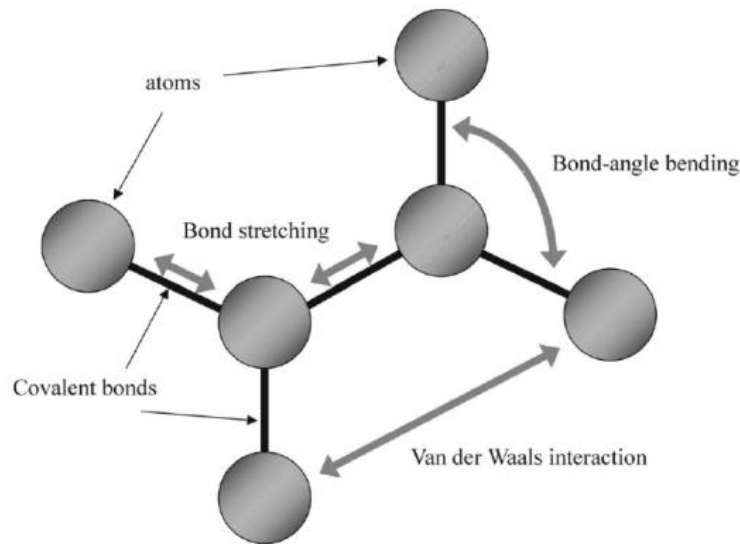


Figure 3-1: The covalent and van der Waals bonds in the CNT lattice which are described by the Brenner and Lennard Jones potential respectively (reproduced from Odegard et al., 2004 [60]).

Since the Brenner potential is used extensively in this study, it is described now in some detail. The original potential [8] is described, since the revised REBO potential [25], is conceptually very similar.

The potential energy of the bond between atoms i and j is:

$$V_{ij} = V_R(r_{ij}) - \bar{B}_{ij} V_A(r_{ij}) \quad 3-1$$

where r_{ij} is the distance between atoms i and j , V_R and V_A are the potential energy for the repulsive and attractive interactions respectively between atoms i and j , and \bar{B}_{ij} is an added term which accounts for changes in potential energy due to variations in bond angle. V_R and V_A are described by the following two equations;

$$V_R(r_{ij}) = f_{ij} \frac{D_e}{S_{ij} - 1} e^{-\sqrt{2S_{ij}}\beta_{ij}(r_{ij} - R_e)} \quad 3-2$$

$$V_A(r_{ij}) = f_{ij} \frac{D_e S_{ij}}{S_{ij} - 1} e^{-\sqrt{\frac{2}{S_{ij}}}\beta_{ij}(r_{ij} - R_e)} \quad 3-3$$

where D_e is the potential well depth. f_{ij} is a smooth, continuous cut-off function which reduces to zero when r_{ij} becomes greater than 2 \AA , according to:

$$f_{ij} = \begin{cases} 1 & \text{if } r_{ij} < 1.7 \text{ \AA} \\ \frac{1}{2} \left[1 + \cos \left[\frac{\pi(r_{ij} - 1.7)}{2 - 1.7} \right] \right] & \text{if } 1.7 \text{ \AA} < r_{ij} < 2 \text{ \AA} \\ 0 & \text{if } r_{ij} > 2 \text{ \AA} \end{cases} \quad 3-4$$

This ensures that the potential effectively only operates over nearest neighbours of each atom. The force between atoms is determined from the rate of change of the potential energy with respect to displacement. More specifically, the force on atom i is the negative of the rate of change of the system's potential energy with respect to a movement of atom i , i.e.

$$F_i = -\frac{\partial V_{SYS}}{\partial r_i} \quad 3-5$$

or in three dimensional cartesian coordinates:

$$\vec{F}_i = -grad(V_{SYS}) = -\left[\frac{\partial V_{SYS}}{\partial x_i} \hat{\mathbf{i}} + \frac{\partial V_{SYS}}{\partial y_i} \hat{\mathbf{j}} + \frac{\partial V_{SYS}}{\partial z_i} \hat{\mathbf{k}} \right] \quad 3-6$$

In a CNT, this equation accounts for the change of potential energy in the bonds between atom i and the three atoms bonded to atom i , due to a movement of atom i . It also takes into account any change of potential energy in bonds between atoms which are not bonded to atom i , due to the movement of atom i . To see how this can arise, figure 3-2 illustrates the bond lengths and angles considered when calculating the potential energies of the bonds between atom i and atoms it is bonded to, while figure 3-3 shows a bond angle which contributes to the potential energy of bond jk_4 and a bond angle which contributes to the potential energy of bond jk_3 . It can be seen that a movement of atom i will affect both of these angles and therefore the potential energy of both these bonds, even though i is not part of either bond. For this reason, the Brenner potential is referred to as a ‘many body’ potential.

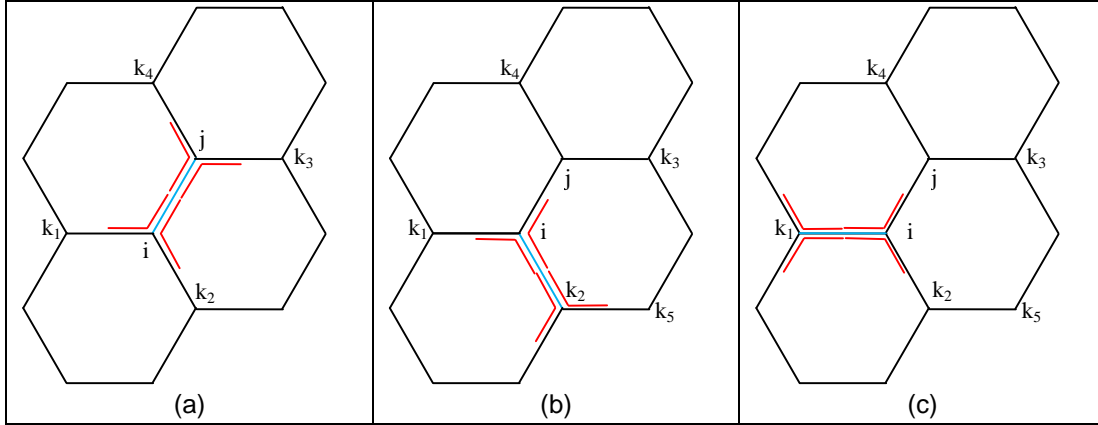


Figure 3-2: Bond lengths and angles considered for the potential energy in the bonds connected to atom *i* using the Brenner potential

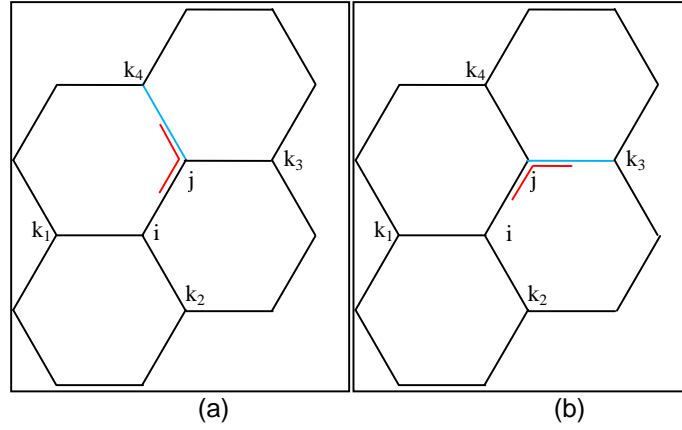


Figure 3-3: One of the bond angles considered in calculating the potential energy of (a) bond *jk*₄ (b) bond *jk*₃ which is affected by movement of atom *i*

After some manipulation the total force on atom *i* can finally be written as:

$$F_{i_x} = - \sum_{j \neq i} \frac{\partial V_{ij}}{\partial x_i} - \sum_{j \neq i} \sum_{k (\neq i, j)} \frac{\partial V_{jk}}{\partial x_i}$$

3-7

This is the equation that must be evaluated at each time step from consideration of the atom positions, and then integrated to find the velocities and displacements at the next time step.

The Brenner potential, like most potentials, was developed for bonded interactions, and not for bond breaking or forming. Molecular mechanics calculations of C–C bond breaking using the REBO potential [25] show inappropriate fracture mechanisms and grossly overestimate the breaking stress, as compared with values predicted by quantum mechanics calculations [35, 37-39]. The inaccuracy stems from the functional form for the above-mentioned cut-off function that greatly increases the bond force for distances between 0.17 and 0.20 nm [25] (it causes a sharp drop-off of the potential energy, hence a spike in the derivative of the potential energy, which is of course the force). For studies only concerned with bond breaking some authors have avoided the non-physical fracture mechanisms by removing the cut-off function [10, 38, 41], which however then leads to an underestimate of the stresses for bond breaking relative to quantum mechanics calculations [10, 12, 37-39, 42] and, moreover, precludes a consideration of bond formation. Since both bond breaking and bond forming are critical to the present study, it was decided to use a modified REBO potential recently presented in [43], where a local environment-dependent cut-off function based on screening concepts [35] allows a bond between two atoms to persist over long distances provided that no third atom moves into the bonding region. This leads to smooth changes in forces and a much better description of bond breaking and reforming compared with first principles calculations.

The public domain parallelized program LAMMPS [48] was used for all simulations in this thesis. The modified REBO potential [43] was incorporated into the LAMMPS program by Dr. Fabio Pavia, a member of Prof. Curtin's group at EPFL, by altering the C++ computer code in the sub-routines `pair airebo.cpp` and `pair airebo.h`.

3.3 Irradiation Simulations:

The irradiation simulations in this thesis mimic the pulsed laser deposition process [36, 44] which produced both C⁺ ions and neutral carbon atoms (as well as slower C₂ and C₃ molecules). Since classical MD does not include charge effects or

electron excitation, this study is constrained, like previous authors [15, 17, 22, 30, 45, 46], to only treating the incident particles as neutral carbon atoms. While it is recognized that particle charge will affect the chemical reactions that occur, it is expected that MD simulation can provide results on the degree of cross-linking and damage that occurs which are qualitatively correct and useful for comparing different irradiation strategies. The simulations performed in this study consider nuclear stopping only, ignoring electron stopping, which is justified based on the low energies involved in this study [17, 47].

3.3.1 Geometry

The irradiated bundles comprised seven or nineteen hexagonally arranged (26,0) SWCNTs (see Figure 3-4 (a)). Each tube had radius 10.18 Å, length 59.6 Å, contained 1456 carbon atoms and was initially defect-free. Periodic boundary conditions (PBCs) were applied in the z direction to simulate an ‘infinitely’ long bundle.

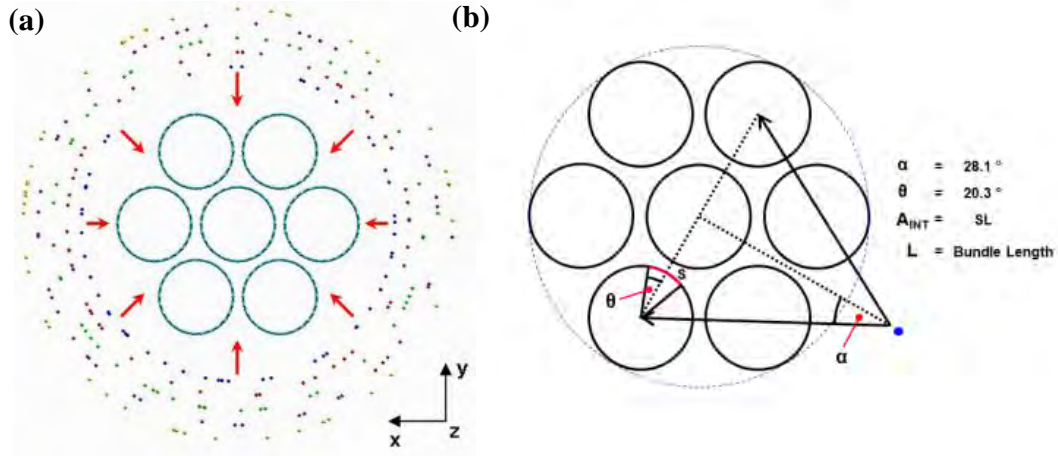


Figure 3-4: (a) Hexagonally arranged 7-tube (26 0) SWCNT bundle model with five “rings” of deposition atoms; the atoms in each ring are distributed randomly in the axial and circumferential directions (b) random deposition atom trajectory parameters and reference area A_{INT} used to determine the number of bonds per area at each interface; the curve segment S is defined to include all atoms in the outer CNT which are within the interaction distance of centre CNT, for the potential function used.

3.3.2 Single-atom Irradiation Simulation Parameters

To validate the irradiation simulation method for multi-atom irradiation of 7 CNT bundle, and investigate the influence of incident energy and trajectory on the formation of defects and inter-tube bonds, single atoms were fired at a defect-free, 7-tube CNT bundle (figure 3-5). Three separate cases were analysed: (a) “**direct impact**”, where the trajectory was normal to one of the outer CNTs and the incoming atom was directly aimed at a CNT atom, (b) “**penetrating impact**”, where the trajectory was normal to one of the outer CNTs but the deposited atom was aimed at the middle of a C6 hexagon on the outer surface of the CNT bundle and (c) “**oblique impact**”, where the deposited atom was given a trajectory 20° off-normal.

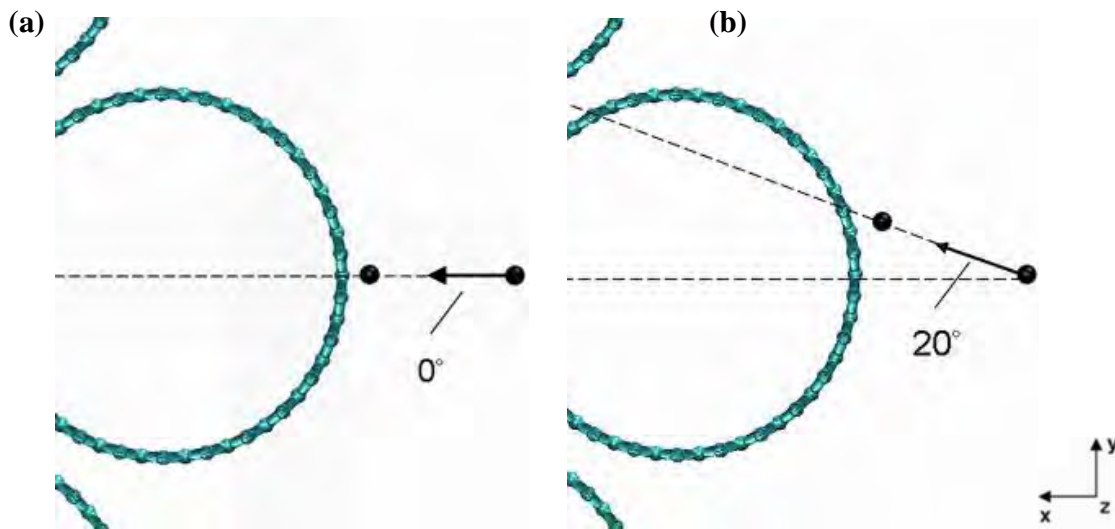


Figure 3-5: Snapshots of incoming atom (black) with incident energy of 21.9 eV directly colliding with a CNT atom (a) 0° impact (b) oblique impact

3.3.3 Multi-atom Irradiation Simulation Parameters

A number of ‘‘rings’’ (in most cases five) of 50 carbon atoms each in the 7-tube case (85 each for the 19-tube case to maintain the same fluence, see below), were initially placed around the CNT bundle, as shown in Figure 3-4 (a). A gap of 4 Å between each ring, and between each atom within each ring, was ensured to avoid initial interactions. Within these constraints, the atoms in each ring were distributed randomly, circumferentially and also along the length of the bundle.

Random incident trajectories within the angle $\pm 28^\circ$, illustrated in figure 3-4 (b) for the 7-tube case, were assigned to each irradiation atom. The strategy behind such a wide angle is to produce inter-tube links which connect the CNTs not just radially, but also circumferentially, which is desirable from the viewpoint of bundle mechanical properties. The irradiation strategy simulated is somewhat idealised, but should be achievable through modification of the pulsed laser deposition procedure used in [44]. In the 7-tube simulations the kinetic energy was the same for all incident atoms, and cases of 50, 100, 150, 200 and 300 eV/ion were examined. For the 19-tube simulations, variable energy strategies were considered in an attempt to achieve as uniform a level of cross-linking within the bundle as possible.

Throughout the irradiation simulations free boundary conditions were applied in the x and y directions. An initial relaxation phase of 3.125 ps was applied to equilibrate the bundle, while the rings of C atoms were held fixed. An NVE ensemble was used with velocity rescaling at 0.5 K, while the velocity Verlet algorithm was used to integrate the equations of motion with a time step of 0.25 fs. The innermost ring was then deposited without a thermostat so the energy of the impinging atoms was added to the CNT bundle. A time step of 0.0625 fs was used during irradiation which allowed the atomic interactions to be determined with sufficient accuracy for all irradiation energies. This was followed by a relaxation phase and a cooling phase. During the relaxation phase, the CNT bundle reached a new equilibrium state as evidenced by the levelling out of the potential energy. In the cooling phase, the bundle was cooled back down to 0.5 K, to

facilitate analysis of defects (as done in [23, 45]). This process was then repeated for the remaining rings.

The irradiation area for the CNT bundle was taken to be the circumference of the circle surrounding the bundle multiplied by the bundle height, which is $125 \times 10^{-14} \text{ cm}^2$ for the 7-tube bundle and $211 \times 10^{-14} \text{ cm}^2$ for the 19-tube bundle. For the majority of the simulations, five rings of atoms were deposited, so the fluence (particles per unit area) ranged from $4.0 \times 10^{13} \text{ cm}^{-2}$ for one ring, up to $2.0 \times 10^{14} \text{ cm}^{-2}$ for five rings; in a few cases extra rings (higher fluence) were considered to extrapolate observed trends, as will be outlined later. According to [45], for Ar ions at 1 keV energy, the number of coordination defect numbers (signifying all kinds of defects, including inter-tube links) increases with fluence up to around $2 \times 10^{14} \text{ cm}^{-2}$ and then levels off. The fluence values are at or below this level and would be classed as “low dosage” in [47]. “Dosage” is defined differently here though as the total incident energy – which is the energy/ion multiplied by the number of incident ions – divided by the mass of the CNT bundle. This differs from fluence in that the energy of the incident ions, not just their number, is accounted for. Apart from the few extra cases mentioned above, the dosages in this study ranged from 2 MGy (i.e. Mega-"Gray" which is a unit used for dosage, or J/kg) for one ring of 50 eV ions to 60 MGy for five rings of 300 eV ions. Any irradiation atoms that rebounded off the CNT bundle and strayed outside a set radius (65 \AA) of the CNT bundle were frozen in space to stop them from exiting and re-entering the periodic simulation box. This caused a small but negligible drop in the total system energy. For the 7-tube bundle, for all incident energies, five runs with varying initial random trajectories of the incident C atoms were performed in order to assess statistical variation. For the 19-tube bundle, due to the computational time required, only a small number of simulations were performed to evaluate strategies suggested by the 7-tube study.

3.4 Mechanical test simulations

3.4.1 Geometry

The mechanical properties of the pristine and irradiated SWCNT bundles were evaluated through MD simulations of “tensile” and “pull-out” tests involving drawing out of the centre CNT. The geometry and boundary conditions for each type of test are shown in Figure 3-6. The bundles tested were those for which one, three and five rings of atoms had been deposited, giving 15 tensile tests and 15 pull-out tests at each irradiation energy. As in the irradiation simulations, periodic boundary conditions were applied for both tests in order to simulate an ‘infinitely’ long bundle and to avoid end effects.

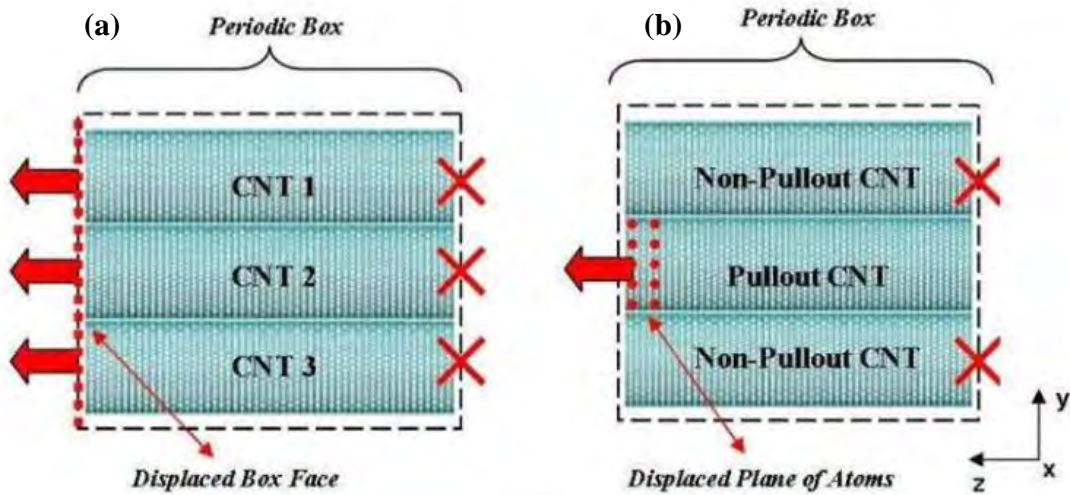


Figure 3-6: Diagrams of (a) pullout and (b) tensile tests for 7 CNT bundles.

3.4.2 Tensile and Pullout test Simulation Parameters

The MD time step was set to 0.25 fs and a velocity re-scaling thermostat was used to maintain the temperature of the CNT bundle models at 0.5 K throughout each test. During the initial relaxation phase which lasted 12.5 ps for the tensile test and 18.75 ps for the pull-out test, both ends of the CNT bundle were fixed in z and free to move in x

and y for both tests. After relaxation, the tensile and pullout tests were performed. An NVE microcanonical ensemble was used for the pull-out tests, whereas an NPT ensemble was used for the tension tests to allow the volume of the simulation box to vary as it is deformed in the z direction. For the tensile test, the top face of the periodic box was displaced 0.025 \AA in the z direction every 0.25 ps, while the bottom face was kept fixed in z, until the bundle failed. The applied stress was measured on the top face. For the pullout test, the bottom two rings of atoms for the outer CNTs were fixed in the z direction, and the centre CNT was drawn out by displacing its upper two rings of atoms 0.025 \AA every 0.25 ps, across the periodic box boundaries. The pull-out force was obtained as the force on these two rings of atoms. Relaxation was performed between displacements. For both test series, the displacement rate was 10 m/s and all CNTs were free to move in the x and y directions throughout.

Chapter 4 Nanostructure Evolution for Single Carbon Atom Irradiation

4.1 Introduction:

In this chapter results from impacts of a single Carbon atom on a 7-tube CNT bundle are presented. This work was carried out in order to validate the use of the modified REBO potential [43] for the problem outlined in this study, and to estimate the impact energies that would be suitable for the later multi-impact simulations. The chapter is divided into sections on "direct impact", where the trajectory was normal to one of the outer CNTs and the incoming atom was directly aimed at a CNT atom, "penetrating impact", where the trajectory was normal to one of the outer CNTs but the deposited atom was aimed at the middle of a C6 hexagon on the outer surface of the CNT bundle and "oblique impact", where the deposited atom was given a trajectory 20° off-normal. These three types of impact are illustrated in Figure 4-1, which supplements the information in Figure 3-5.

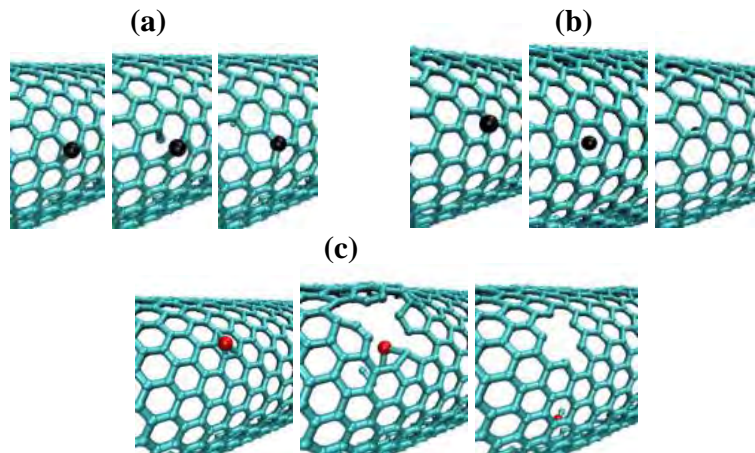


Figure 4-1 - Single C atom impacts, (a) direct impact sequence, (b) penetrating impact sequence, (c) oblique impact sequence for 200 eV case

4.2 Direct Impact

4.2.1 Threshold Kinetic Energy to Displace an Atom from the CNT (E_{th})

The first set of simulations on direct impact was aimed at identifying the threshold kinetic energy E_{th} that the irradiation atom needs to fully displace an atom from the CNT lattice. This value was found after several simulations to be $E_{th} = 21.9$ eV. At this energy, the displaced atom travels to the far wall of the impacted CNT and deposits there as an adatom, while the irradiation atom takes its place in the lattice (see Figure 4-1(a)). Unlike most solids, the open structure of nanotubes allows this type of large interstitial-vacancy Frenkel pair separation, so instant recombination does not necessarily occur [47]. To knock out an atom from the lattice, a displacement threshold energy T_d must be transferred to the atom [47]. For most types of irradiation ions, the energy of the impinging ion needs to be substantially larger than this, e.g. classical binary collision theory gives [47]:

$$E_{TH} = \frac{(m_c + m_l)^2}{4m_c m_l} T_D \quad 4-1$$

where m_l is the mass of the ion and m_C is the mass of the carbon atom. However from equation 4-1, when the impinging ion is carbon, $E_{th} = T_d$, i.e. complete energy transfer occurs, and the velocity of the ion after the impact is zero (regardless of the initial energy of the ion). In comparison, for Ar ions, $E_{th} = 1.4 T_d$ and for electrons $E_{th} = 5469 T_d$. The simulations confirm that for a direct impact, with energies ranging from 21.9 to 300 eV, no damage occurs at the impact site, and the impinging ion simply replaces the impacted ion in the lattice. Studies using molecular dynamics with the non-orthogonal density functional based tight binding (DFTB) force model [28, 48] give $T_d \sim 20$ eV for “dynamic” simulations (initial kinetic energy that needs to be given to a lattice atom for

it to escape the system) and $T_d \sim 13$ eV for “static” simulations (energy to create a vacancy and an adatom – i.e. a widely separated vacancy-interstitial Frenkel-pair – from a perfect CNT lattice) for zigzag CNTs with diameter 2 nm. According to [46] the true value lies between these values, probably closest to the dynamic value. Thus the value of $E_{th} = 21.9$ eV, being just above the dynamic DFTB value for T_d in [29, 49], is a very reasonable one, considering that binary collision theory is only an approximation so that E_{th} is likely to be somewhat above T_d .

4.2.2 Effects on CNT Bundle at Energies above E_{th}

Figure 4-2 – Figure 4-5 show the cascade collisions (for “direct impact”) for 50-200 eV. For 50 eV (Figure 4-2), the ejected atom in turn ejects an atom on the opposite side of the target CNT, which ends up as an interstitial atom, creating a bond between the target and centre CNTs. An impact energy of 100 eV (Figure 4-3) is sufficient to lead to an atom being ejected from the centre CNT, and the final situation is one bond with the centre CNT, and one deposited atom on a CNT far from the target CNT. The main difference on moving to 150 eV (Figure 4-4) is that atoms are ejected from both sides of the centre CNT. One inter-tube bond is formed, but not with the centre CNT. Finally, an impact at 200 eV leads to atoms punching through to the furthest CNT from the target CNT and two (quite complex) inter-tube bonds. Three-dimensional views in Figure 4-5 also show the minor damage created at this energy.

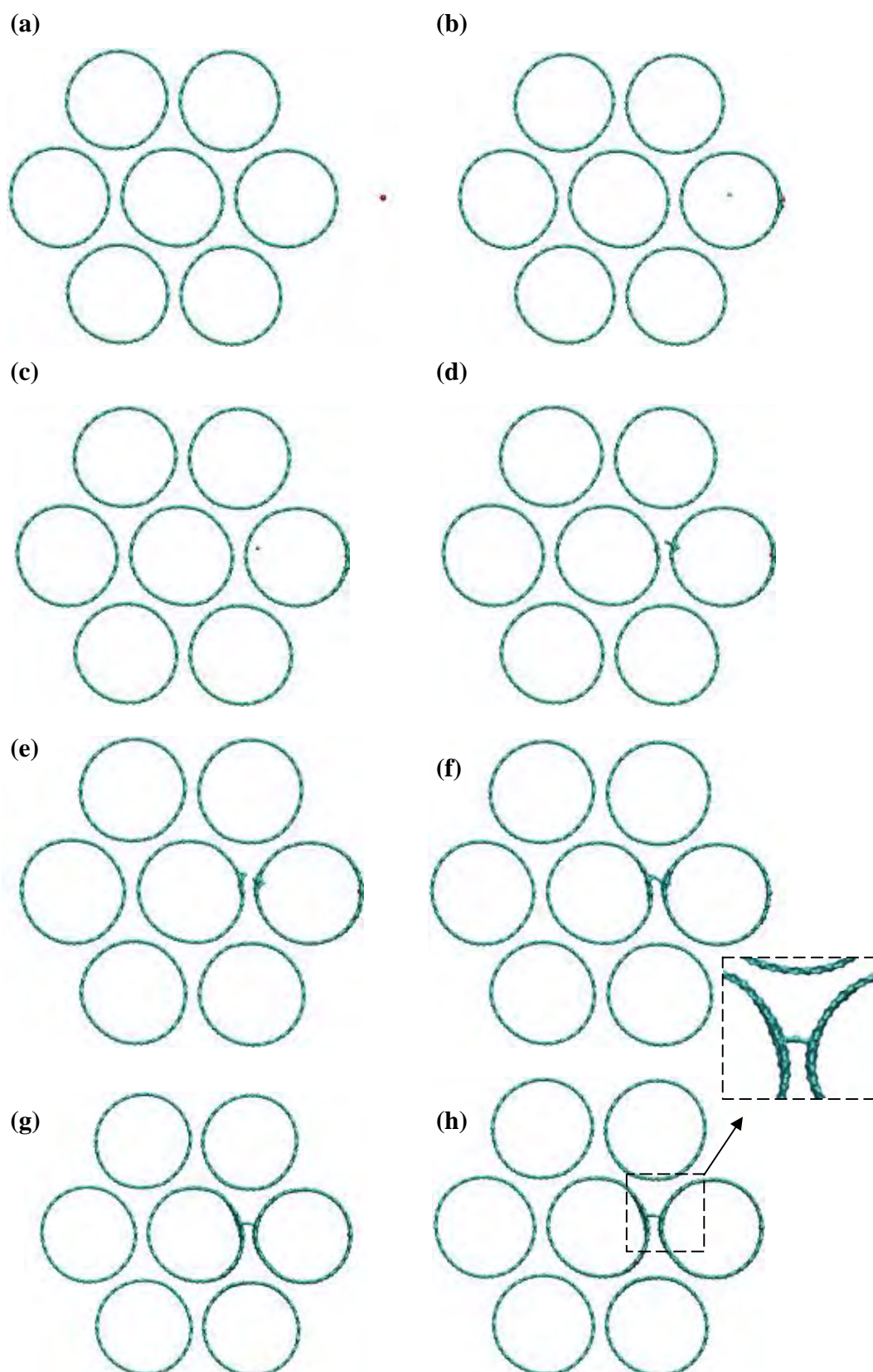


Figure 4-2: Snapshots in time for direct impact of atom with 50 eV incident energy

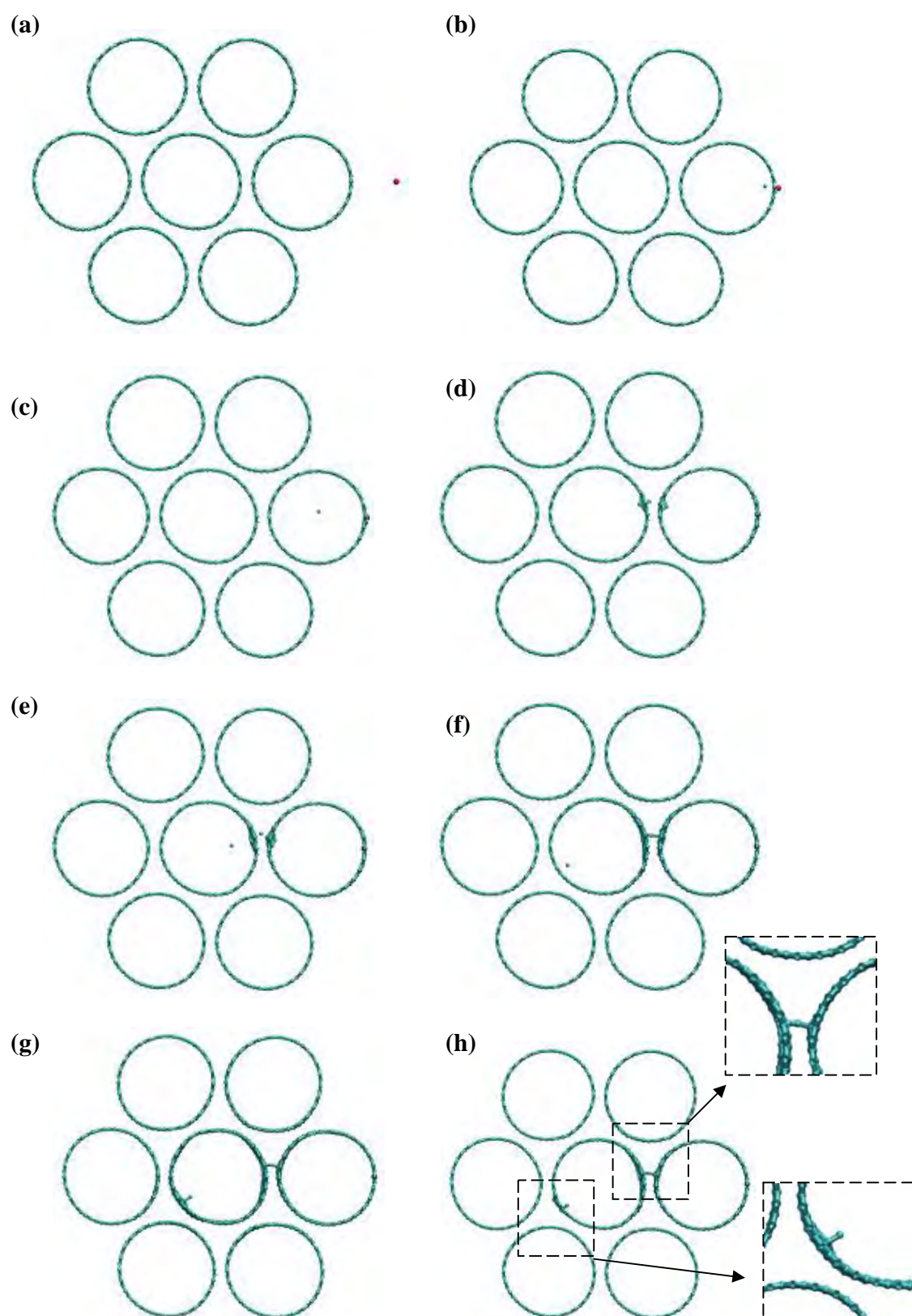


Figure 4-3: Snapshots in time for direct impact of atom with 100 eV incident energy

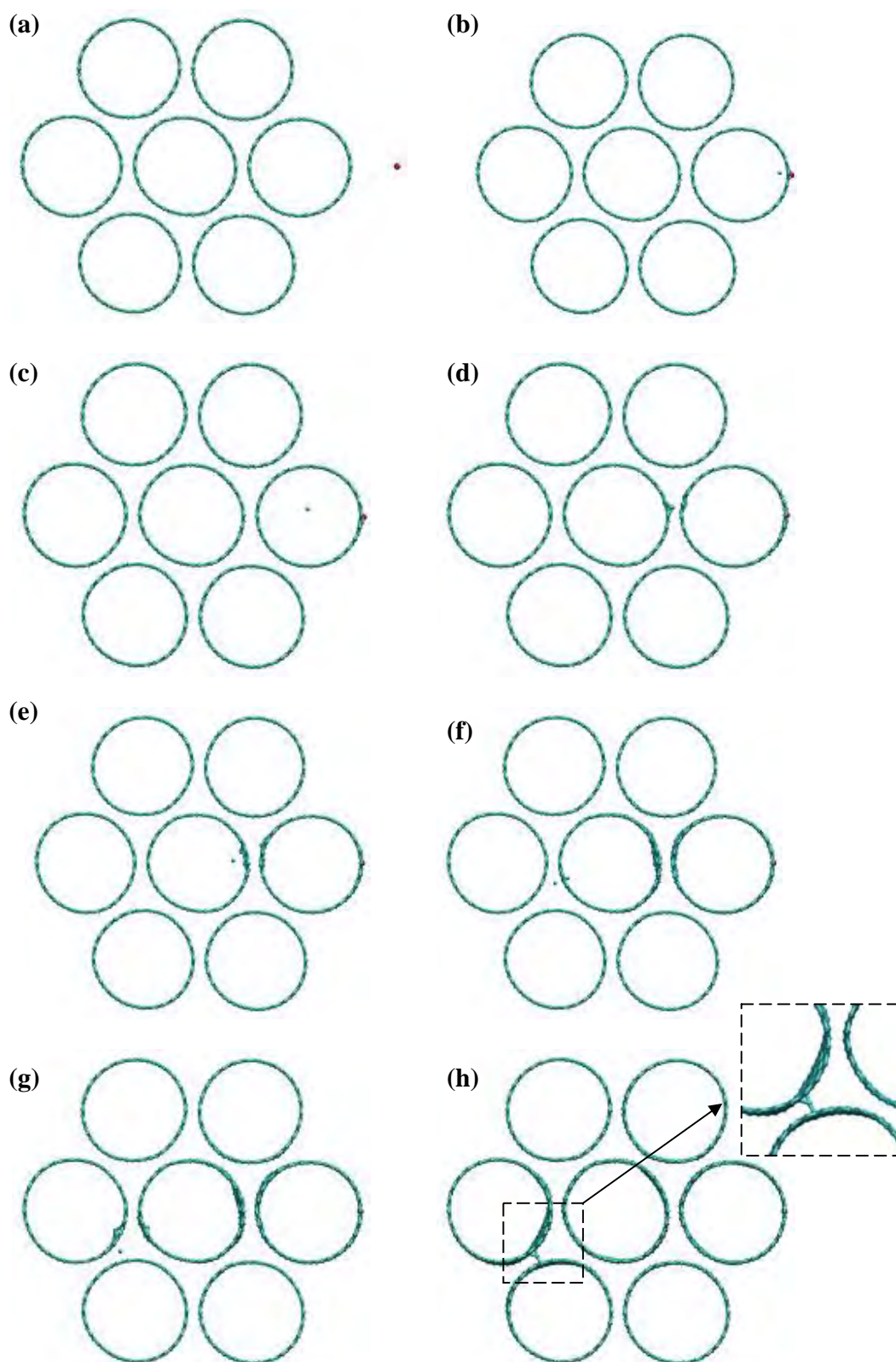


Figure 4-4: Snapshots in time for direct impact of atom with 150 eV incident energy

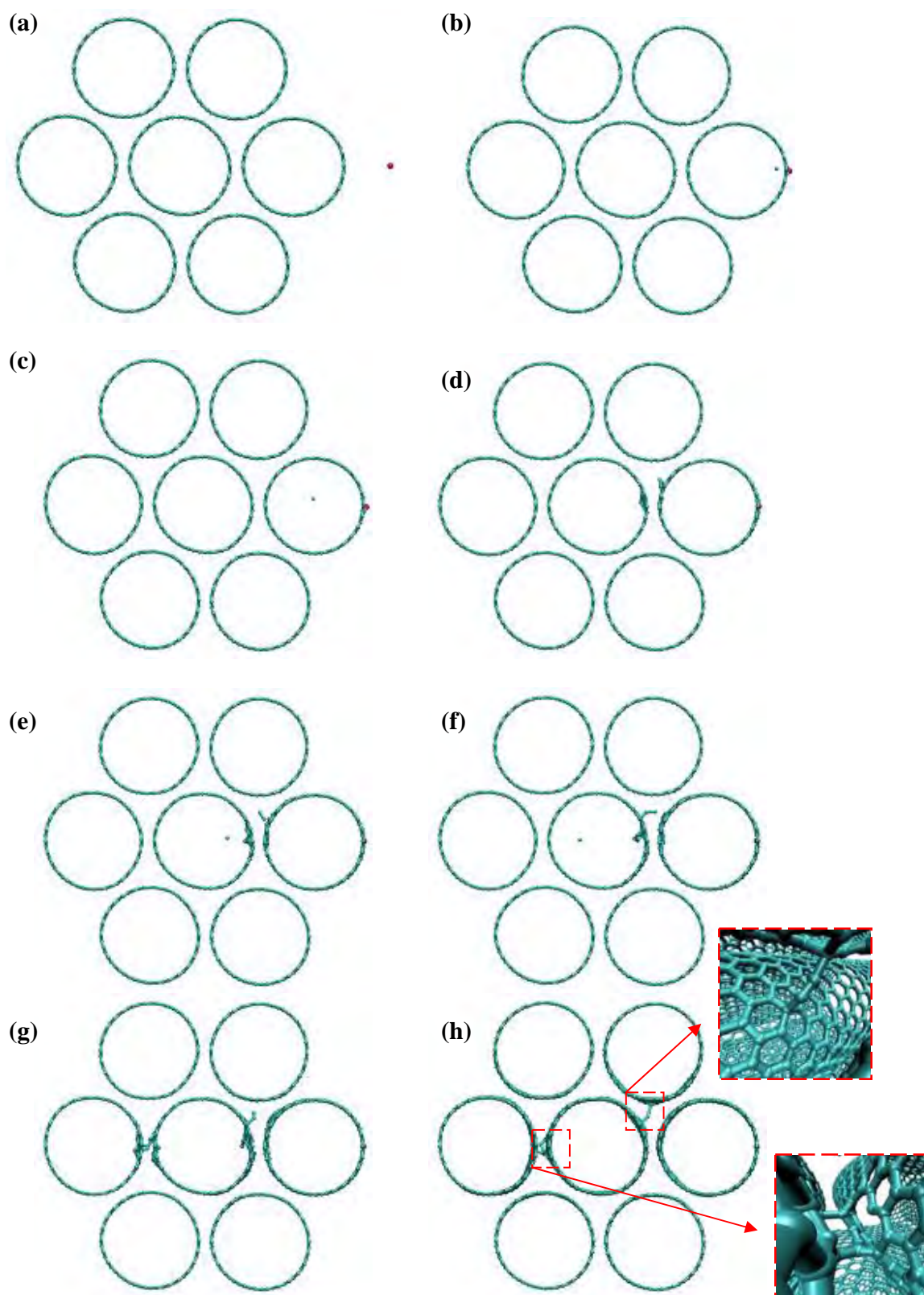


Figure 4-5: Snapshots in time for direct impact of atom with 200 eV incident energy eV

4.2.3 Energy Analysis for Direct Impact

An energy analysis was performed for the initial impact in the 50 eV, direct impact case, in which the kinetic energy of the impacting *and* ejected atom was recorded. Figure 4-6 shows the results (note the two y-axis scales, on the left for kinetic energy, on the right for potential and total system energy). Note that no thermostat was used in these simulations, so the total system energy remains constant. The initial potential energy of the system is set to an arbitrary datum of -50 eV, so the total initial system energy equals zero since the initial kinetic energy of the incoming atom is 50 eV, which is also approximately the initial kinetic energy of the system, since the CNT bundle is initially at rest apart from small vibrational fluctuations. Choosing this datum for the potential energy was purely for visualisation purposes in Figure 4-6.

From Figure 4-6, it can be observed that for the initial impact, the impacting atom loses all of its initial 50 eV, the ejected atom gains 37 eV of kinetic energy, the total system kinetic energy decreases by 6.5 eV and the total system potential energy increases by 6.5 eV. This indicates that 13 eV of kinetic energy is transferred to the CNT bundle for the first impact, which sets up vibrations in the bundle. The kinetic energy of the ejected atom was also checked by deducing its velocity from its position-time data, which confirmed it was 37 eV.

For the second impact (when the ejected atom collides with the target CNT's innermost wall), the kinetic energy of the ejected atom drops to zero which demonstrates that the atom has bonded to the CNT wall. This ejected atom has sufficient energy to displace an atom from the CNT wall and form an inter-tube bond (shown in Figure 4-2(h)).

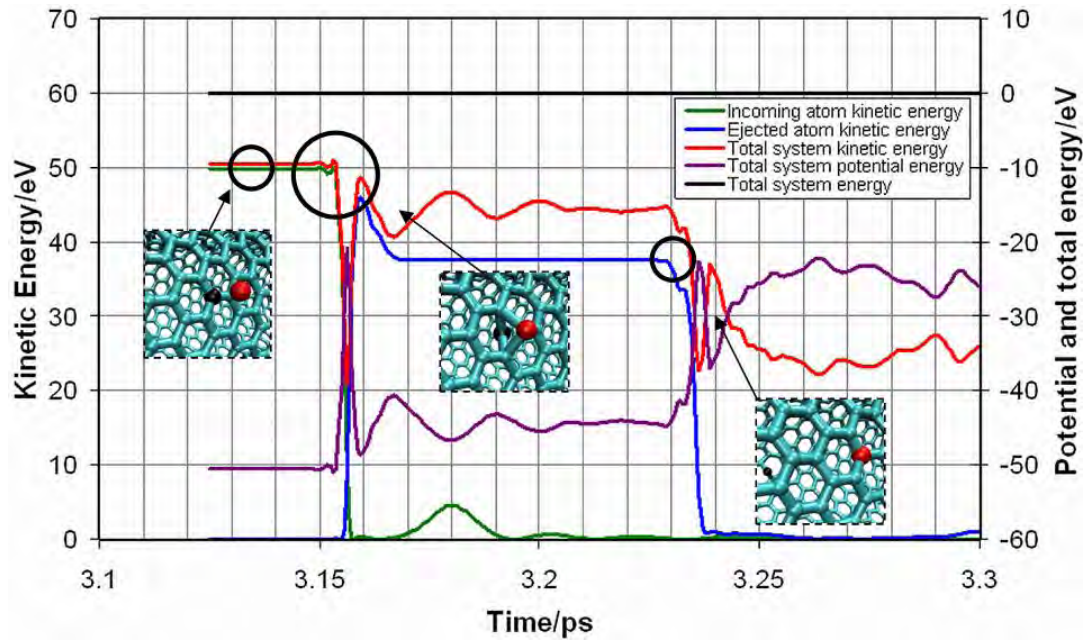


Figure 4-6: Time versus energy for direct impact of atom with 50 eV incident energy and snapshots of incoming and ejected atom's trajectory (Incoming atom = Red; Ejected atom = Black)

4.3 Penetrating Impact

4.3.1 Energy Analysis for Penetrating Impact

A “penetrating” impact was considered next, i.e. an irradiation atom aimed directly at the centre of a CNT hexagon, (shown in Figure 4-1(b)). The energy analysis is shown first in this section, as it helps to explain the effects on the CNT bundle to be presented next. Results are shown in Figure 4-7. The initial potential energy of the system is again set to an arbitrary datum of -50 eV, so the total initial system energy equals zero. The simulations indicate that the kinetic energy of the irradiation atom decreases when it gets within the interaction distance of the CNT atoms, attains a minimum as it passes through the hexagon and then increases slightly thereafter until it leaves the interaction region and continues on. The net energy loss after passing through varied from 22 eV for 50 eV initial energy to 16 eV for 300 eV initial energy. Unfortunately no results in the literature using more exact simulation techniques than MD could be found to verify whether these values are correct. Intuitively though they seem reasonable.

To explain the occurrence of a minimum, it is noted that while the irradiation atom interacts with the lattice atoms, their coordination number increases giving an equilibrium bond distance greater than 1.42 Å. To squeeze through the hexagon, the irradiation atom must pass within 1.42 Å of all the hexagon atoms, resulting in a repulsive force which gives the atom a kick once it passes through; hence the small recovery of kinetic energy. The energy lost by the irradiation atom is transferred to the lattice (11 eV of kinetic energy and 11 eV of potential energy), setting up vibrations and potentially forming defects, and has been termed “chemical erosion” in [23]; this process obviously does not occur for non-bonding ions like He, Ar, and Ne. This observation for non-direct impacts, combined with consideration of Eq. 4-1 for direct impacts, explains results in the literature wherein considerably higher irradiation energies (around 50 eV) were required to effect modification of the CNT lattice using noble gas ions such as Ar [15, 23, 30, 47, 50] than for the C ions studied here.

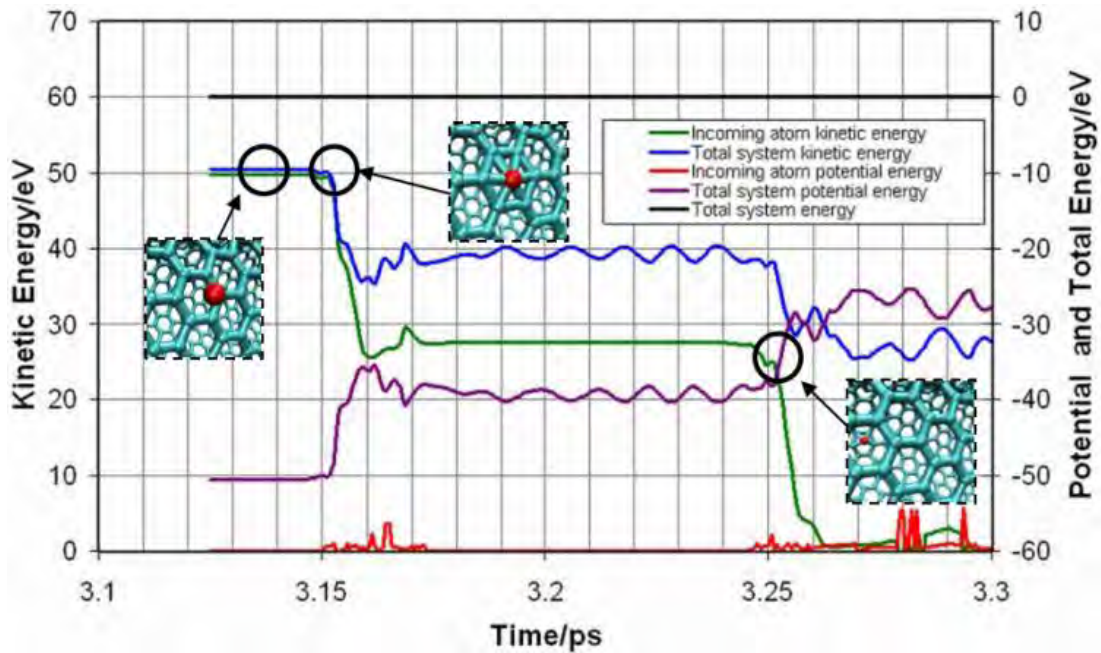


Figure 4-7: Time versus energy for atom penetrating C6 hexagon for CNT bundle (incoming atom energy = 50 eV) and snapshots of incoming atom's trajectory (Incoming atom = Red)

4.3.2 Effects on CNT Bundle at Energies of 50-200 eV

Figure 4-8 - Figure 4-11 show snapshots of inter-atomic collisions for a penetrating impact for energies ranging from 50-200 eV. For the 50 eV case (Figure 4-8), unlike the direct impact case (see above) an inter-tube bond is not formed. In the direct impact case, the ejected atom was found above in Section 4.2.3 to possess 37 eV of kinetic energy after impact, whereas for the penetrating case, the impacting atom was found in Section 4.3.1 to have only 28 eV kinetic energy after passing through the lattice. This penetrating atom has insufficient energy coming into the second collision to fully knock an atom out of the far wall of the target CNT (and hence no inter-tube bond is formed).

At an incident energy of 100 eV (Figure 4-9), the impact cascade again does not penetrate as far into the bundle as the direct impact case, and no atoms reach the far side of the centre CNT; one inter-tube bond with the centre CNT is formed. Remarkably the same is true for both 150 eV and 200 eV (Figure 4-10 and Figure 4-11 respectively) – no atoms reach the far side of the centre CNT and only one inter-tube bond is formed. Thus, it can be said that direct impacts lead to deeper penetration into the bundle and more inter-tube bonds than penetrating impacts. However, this must be said with caution since, as noted above, no results in the literature using more exact methods than the MD method were found for the penetrating impact case, so it cannot be said with certainty that the modified REBO potential is giving correct answers for that case.

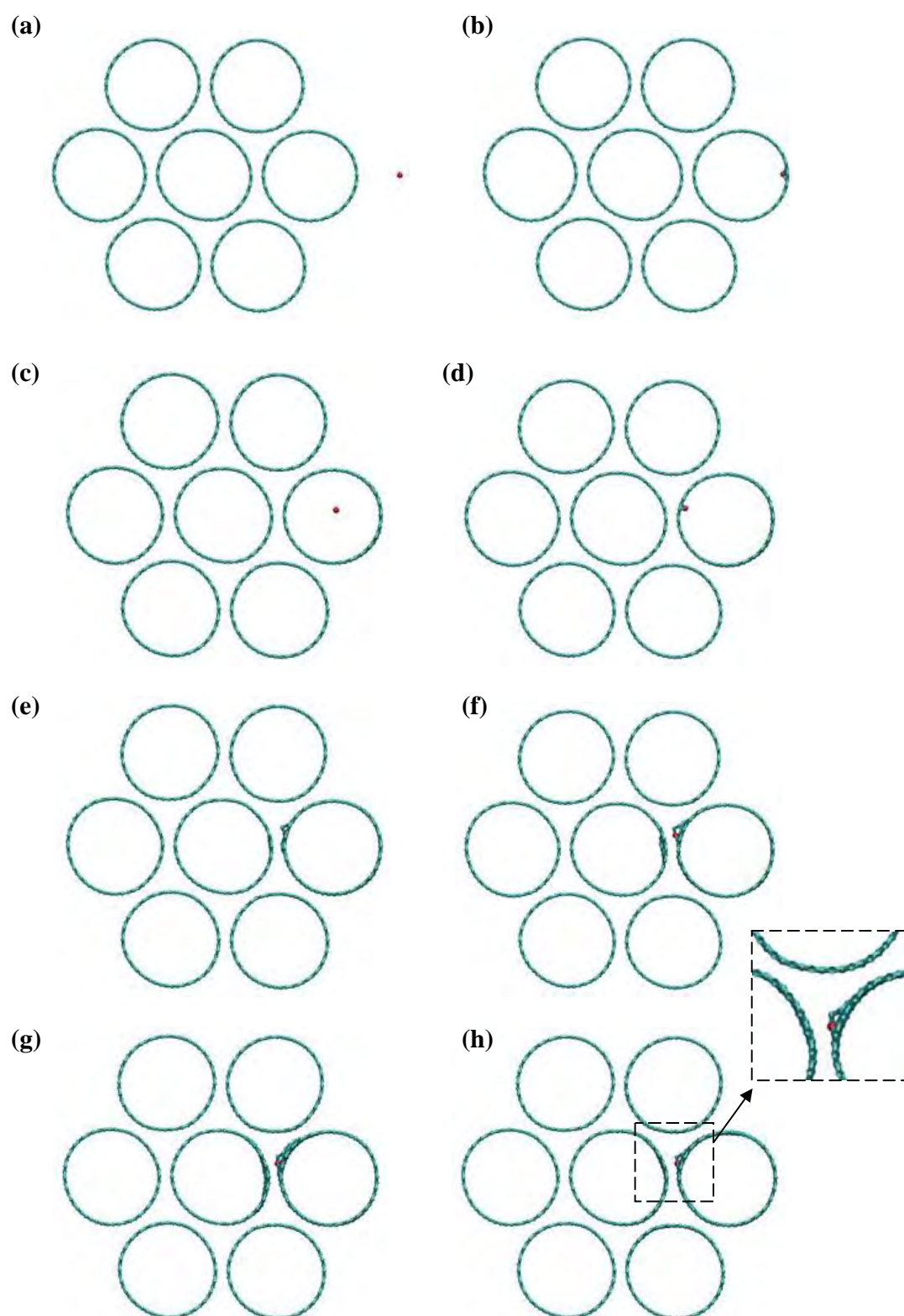


Figure 4-8: Snapshots in time for penetrating impact of atom with 50 eV incident energy

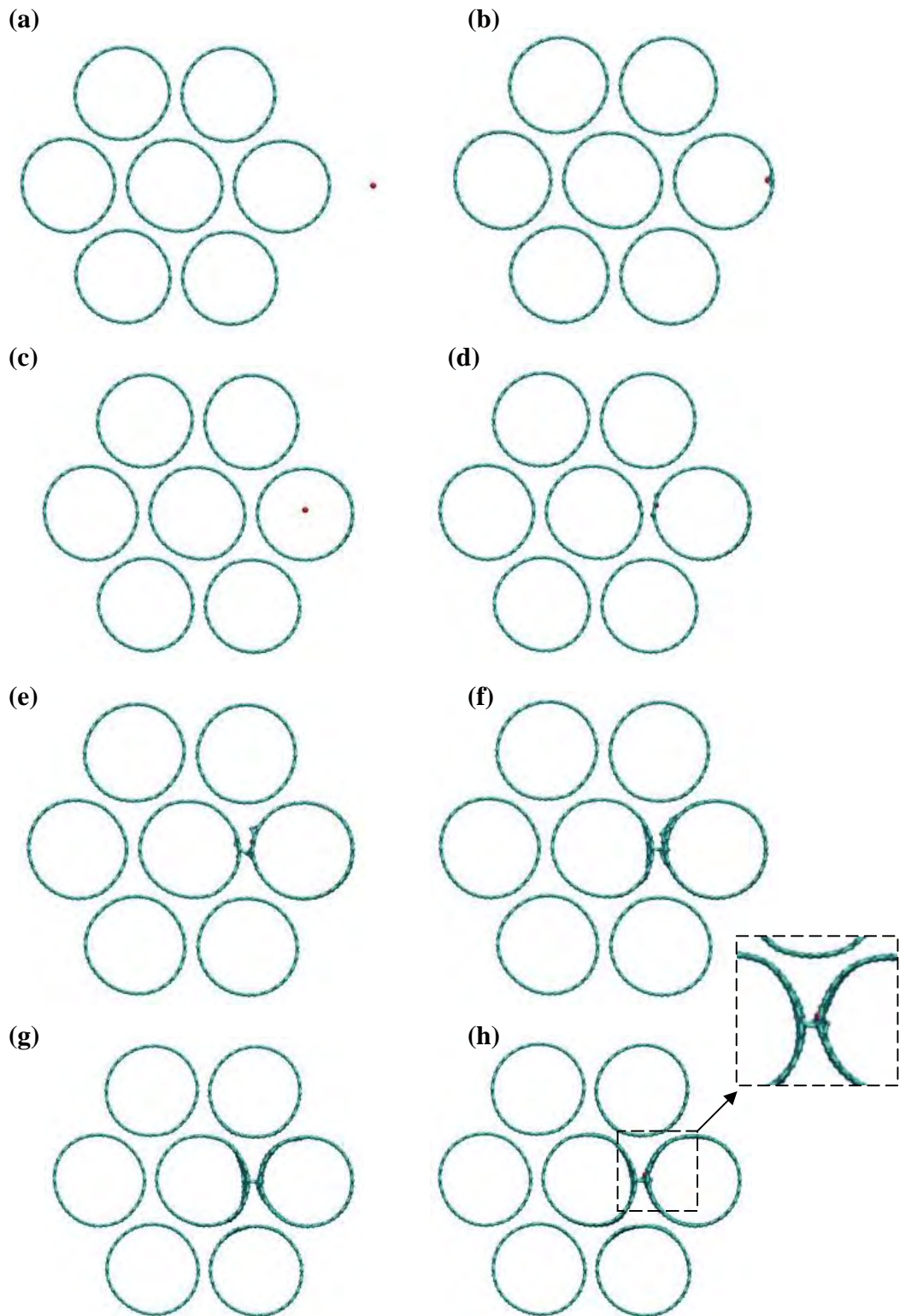


Figure 4-9: Snapshots in time for penetrating impact of atom with 100 eV incident energy

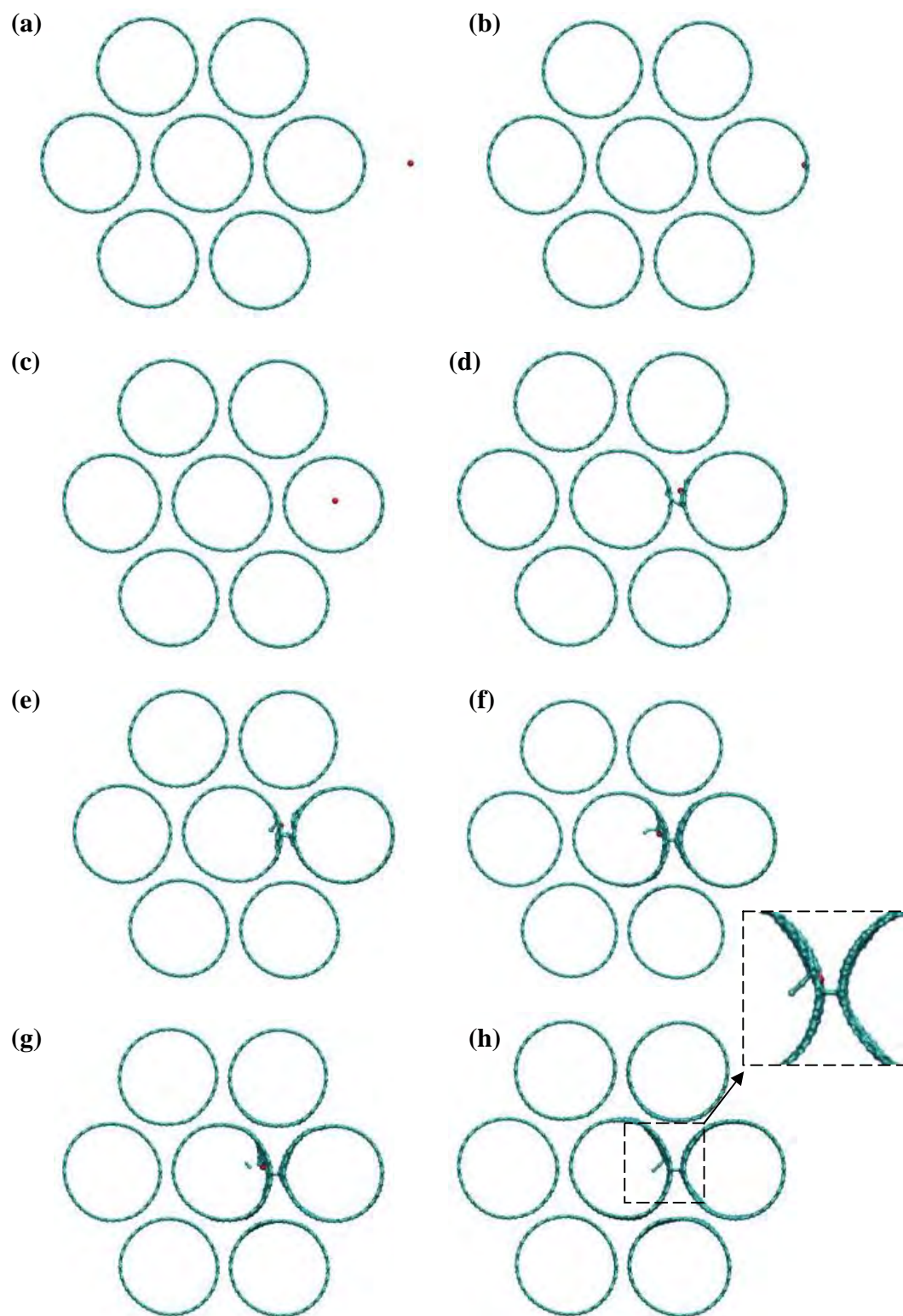


Figure 4-10: Snapshots in time for penetrating impact of atom with 150 eV incident energy

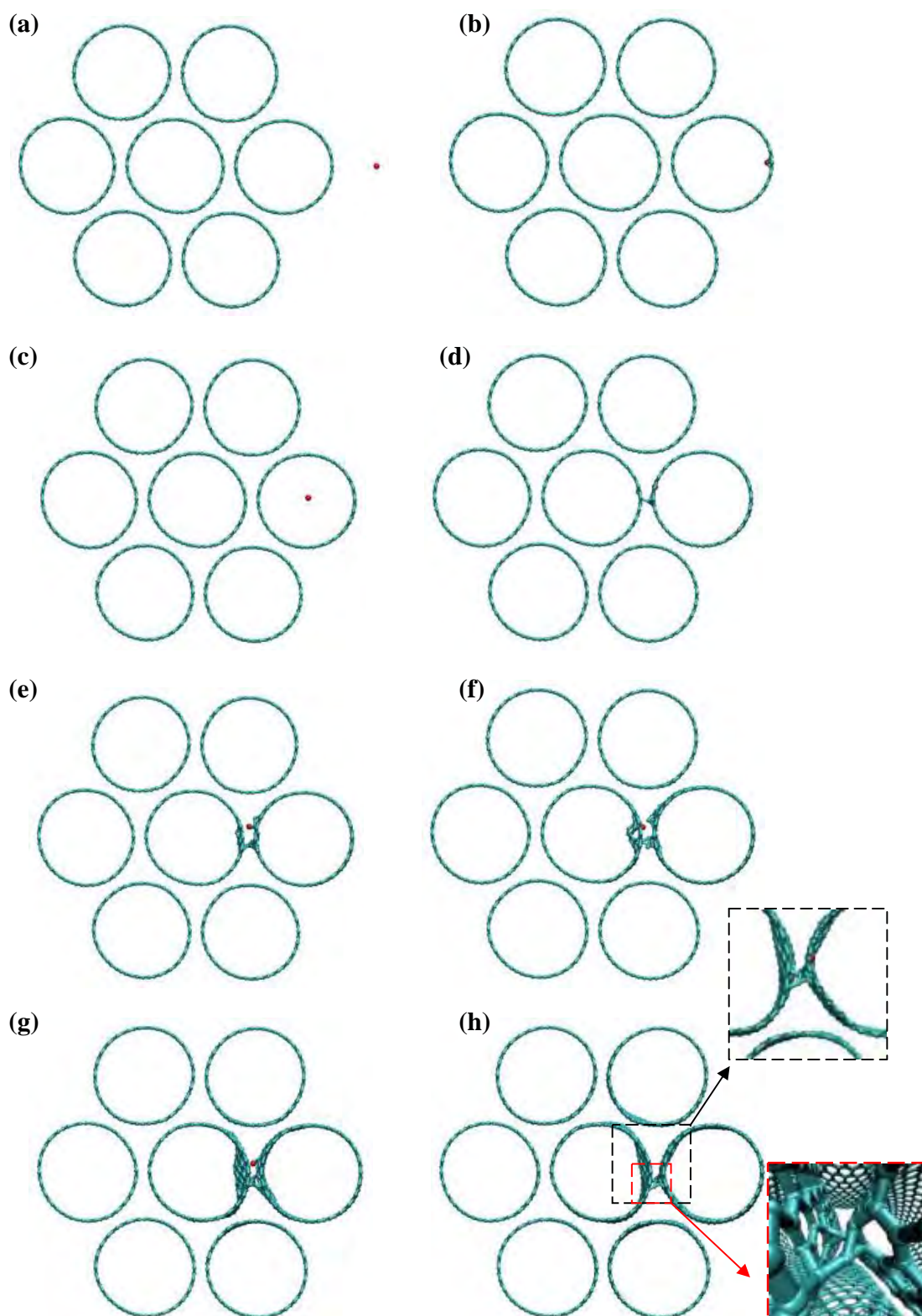


Figure 4-11: Snapshots in time for penetrating impact of atom with 200 eV incident energy

4.4 Oblique Impact

The final single atom impact considered is an oblique impact, 20° from the normal direction, (Figure 4-1 (c)). Figures 4-12 – Figure 4-15 show the results for energies between 50 and 200 eV. This time the behaviour at first impact changes with energy, so separate plots of this initial impact event at each energy are shown. For these oblique impacts, significant damage initially occurs at the impact site, in keeping with [47] which stated that multi-vacancies normally appear for tangential hits. However, the unique ability of CNTs to “self-heal” themselves [47] by saturating dangling bonds is clearly visible as the simulations progress in Figures 4-12 – Figure 4-15, and is certainly an advantageous feature for the overall goals of this work.

At 50 eV (Figure 4-12), the end result after the "healing" process is that no defect is formed. But for 100, 150 and 200 eV, defects are formed which get progressively larger with increasing energy. At 100 eV (Figure 4-13), a two atom asymmetric vacancy is formed, while for energies of 150 and 200 eV (Figure 4-14 and Figure 4-15), the created defects are greater than two atoms in size. This behaviour directly correlates with results in Chapter 5 for multi-atom impacts which show that for 100 eV, the two atom vacancy is most common type of defect formed, while for 150 and 200 eV, the greater-than-two atom vacancy is the most common. Note that the impacting atom bounces off for ≤ 150 eV but penetrates the target CNT at 200 eV. Secondary impacts due to the irradiation atoms or displaced atoms did not cause defects to form for the 150 and 200 eV cases. Importantly *no inter-tube bonds formed* for the oblique impact angle studied here (20°) for any of the incident energies applied. Oblique impacts can thus be seen as detrimental to the purpose of this study, whereas impacts at 0° (or close to it) are much more desirable.

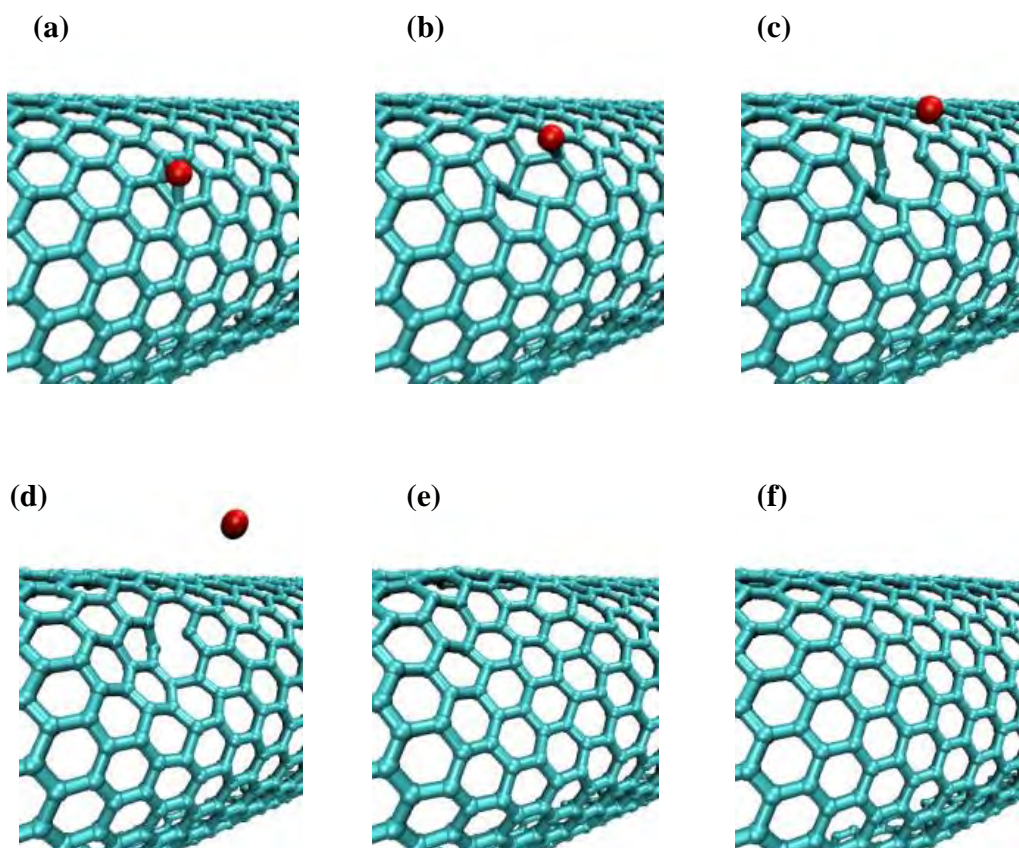


Figure 4-12: Snapshots in time of CNT bundle outer surface for oblique impact with incident energy of 50 eV

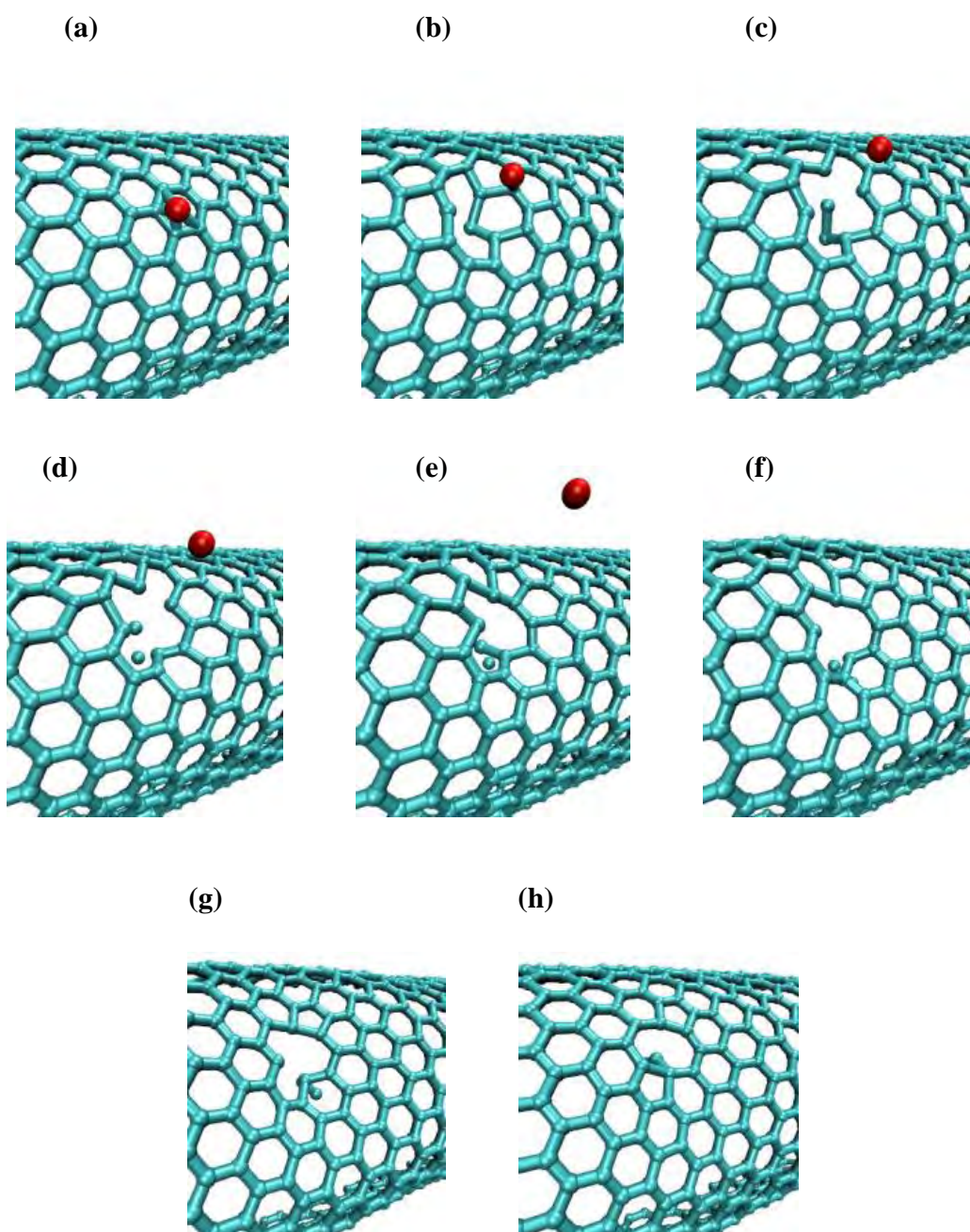


Figure 4-13: Snapshots in time of CNT bundle outer surface for oblique impact with incident energy of 100 eV

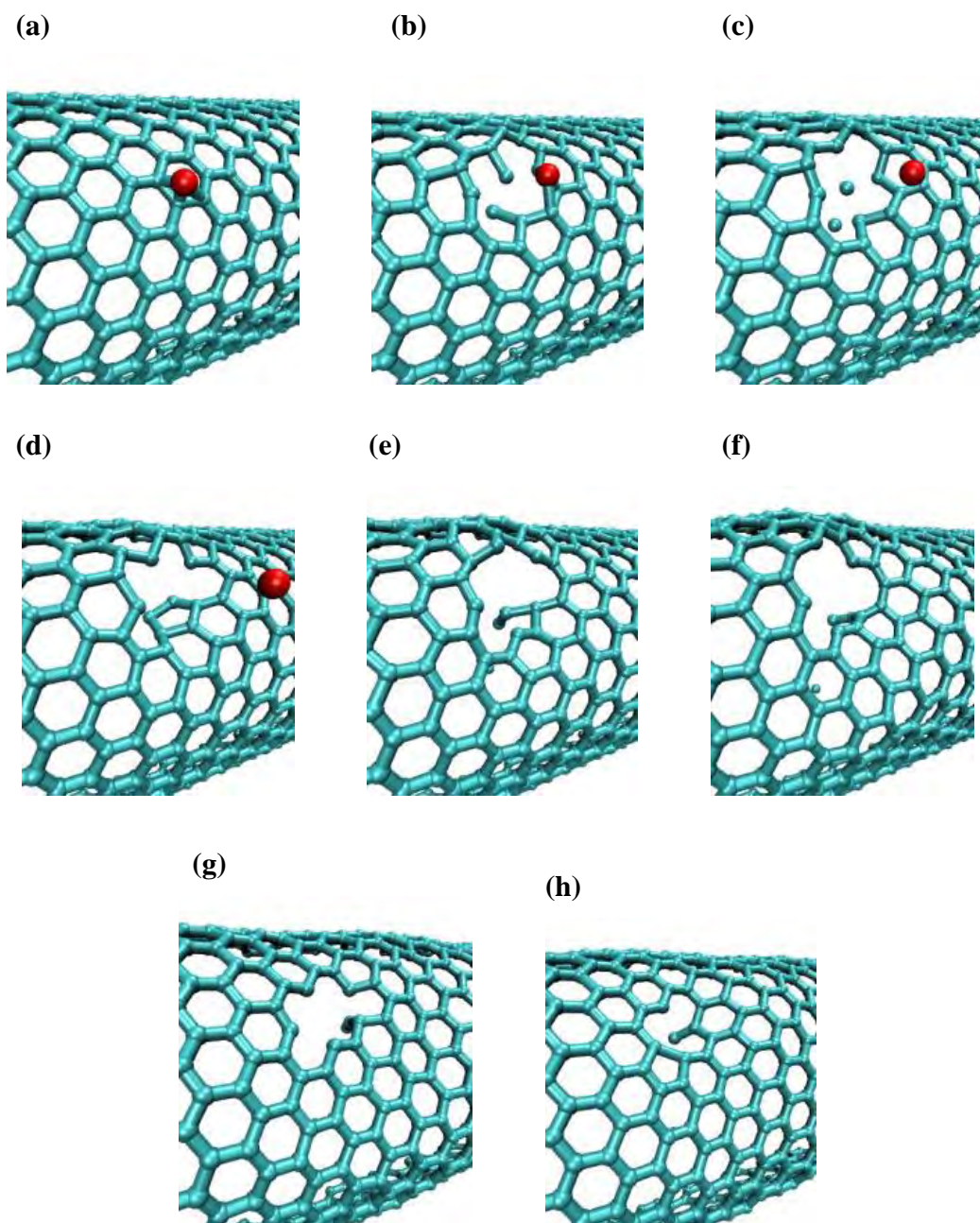


Figure 4-14: Snapshots in time of CNT bundle outer surface for oblique impact with incident energy of 150 eV

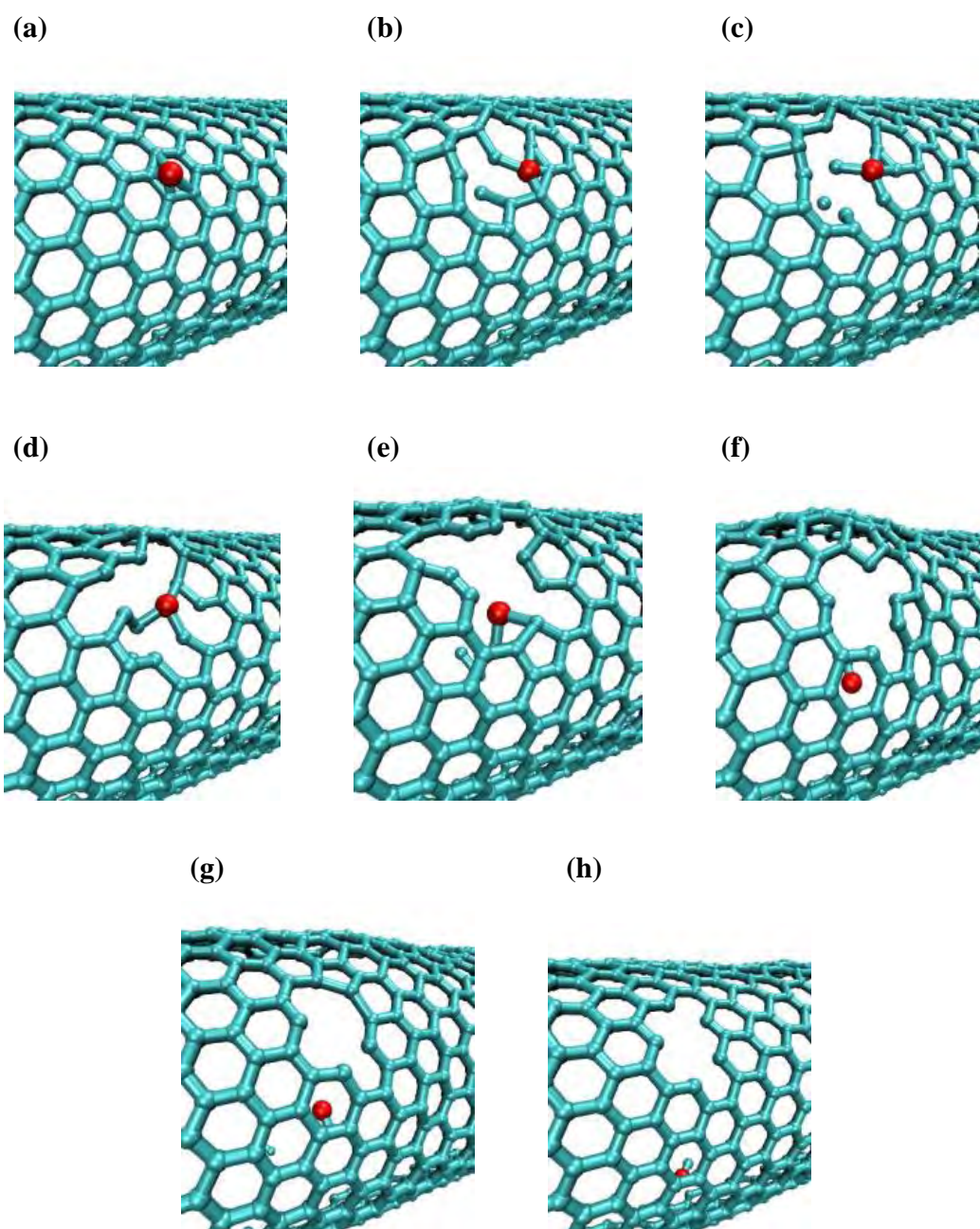


Figure 4-15: Snapshots in time of CNT bundle outer surface for oblique impact with incident energy of 200 eV

Chapter 5 Nanostructure Evolution for Multi-Carbon Atom Irradiation of Pristine SWCNT Bundles

5.1 Introduction

In this chapter, the results from multi-carbon atom irradiation of pristine SWCNT bundles are presented. The simulation details were provided in Section 3.3, especially sections 3.3.1 and 3.3.3. Of interest is the formation of inter-tube covalent bonds in the bundle which are desirable for improving load transfer within the bundle, as well as the formation of defects in the CNTs which are undesirable, but inevitable. The dependence of the formation of these features on energy and dosage of the irradiation is also of interest. The chapter is divided as follows: Section 5.2 discusses the types of inter-tube link formed by multi-atom irradiation and qualitatively how their number depends on irradiation parameters. Section 5.3 outlines the defects formed by multi-atom irradiation. Section 5.4 discusses quantitatively the effects of irradiation parameters on inter-tube cross-link and defect characteristics. In Section 5.5 irradiation strategies to improve mechanical performance in 7-tube bundles are put forward and finally in Section 5.6 extension of the work to larger bundles is considered, with results presented for 19-tube bundles.

5.2 Inter-tube Links Formed by Multi-atom Irradiation

Figure 5-1 illustrates the level of inter-tube cross-link formation for multi-atom irradiations of 7-tube bundles for a variety of energies and fluences. It is observed that very few bonds with the centre CNT are created at 50 eV/ion, Figure 5-1 (a), and none involve irradiation atoms (colored red), even at a fluence of $2 \times 10^{14} \text{ cm}^{-2}$ (five rings of 50 atoms). The number of such bonds increases for 100 eV/ion, Figure 5-1 (b), and 150 eV/ion, Figure 5-1 (c), and it is observed that some irradiation atoms make it to the centre of the bundle at these energies. At 200 eV/ion, significant bonding with the centre CNT can be achieved with a lower fluence of $1.2 \times 10^{14} \text{ cm}^{-2}$, Figure 5-1 (d), although because of the random positioning and trajectories of the irradiation atoms, the bonding is unevenly distributed; for a higher fluence of $2 \times 10^{14} \text{ cm}^{-2}$ at this energy, Figure 5-1 (e), a high level of inter-tube bonding is achieved. Similar observations can be made for 300 eV, Figure 5-1 (f), where significant inter-tube bonding occurs for a fluence of just $4 \times 10^{13} \text{ cm}^{-2}$ (just 50 atoms). At a fluence of $1.2 \times 10^{14} \text{ cm}^{-2}$, Figure 5-1 (g), the damage to the CNTs becomes excessive, and at 300 eV, $2 \times 10^{14} \text{ cm}^{-2}$, the centre CNT is virtually amorphised, which is obviously undesirable for structural applications.

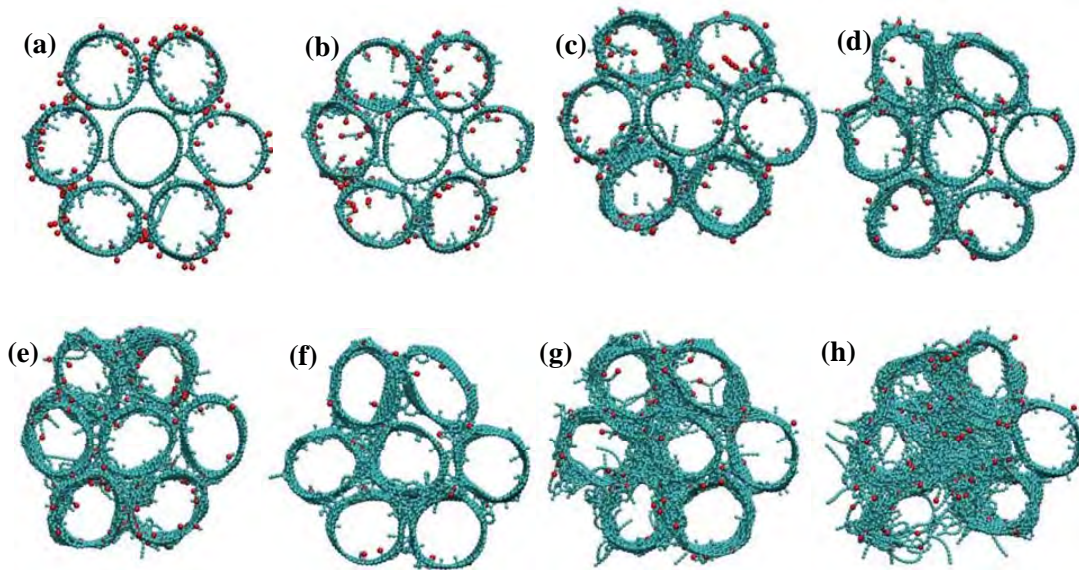


Figure 5-1: Irradiated SWNT bundles for: (a) 50 eV/ion, fluence = $2 \times 10^{14} \text{ cm}^{-2}$, (b) 100 eV, fluence = $2 \times 10^{14} \text{ cm}^{-2}$, (c) 150 eV, fluence = $2 \times 10^{14} \text{ cm}^{-2}$, (d) 200 eV, fluence = $1.2 \times 10^{14} \text{ cm}^{-2}$, (e) 200 eV, fluence = $2 \times 10^{14} \text{ cm}^{-2}$, (f) 300 eV, fluence = $4 \times 10^{13} \text{ cm}^{-2}$, (g) 300 eV, fluence = $1.2 \times 10^{14} \text{ cm}^{-2}$, (h) 300 eV, fluence = $2 \times 10^{14} \text{ cm}^{-2}$, (Original irradiation atoms = Red; Original CNT bundle atoms = Blue)

Figure 5-2 shows the large variety of inter-tube link types formed. The bonds involved in the cross-link are labelled according to the hybridization of the participating carbon atoms, e.g. a bond between two four-coordinated C atoms is labelled an $\text{sp}^3\text{-sp}^3$ bond and so on. The bond lengths and angles are given in Table 1. Link types (c)–(f) were found to be relatively common, so an average and a range over five different instances of each type is given in Table 1. Link types (a), (b) and (g–j) were very rare (less than five instances) so a range is not given.

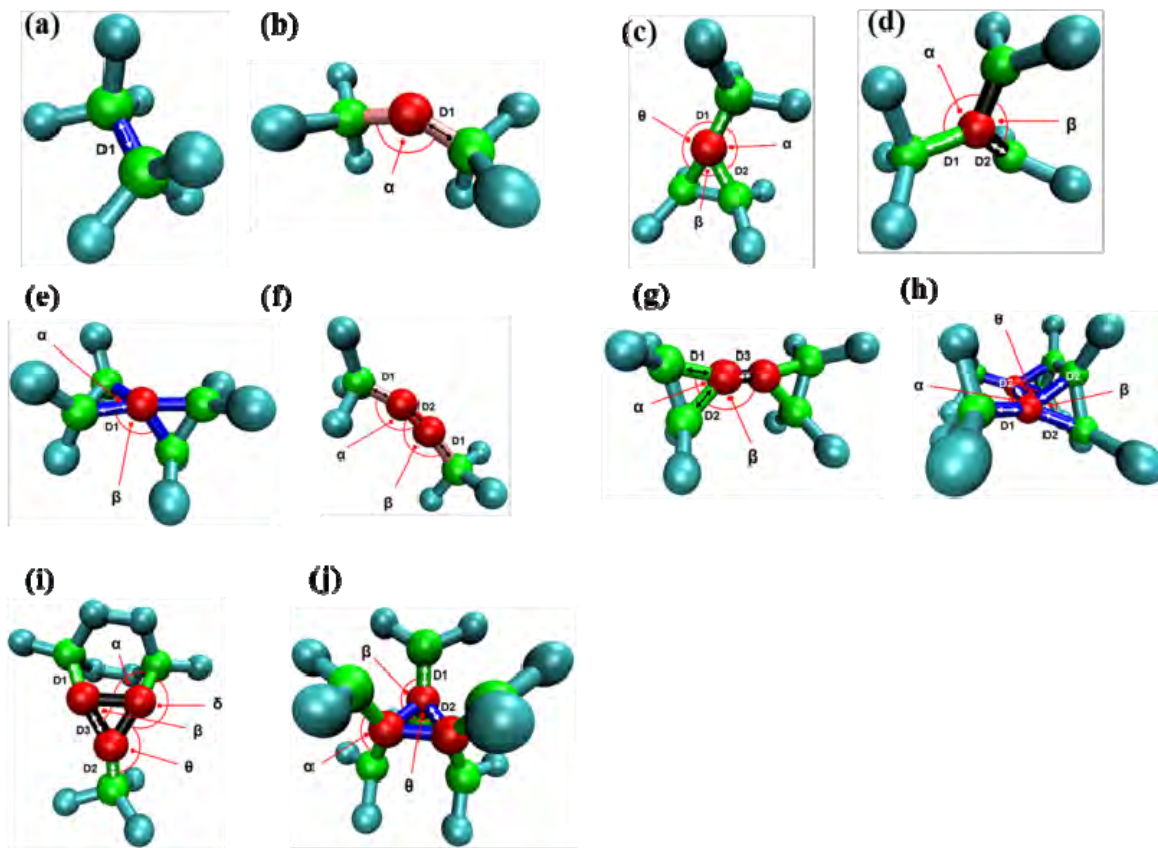


Figure 5-2: Inter-tube cross-link types, (a) direct sp^3 - sp^3 bond (b) two sp^3 - sp bonds with one interstitial atom, (c) three sp^3 - sp^2 bonds with one interstitial atom, (d) one sp^3 - sp^2 and two sp^2 - sp^2 bonds with one interstitial atom, (e) four sp^3 - sp^3 bonds with one interstitial atom, (f) one sp - sp and two sp^3 - sp bonds with two interstitial atoms, (g) one sp^2 - sp^2 and four sp^3 - sp^2 bonds with two interstitial atoms, (h) seven sp^3 - sp^3 bonds, and two interstitial atoms, (i) three sp^3 - sp^2 and three sp^2 - sp^2 bonds, and three interstitial atoms, (j) six sp^3 - sp^2 and three sp^3 - sp^3 bonds, and three interstitial atoms. Atoms: Red = interstitial, Green: CNT atom directly involved in cross-link, Blue: CNT atom not involved in cross-link. Bonds: Blue = sp^3 - sp^3 , Pink = sp^3 - sp , Green = sp^3 - sp^2 , Black = sp^2 - sp^2 , Red = sp - sp .

Table 1 - Inter-tube cross-link bond lengths and angles									
Cross link type*	N _I [†]	Bond types (no. of)	D1 (Å)	D2 (Å)	D3 (Å)	α (°)	B (°)	θ (°)	δ (°)
(a)	0	sp ³ -sp ³ (1)	1.63						
(b)	1	sp ³ -sp (2)	1.56			147			
(c)	1	sp ³ -sp ² (3)	1.51±0.05	1.67±0.07		128	58	163	
(d)	1	sp ³ -sp ² (1)	1.55±0.07			126			
		sp ² -sp ² (2)		1.42±0.02			109		
(e)	1	sp ³ -sp ³ (4)	1.67±0.08			58	117		
(f)	2	sp-sp (1)		1.22±0.01		150	168		
		sp ³ -sp (2)	1.57±0.07						
(g)	2	sp ² -sp ² (1)			1.25		135		
		sp ³ -sp ² (4)	1.68	1.65		58.4			
(h)	2	sp ³ -sp ³ (7)	1.54	1.69		110	57	86	
(i)	3	sp ³ -sp ² (3)	1.57	1.49		112		147	152
		sp ² -sp ² (3)			1.61		60		
(j)	3	sp ³ -sp ² (6)	1.49			128	112		
		sp ³ -sp ³ (3)		1.65				60	

Refer to Fig. 4, [†] N_I = number of interstitial atoms

Even more complex links involving more than three interstitials were also found; the more complex links were mostly found at high dosages, perhaps through amalgamation of adjacent simpler links. It is observed that the bond lengths and angles differ somewhat from the equilibrium distances for pure sp, sp², and sp³ bonds, indicating the bonds are stretched and distorted. Overall, bond type (d), in which a single interstitial atom is bonded to one atom in one CNT and two atoms in another CNT, was the most common type of cross-link. Bond types (a), (b), (d) and (f) were reported for C atom irradiation on CNT bundles in [17], but the other types have not been reported before. Bond lengths, angles and frequency of occurrence are quite different from [17], e.g. direct bonding without an interstitial (bond type (a)) was found to be rare here, but more common in [17]. The potential function used in [17] was a relatively old Tersoff potential [51], which helps to explain these differences. Chainlike crosslinks of sp-hybridised atoms, like bond type (f), have been reported before between MWCNT walls in [14]

following CH_3^+ ion irradiation. The cross-links formed will provide inter-tube mechanical coupling as desired. The stiffness and strength of each of these types of cross-link are likely to vary, although should be governed by the weakest bond in the link. For example, bond type (f) contains a high-strength triple C–C bond, but the other bonds in the chain will determine the strength of the cross-link. The effects of these inter-tube bonds on mechanical properties of the bundle will be quantified in the next chapter.

5.3 Defects Formed by Multi-atom Irradiation

The side effect of irradiation is the formation of defects which weaken the structure. Figure 5-3 shows the variety of defects formed during the simulations performed in this study, which include single atom vacancies, two-atom vacancies, larger vacancies, Stone–Wales defects and a pentagon–hexagon (5665) defect which has not been observed before in the literature to the author's knowledge. Stone–Wales defects are thought to be responsible for the release of excessive strain under axial mechanical load of nanotubes [47], which ties in with an observation that after irradiation, the CNT bundle was in a state of tension due to the geometric changes caused by defects and cross-links.

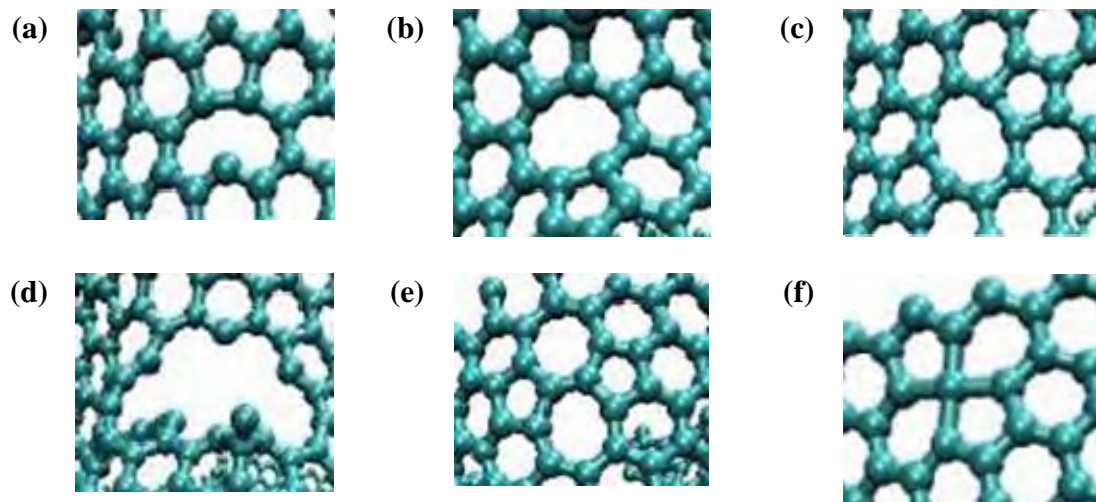


Figure 5-3: Vacancies/defects formed for irradiated CNT bundle models (a) one atom vacancy (symmetric reconstruction), (b) two atom vacancy (symmetric reconstruction), (c) two atom vacancy (asymmetric reconstruction), (d) greater than two atom vacancy, (e) Stone-Wales (5775) defect, (f) pentagon-hexagon (5665) defect

5.4 Effects of Irradiation Parameters on Inter-tube Cross-link and Defect Characteristics

In this section we examine the effect of the irradiation parameters on the inter-tube cross-link and defect characteristics. The CNT bundle models were first analysed for the number of irradiation atoms trapped (defined as the number of irradiation atoms remaining within a cylinder of radius $3R + G + 5 \text{ \AA}$ (38.28 \AA)) centred at the middle of the centre CNT, where R = CNT radius and G = interspatial gap) and the number of atoms displaced from the CNT bundle lattice (defined as the number of atoms no longer existing within the aforementioned cylinder). Note: displaced atoms are removed from the data file before mechanical testing in the CNT bundle. Figure 5-4 (a) shows the number of trapped CNT atoms versus incident energy. It can be seen that the number of trapped irradiation atoms is remarkably constant with respect to incident energy, decreasing only slightly with increasing energy. Each ring of atoms consists of 50 atoms, and it can be seen that the number of trapped atoms after 1, 2, 3, 4 and 5 rings is approximately 40, 80, 120, 160 and 200 respectively i.e. about 80% of incoming atoms are trapped. At higher energies, it might be expected that more incoming atoms would pass completely through the CNT bundle, resulting in fewer atoms getting trapped. But such a drop-off with energy is not seen. On close examination of the atom trajectories, it became clear that the reason for this is that, due to the bounds on the atom trajectories, shown in Figure 3-4 (b), most of the atoms would have to penetrate six walls to completely pass through the CNT bundle, and even at the maximum energy of 300 eV, there is insufficient energy for them to do this. Thus only the atoms with more “glancing” trajectories, which would only have to penetrate 4-5 walls, escape from the system. Figure 5-4 (b) demonstrates that as the incident energy is increased, the number of atoms displaced from the original ideal SWCNT increases. The increase with energy appears exponential in nature. The number of displaced atoms at 300 eV incident energy is far higher than for energies of 200 eV and below, which correlates with the excessive damage depicted in Figure 5-1 (h).

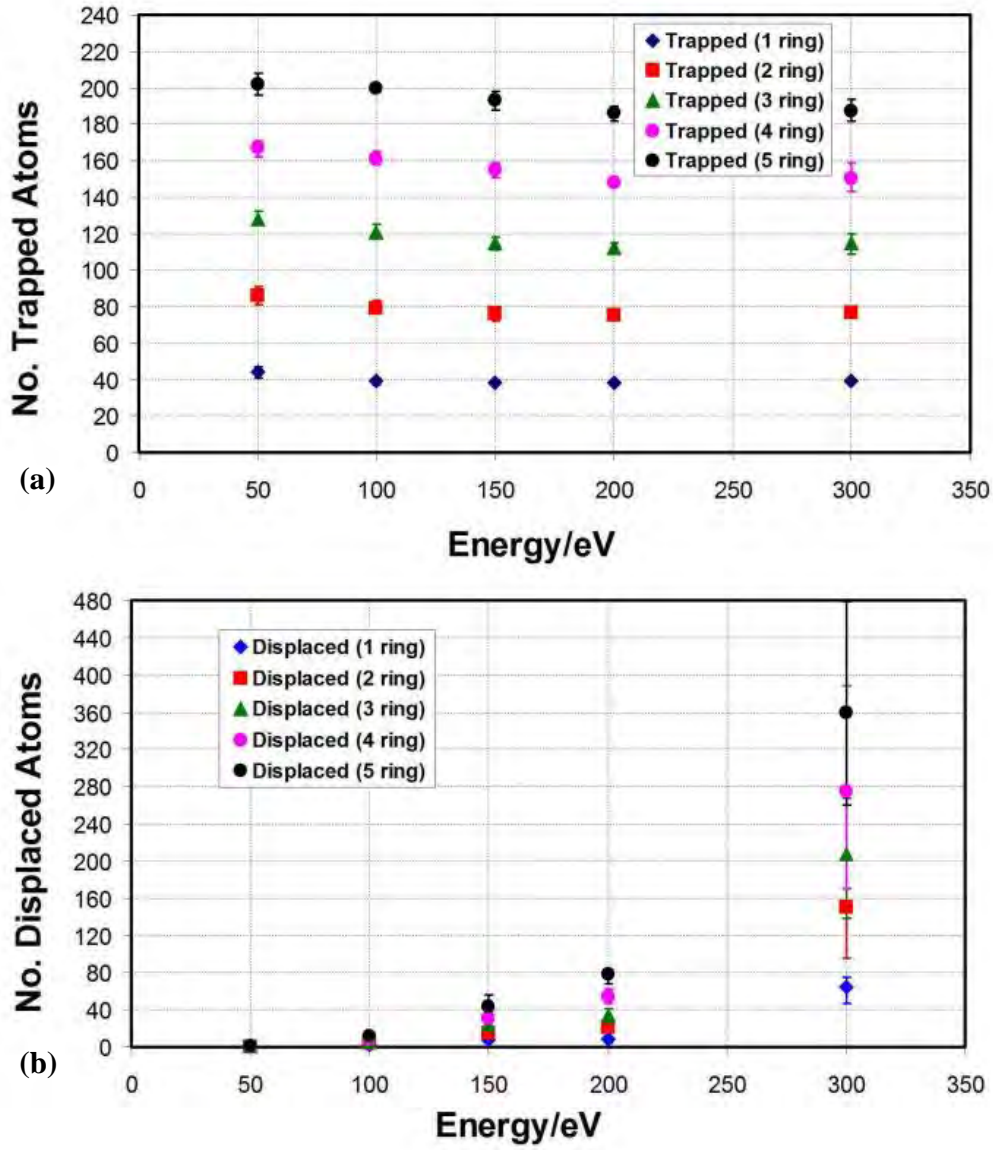


Figure 5-4: Number of irradiation atoms trapped (a) and displaced (b) in the CNT bundle as a function of incident energy, for five rings of 50 incident atoms

Figure 5-5 shows the number of “centre links”, i.e. links formed between the centre CNT and the surrounding CNTs, and the number of “circumferential links”, i.e. the links between the outer CNTs only, as a function of dosage, for 50–300 eV/ion energy levels. The results are presented per interface area, where the interface area for one CNT-CNT interface, A_{INT} , is defined in Figure 3-4(b). There are six interfaces

involved in both the centre links and the circumferential links so the number of bonds is divided by $6A_{INT}$ in each case. To enable comparison of different energy levels at similar dosages, additional rings of irradiation atoms (beyond five) were examined for the 50 and 100 eV cases (total 15 rings for 50 eV, 10 for 100 eV). The error bars demonstrate the variation obtained from the five different random trajectories applied for each data point. For irradiation at 300 eV, it was only possible to count the cross-links after one ring of atoms was deposited – after that the bundle became nearly amorphous. It is observed that for energies in the range 100–200 eV, both the number of centre links and the number of circumferential links increase almost linearly with dosage, with only a slight dependency on energy. Thus, within this energy range, a given percentage increase in either energy/ion or fluence has the same effect on cross-link density, giving us two ways to control the level of cross-linking. Below this energy range, i.e. for 50 eV/ion, the efficiency of bond formation with the centre CNT is significantly less. As noted above, it was observed that, for all simulations in this study, the number of irradiation atoms staying in the system (“trapped atoms”) was approximately constant at 80%, with the remainder being deflected out on first impact during oblique impacts. Thus, it is shown that within the 100–200 eV energy range, as the incident energy increases, a higher percentage of the trapped atoms result in inter-tube links, whereas at lower energy, many trapped atoms merely “stick” (as adatoms) to the bundle, but do not cause inter-tube links. It is also observed that the number of circumferential links is approximately double the number of centre links. It is anticipated the distribution could be made more uniform by decreasing α in Figure 3-4 (b). The single data points for 300 eV show a dramatic variation from the trends shown at lower energy levels. At 300 eV, $\sim 2 \text{ nm}^{-2}$ links can be achieved radially and circumferentially with a fluence of just $4 \times 10^{14} \text{ cm}^{-2}$ or 50 irradiation atoms. However, the fluence would have to be very carefully controlled at this energy level to avoid excessive damage to the bundle. As noted in [45], this continuing increase in defect numbers (considering cross-links to be a type of defect) with irradiation energy is a result of the irradiation atoms being primarily trapped in the system.

Above 300 eV, it is expected that the level of defects produced will level off as irradiation atoms would start to pass right through the bundle, limiting the number of

recoils. The results shown in this study are also in accord with [23], where for C ion irradiation on a single SWCNT, the number of coordination defects increased linearly with ion energy up to 200 eV/ion and then started to level off as the ions started to pass through the CNT.

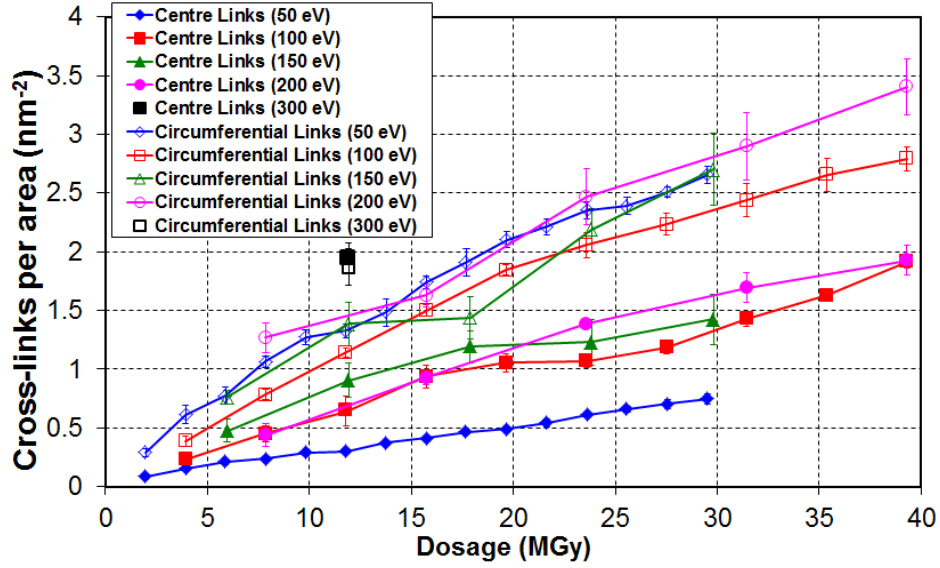


Figure 5-5: Number of inter-tube links per area (A_{INT} in Fig. 3-4 (b)), between centre CNT and outer CNTs (“Centre Links”), and between outer CNTs only (“Circumferential Links”) as a function of dosage, with incident beam energies of 50-300 eV; error bars show standard error or σ / \sqrt{N} where N is the number of repeats with different random trajectories

The variation of defect numbers with simulation parameters was also analysed and is presented in Figure 5-6. It can be seen that as energy/ion increases from 50 to 200 eV, the number of single atom vacancies decreases sharply (by a factor of 4), the number of two atom vacancies stays relatively constant, the number of larger (more than two-atom) vacancies increases sharply (by a factor of 4), and the number of Stone–Wales and pentagon–hexagon defects (small at all energies) stays constant. The overall conclusion is that at higher energy, larger holes are formed either from the first impact or through hole enlargement via subsequent impacts which overwhelm the self-healing ability of the CNTs. These results are in line with the findings in [29] which show that the

transformation of single atom vacancies to double vacancies has quite a low energy cost relative to formation of single atom vacancies from pristine tubes, because only two bonds need to be broken instead of three, and the double vacancy reconstruction, Figure 5-3 (b), is more stable than the one vacancy reconstruction, Figure 5-3 (a), due to the absence of dangling bonds.

The number of Stone–Wales and pentagon–hexagon defects is relatively independent of the energy of the incident atoms, while the total number of defects reduces at higher energies – this is logical since a large hole will count as one defect, whereas a number of one-atom defects in the same region will count as multiple defects. This also indicates that there may be merging of defects or changing of defects from one type to another.

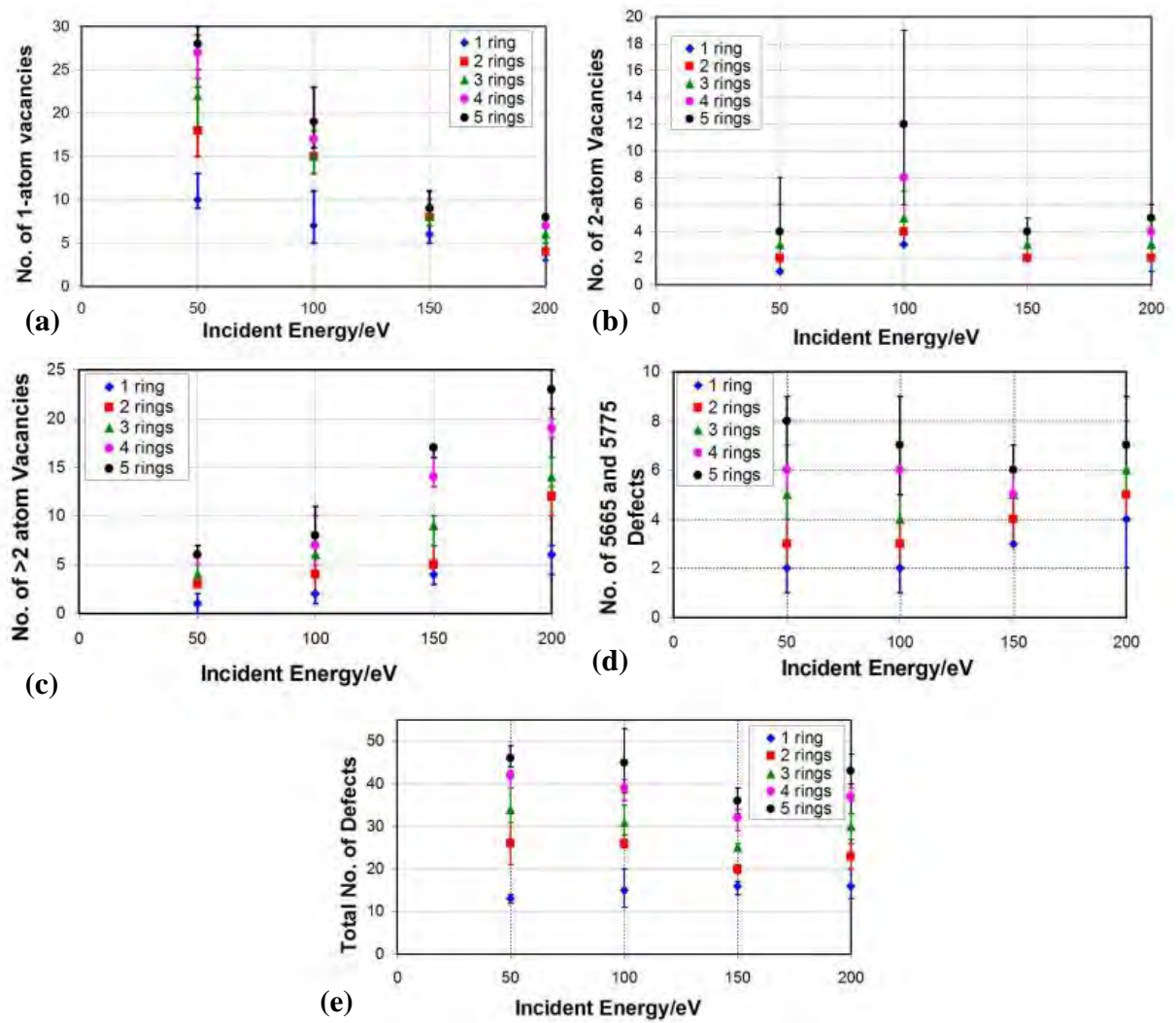


Figure 5-6: Number of defects as a function of incident energy, for five different numbers of incident atoms (a) One-atom vacancies, (b) Two-atom vacancies, (c) Greater-than-2-Atom vacancies, (d) 5665 and 5775 defects and (e) Total number of defects

A feature that is likely to strongly influence bundle tensile strength is the largest hole in the bundle. Fig. 5-7 shows the largest hole size (measured as the largest distance across the hole) as a function of dosage for various energies. We see that largest hole size increases with dosage, but there is also a dependency on energy, with lower energies producing smaller holes for the same dosage and thus being preferable.

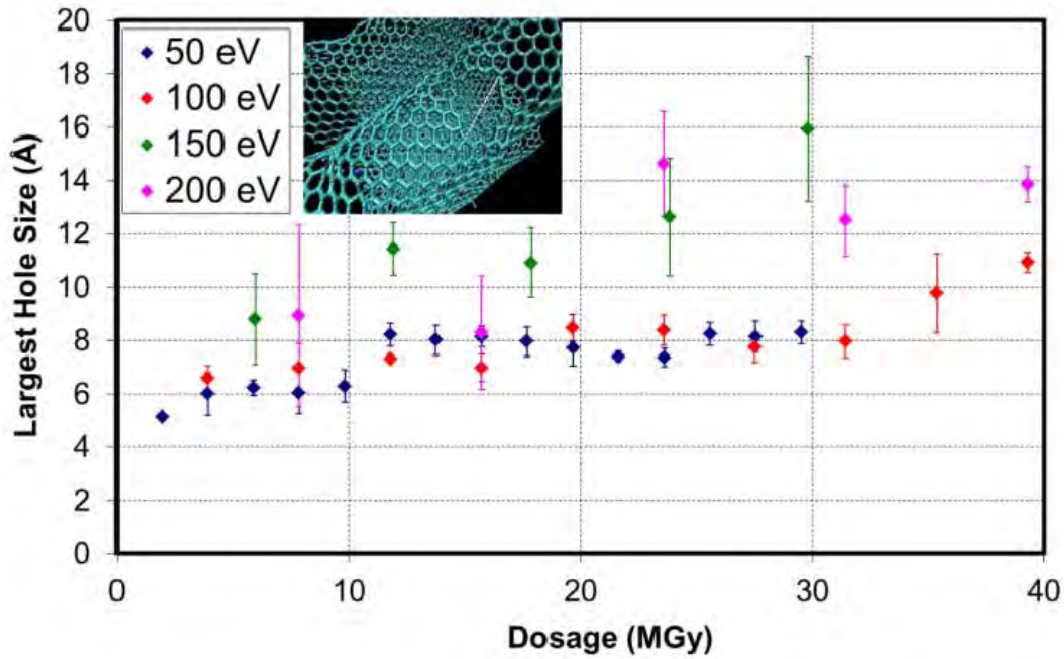


Fig. 5-7 - Largest hole size as a function of dosage, with incident beam energies of 50-200 eV; error bars show standard error or σ / \sqrt{N} where N is the number of repeats with different random trajectories

5.5 Irradiation Strategies to Improve Mechanical Performance in 7-tube Bundles

As stated at the start, the ideal result for the purposes of this study would be a controllable, uniform level of inter-tube cross-links between all adjacent tubes with a minimum level of defects in the CNT walls. This would allow transfer of load between CNTs, enabling all of them to engage in loading, with the least loss in strength due to intra-wall defects. From the previous section, in conclusion for 7-tube bundles, the achievement of a uniform and controllable level of inter-tube cross-links via C ion irradiation is possible within the energy range of 100–200 eV/ion. To keep the largest hole size to a minimum, which is likely to be the key parameter for tensile strength, lower energy is best, so the optimum strategy is to use energy/ion of ~ 100 eV, and to control the cross-link density through the fluence. The desirable level of cross-link density will

be discussed in the next chapter, but in general terms, higher density will give higher interface shear stiffness and strength, and based on results in [13] for CNT-diamond matrix composites, is likely to produce higher sliding stress during pull-out of a CNT from the bundle, which increases toughness. Too high a level, however, could lead to CNT breakage during pull-out giving a brittle response. The results show that for 7-tube bundles, it is possible to engineer the interface to achieve the desired response.

5.6 Extension to Larger Bundles

To examine if a satisfactory irradiation strategy can also be found for larger bundles, the next largest hexagonally-packed bundle arrangement is now considered which consists of 19 tubes. Six different irradiation strategies, all involving the same overall dosage (24.6 MGy), are considered. The final state of the bundle and the number of inter-tube links per interface area at each interface are shown in Figure 5-8. Note that there does seem to be some bias towards more cross-links on the left, suggesting the positions of the irradiating atoms were not truly random, but the effect of this on the results is of minor importance. The first strategy involved irradiation at a constant energy level of 100 eV/ion and the results in Figure 5-8 (a) show that the two outer layers of the bundle are very well-connected both circumferentially and radially, but the centre CNT remains almost completely unconnected. In the second strategy the energy level is doubled to 200 eV/ion (while the fluence is halved), and Figure 5-8 (b) shows that the resulting level of cross-linking is very similar to the first strategy. This is quite an interesting result as it shows that within the range 100–200 eV/ion, the cross-link density between the outer CNTs and the next innermost layer of CNTs is a function of dosage and thus can be controlled either through fluence or energy/ion; this is the same result as was found for 7-tube bundles. In the third strategy, a variable energy approach was used, applying a $8 \times 10^{13} \text{ cm}^{-2}$ fluence at 300 eV/ion, then $8 \times 10^{13} \text{ cm}^{-2}$ fluence at 150 eV/ion and then $4 \times 10^{13} \text{ cm}^{-2}$ fluence at 100 eV/ion. Given the results for 7-tube bundles, in which 300 eV/ion was deemed to be too high an energy level due to the excessive

damage caused, it was expected that this strategy would be successful in forming cross-links with the centre CNT. However, over the six interfaces with the centre CNT, Figure 5-8 (c) shows that the average number of cross-links per interface area is only 0.42 nm^2 , which is very low in comparison to the results for 7-tube bundles (see figure 5-5).

In the fourth strategy, the initial energy is increased to 400 eV/ion ($4 \times 10^{13} \text{ cm}^{-2}$ fluence) followed by $8 \times 10^{13} \text{ cm}^{-2}$ fluence at 200 eV/ion , then $8 \times 10^{14} \text{ cm}^{-2}$ fluence at 100 eV/ion , but this gives just 0.31 nm^2 links to the centre CNT (Figure 5-8 (d)). The best results are found with the fifth strategy of 500 eV/ion (fluence of $4 \times 10^{13} \text{ cm}^{-2}$), followed by 150 eV/ion (fluence $8 \times 10^{13} \text{ cm}^{-2}$) and then 100 eV/ion ($8 \times 10^{13} \text{ cm}^{-2}$ fluence), which gives 0.70 nm^2 links to the centre CNT (Figure 5-8 (e)). However, damage to some of the outer tubes is becoming excessive, and a few interfaces are so amorphous that counting links is impossible (signified by ‘M’ for ‘multiple links’). In the last strategy, the initial energy is increased to 600 eV/ion ($4 \times 10^{13} \text{ cm}^{-2}$ fluence), followed by $1.6 \times 10^{14} \text{ cm}^{-2}$ fluence at 100 eV/ion . This again gives 0.70 nm^2 links with the centre CNT (Figure 5-8 (f)), but in a less desirable way in that 16 of them are with just two of the surrounding CNTs, with no links at all to two adjacent CNTs. In this last case, the centre CNT has moved off-centre to the left, making links with CNTs from further irradiation impossible, and the level of damage is also clearly excessive. Further improvements could be obtained through variations on the fifth strategy, but the overall trends are clear, and given the long computation time for the 19-tube simulations, it was decided not to optimise further.

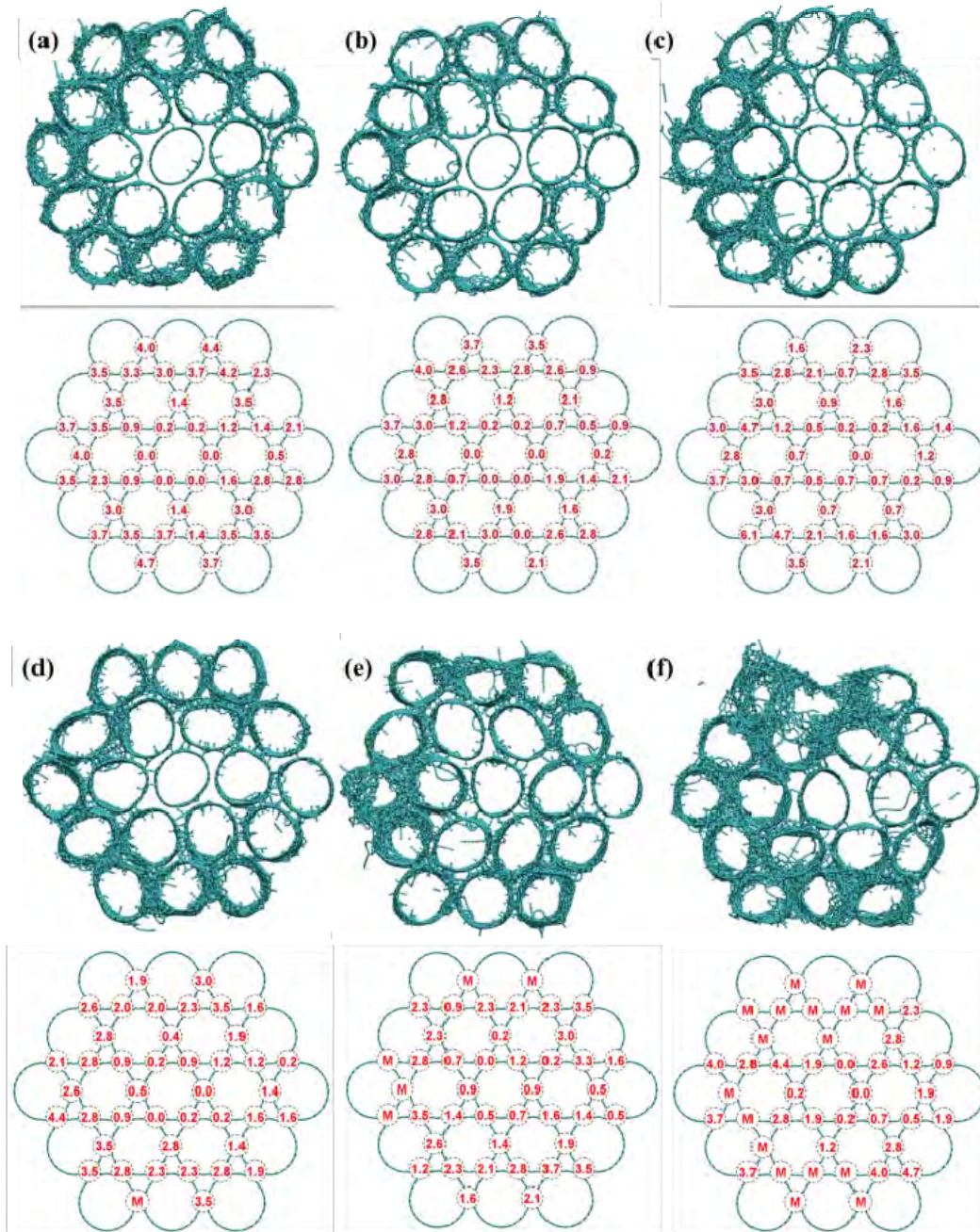


Figure 5-8: Final state and number of inter-tube cross-links at each CNT-CNT interface for various irradiation strategies with same overall dosage, (a) 850 ions at 100 eV/ion, (b) 425 ions at 200 eV/ion, (c) 170 ions at 300 eV/ion, then 170 ions at 150 eV/ion, then 85 ions at 100 eV/ion, (d) 85 ions at 400 eV/ion, then 170 ions at 200 eV/ion, then 170 ions at 100 eV/ion, (e) 85 ions at 500 eV/ion, then 170 ions at 150 eV/ion, then 170 ions at 100 eV/ion, (f) 85 ions at 600 eV/ion, then 340 ions at 100 eV/ion. “M” stands for multiple links in cases where the interface is too amorphous to allow counting of links.

The results obtained in this study are in line with those in [17] and [30]. In [17] C ion irradiation on CNT bundles, with energies up to 200 eV/ ion, produced only a few cross-links with the third CNT layer. In [30], Ar ion irradiation on CNT bundles with energies up to 250 eV/ion caused no cross-links beyond the first interface layer, and irradiation at 500 eV/ion produced very few links beyond the third CNT layer. Neither [17] nor [30] presented explicit information on the damage produced by irradiation though, as has been investigated here.

It is clear from the results that controlling the cross-link density in bundles containing more than 7 tubes, while simultaneously limiting the damage to acceptable levels is a much more difficult task as the bundle size increases. One can imagine that for the next size bundle up (37 tubes) it will be extremely difficult to reach the centre CNT without destroying the outer layer of CNTs completely. Electron irradiation will be more successful in penetrating to the centre of large bundles, and the most successful experimental demonstrations of inter-wall and inter-tube cross-linking to date have involved electron irradiation [14, 52]. However, in electron irradiation all the interstitial C atoms in the cross-links must come from the CNT lattice, so the level of damage is likely to be high (CNT structure becomes frayed and tensile strength is sacrificed), e.g. in the CNT bundles in [52] the highest tensile strength achieved was 17 GPa, which while impressive is well below achievable CNT strengths [14].

One possible future scenario to achieve highly cross-linked CNT fibres through C ion irradiation is through a modification of the method in [5, 41, 53] in which CNT yarns are created by drawing multiple small bundles of CNTs simultaneously from a CNT forest and then twisting them into a bundle. Significantly, the small bundles are described in [41] as containing just ‘‘a few’’ CNTs and prior to twisting are laid out parallel to each other (Figure 1 in [41]). Irradiation at that point in the process with C ions at 100–200 eV/ion could produce excellent results due to the small size of the bundles being pulled off. The extra C adatoms deposited might also lead to cross-links between the bundles as they are brought into intimate contact through the twisting process. However, it needs to be pointed out that the CNTs in [5, 41, 53] are MWCNTs unlike the SWCNTs studied here. The optimal irradiation parameters for MWCNT bundles would be quite different

from those found here for two reasons. Firstly, the objective would be different for MWCNT bundles in that not only inter-tube but also inter-wall cross-links would be desired for optimal mechanical performance, making the overall problem significantly more complex. Secondly, MWCNTs perform differently to SWCNTs under irradiation, being generally more stable because the atoms sputtered from inner shells remain in the MWCNT and Frenkel pairs created inside the MWCNT can easily recombine [47]. Thus further study is needed to establish suitable irradiation parameters for MWCNT bundles, and to determine if the suggested method of irradiating CNTs prior to twisting into a yarn would produce useful results.

Chapter 6 Interface Friction Behaviour and Tensile Strength of Pristine and Irradiated SWCNT Bundles

6.1 Introduction

In this chapter, the results are presented for mechanically testing (by simulation) the irradiated 7-tube CNT bundles analyzed in Chapter 5. The chapter is divided into Section 6.2, which deals with the beneficial effects in terms of improved inter-tube shearing response due to CNT bundle irradiation, and Section 6.3 which covers the detrimental effects on tensile properties.

6.2 Irradiation Effects on Inter-tube Shearing

As seen in Chapter 5, the irradiation simulations resulted in inter-tube cross-links. More than ten different types of cross-link were observed, including direct sp^3 bonded links with no interstitial C atom, and links mediated by one or more interstitial C atoms. The cross-links relevant to the pullout tests are those between the outer tubes and the centre tube, hereafter referred to as “centre links”. A reference area for shear resistance is defined as $A_{SH} = 6A_{INT}$ where A_{INT} is as defined in Chapter 5 and Figure 3-4(b). This area includes all atoms in the outer CNTs which are within the interaction distance of the centre CNT atoms for the potential [43] used here (prior to irradiation) and all centre

links post-irradiation. The number of centre links is divided by A_{SH} to get an areal inter-tube link density (ITLD or ρ). Figure 6-1 shows ρ as a function of dosage for energy/ion of 50– 300 eV (this data was also shown in Figure 5-5 but here only the centre links are included). It can be seen that within the range of 100–200 eV/ion, ρ is proportional to dosage, and thus can be controlled by varying either the fluence or the energy/ion. Lower energy irradiation (50 eV/ ion) was relatively ineffective in forming centre links. Higher energy irradiation (300 eV/ion) was highly effective in forming centre links, but the production of defects was excessive, as noted in Chapter 5.

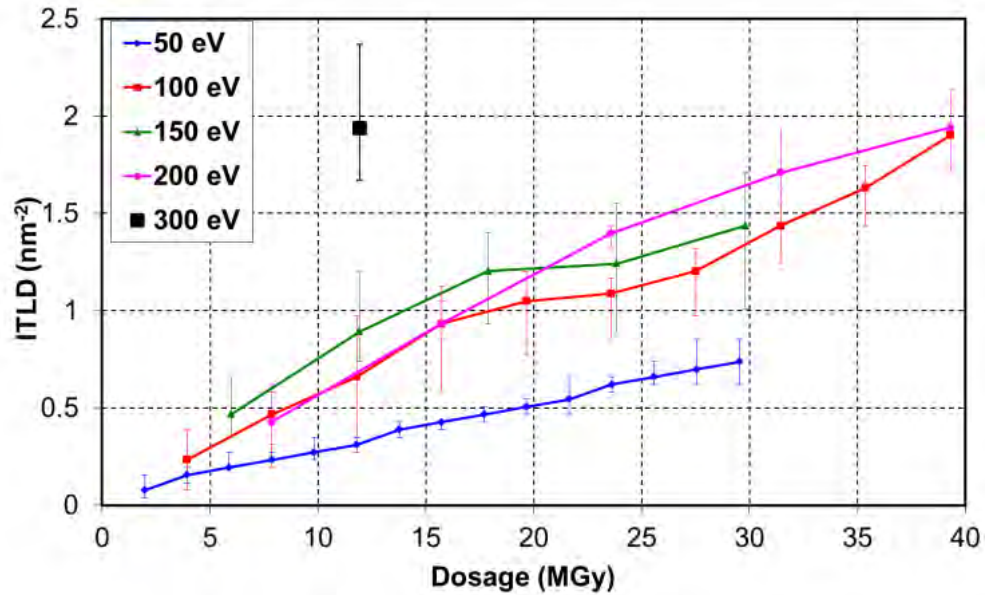


Figure 6-1: Areal inter-tube link density (ITLD or ρ), as a function of dosage, with incident beam energies of 50-300 eV (only links to centre CNT included)

The average interfacial shear stress is calculated as the pull-out force divided by A_{SH} . Figure 6-2 shows the pull-out stress versus pull-out distance for the irradiated SWCNT bundles (for all five random trajectory instances). For comparison, the result for the pristine case is shown in Figure 6-2(a). We see that the nano-scale interface response resembles that of traditional micro-scale composites: pull-out is characterized by an elastic stretching region at small displacements ($x < 1 - 2 \text{ \AA}$), followed by the onset of

debonding, in which inter-tube bonds are broken, up to a displacement of 2 - 3.5 Å and then a drop to a lower oscillating sliding stress (“pull-out sliding” regime). The only exception to this behaviour is the highest dosage case (39.3 MGy) where the shear stress reaches a peak of 10.1 GPa and then drops to zero. In this case, the centre CNT did not pull out and instead failed in tension. Both the elastic and sliding response vary with dosage, which as mentioned above is directly related to ρ . Notably, the effective frictional stresses at the interface after debonding are quite high (several GPa) for higher cross-link densities.

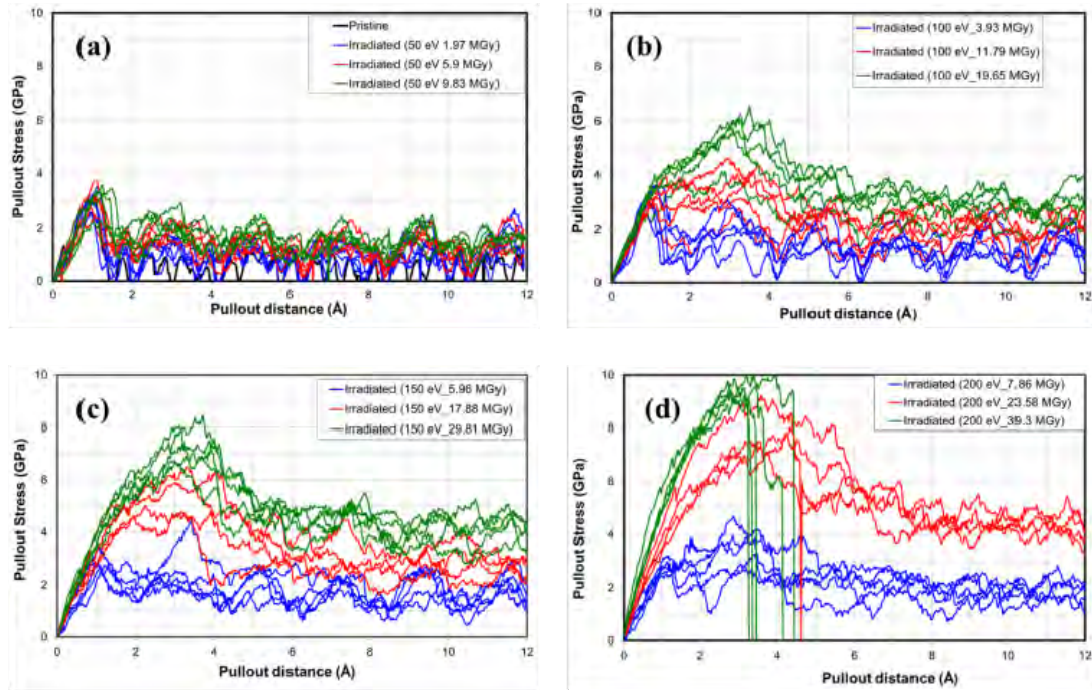


Figure 6-2: Pull-out stress versus pull-out distance for irradiated CNT bundles with incident energies of (a) 50 eV, (b) 100 eV, (c) 150 eV, and (d) 200 eV

The nano-scale pull-out behaviour shown in Figure 6-2, resembles micro-scale composite response, and can be understood by analysing the atomic deformation mechanisms at the interface. As noted above, more than ten different types of inter-tube cross-link were found post-irradiation. Figure 6-3 shows snapshots in time of the pull-out behaviour of three of them: a direct link, a link involving one interstitial carbon atom, and a link involving two interstitial carbon atoms. For pictures of the pull-out behaviour of all

ten types of cross-link refer to Appendix A. The key finding from this figure is that cross-links involving an interstitial atom (Figure 6-3 (b) and (c)) break (at the end of the elastic region of pull-out), new links are formed and broken several times subsequently. On the other hand, direct links in which no interstitial is present (Figure 6-3 (a)), once broken, do not reform, and so do not contribute to the pull-out force in the sliding regime. The bond breaking and re-forming processes for interstitial-mediated cross-links are responsible for the overall ‘stick and slip’ behaviour observed. The directly bonded cross-links contribute to the initial elastic behaviour but not to the sliding stress. In conclusion, in order to produce tough CNT-fibres, in which significant energy is absorbed during CNT pull-out from the fibre, it is desirable to have C interstitials at CNT interfaces, since inter-tube links will spontaneously form and break during sliding. This makes C ion irradiation an attractive option over irradiation by electrons or other types of ions, since extra C atoms are added to the system, so not all interstitials have to come from knocking out atoms from the CNT lattice (thereby reducing tensile strength).

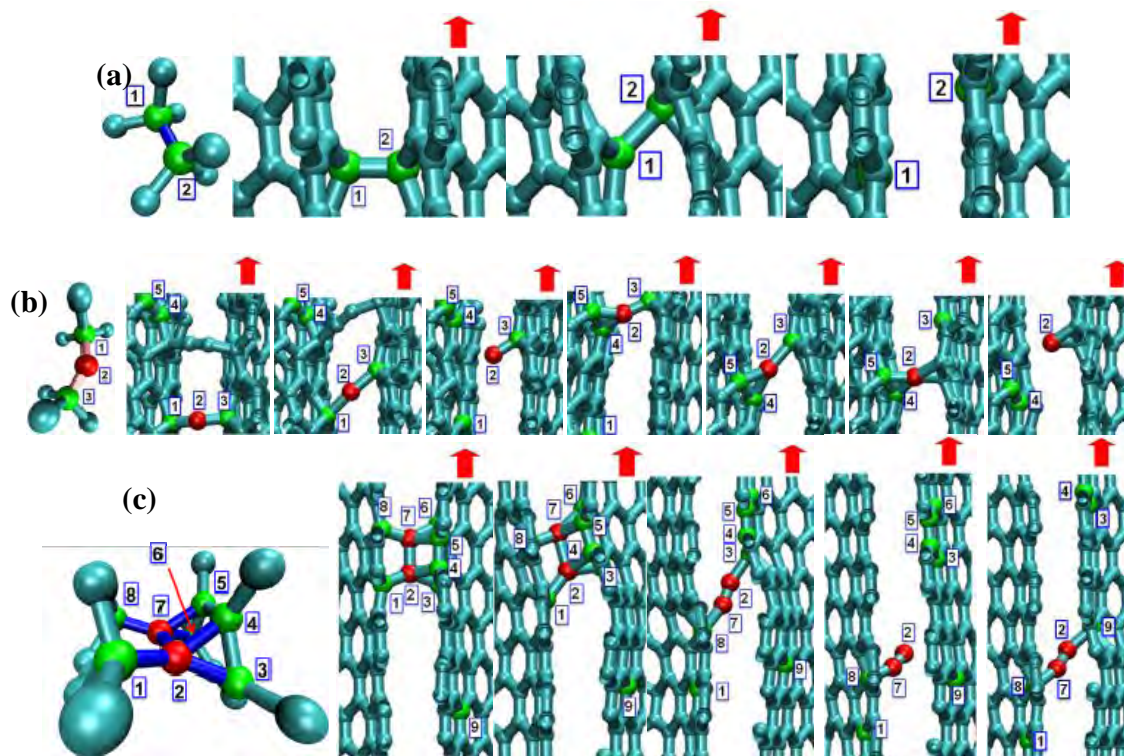


Figure 6-3: Bond breaking and re-forming during pull out of centre CNT. Snapshots in time, time increasing from left to right, numbers are to guide eye in following individual atoms over time, (a) direct sp^3 - sp^3 bond, (b) cross-link with one interstitial and two sp^3 - sp bonds, (c) cross-link with two interstitials and seven sp^3 - sp^3 bonds

The pull-out force was divided by the number of centre links to give the pull-out force per centre link, which is plotted against pull-out distance in Figure 6-4, for energies ranging from 50 eV to 200 eV; only representative instances among the five random trajectories for each case are shown for clarity. The ITLD (ρ) is also shown in the legend. In [13], the pull-out force per cross-link involving a single interstitial carbon atom between a CNT and a diamond matrix was found to collapse all the data for different interstitial densities onto a nearly single universal curve for interstitial C atom densities of 0.73 – 2.18 nm². The system studied here differs from that in [13] in that the cross-links are between two CNTs rather than between a CNT and diamond matrix, and there are several different types of cross-link, some of which are direct links and some of which involve one or multiple interstitials. Figure 6-4 illustrates that for low cross-link densities, $\rho < 0.7$ nm², the force per cross-link is high and oscillates erratically. This is due to the small number of inter-tube links at this density, given the short length of the tubes studied. With just a few links distributed randomly axially and circumferentially, very unsymmetrical loads on the centre CNT occur, with large relative force oscillations as individual cross-links break and re-form. However, as ρ increases into the range considered in [13], i.e. $\rho > 0.7$ nm², (which corresponds to > 18 centre links in total in the system) the curves collapse quite well onto a single curve, as in [13]. Therefore, the varying strength of the different cross-link types averages out if enough of them are present, and this can be directly related to the shear mechanical properties to the ‘number of cross-links present’, or ρ . Unlike [13] however, an upper limit to this is observed, since above $\rho = 1.7$ nm², Figure 6-4 (d) shows that failure of the centre CNT during pull-out can occur since the interfacial shear stress is too large. It needs to be borne in mind that, unlike in [13], the centre CNT, like all the CNTs in the bundle, contains defects such as vacancies and Stone–Wales defects due to the irradiation process, so the value of ρ needed to cause pull-out CNT failure would vary somewhat depending on the damage level in the pull-out CNT.

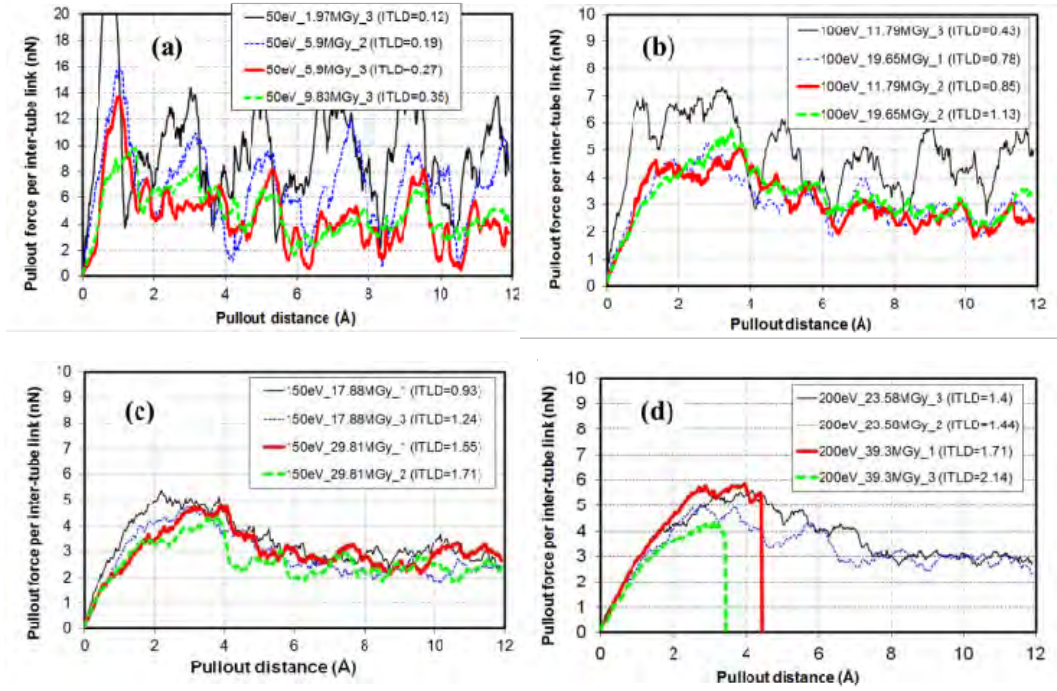


Figure 6-4: Pull-out force per inter-tube cross-link with the centre CNT versus pull-out distance for irradiated CNT bundles with incident energies of (a) 50 eV, (b) 100 eV, (c) 150 eV, and (d) 200 eV (ITLD = inter-tube link density or ρ in $1/nm^2$)

In Figure 6-5, some key parameters are plotted against ρ , for $\rho > 0.7 \text{ nm}^2$. Figure 6-5 (a) shows the “interface shear modulus” μ prior to debonding. Here, the interface shear strain γ_{xy} was defined as the applied displacement divided by the intertube gap. From the graph, it is shown that μ scales linearly with ρ , in the range $\rho = 0.7\text{--}1.7 \text{ nm}^2$,

$$\mu \cong 10\rho \text{ GPa nm}^2 \quad \text{6-1}$$

This is more than double the value $\mu \sim 4.6\rho \text{ GPa nm}^2$, found in [13] for CNT sliding in a diamond matrix with interstitial carbon atoms. On the other hand, in [21] an effective shear modulus for the interface between walls of a DWNT directly bonded with sp^3 -bonds was found that scales with the bond fraction f . Converting their bond fraction f to an areal density of bonds ρ , their result is

$$\mu \cong 12\rho \text{ GPa nm}^2 \quad \text{6-2}$$

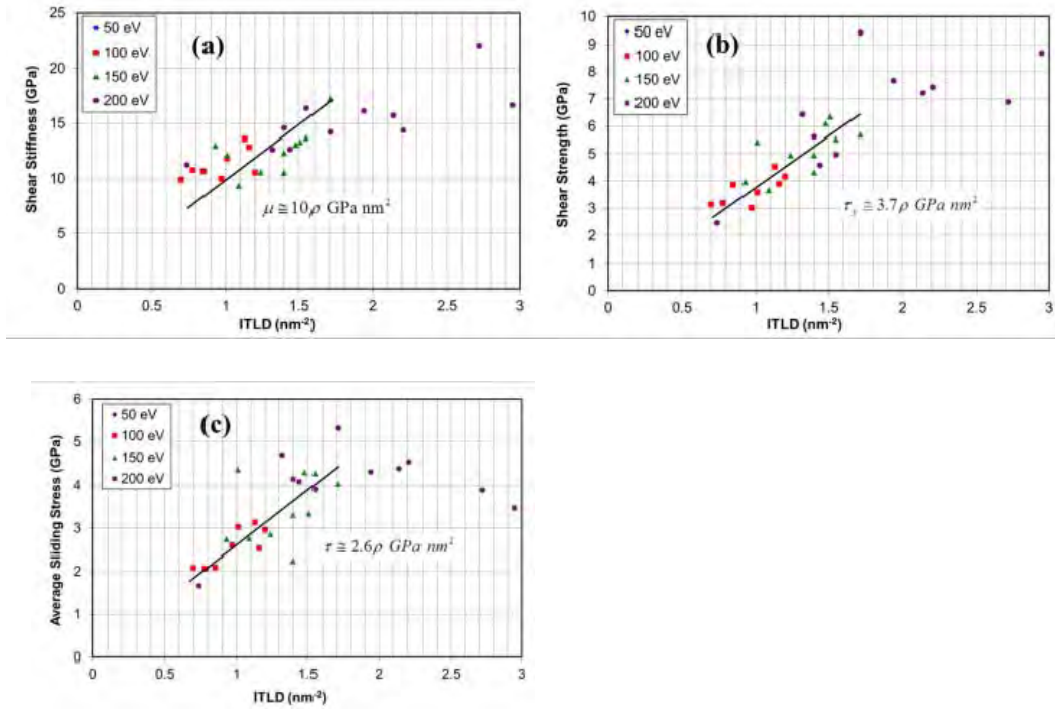


Figure 6-5: Elastic and sliding parameters for pull-out versus ITLD (or ρ) for irradiated CNT bundles (a) interface shear modulus, (b) interface shear strength, and (c) interface sliding stress. Lines show linear relationships in the range $\rho = 0.7 - 1.7 \text{ nm}^{-2}$.

Since both direct bonds and bonds mediated by interstitial C atoms are present for the system in this study, it is reasonable that the result shown should be between the values found in [13, 21]. Furthermore, the bonds in [13] involved one interstitial C atom initially bonded to just one CNT atom and one diamond matrix atom. As described in [20], many of the interstitial atoms in the system studied were initially bonded to more than one atom in each CNT – an example can be seen in Figure 6-3 (c) – which is a stiffer arrangement, so the interstitial-mediated bonds here are on average stiffer than in [13]. It is shown that with an areal density of cross-links, $\rho = 1.7 \text{ nm}^{-2}$, an interface shear modulus of 17 GPa is obtained. This is more than three times the value of 5 GPa found from simulations performed for CNT bundles without cross-linking.

In figure 6-5 (b) and (c), it is shown that in the range $\rho = 0.7 - 1.7 \text{ nm}^{-2}$, the interface shear stress at the onset of debonding or yield stress, τ_y (note this is not the maximum shear stress during pull-out, it is the stress at the end of the linear region of the

load–displacement curve), and the frictional sliding stress after debonding, τ (calculated for pull-out distance $x > 8 \text{ \AA}$) are both linearly dependent on ρ , scaling as

$$\tau_y \cong 3.7 \rho \text{ GPa nm}^2 \quad \mathbf{6-3}$$

$$\tau \cong 2.6 \rho \text{ GPa nm}^2 \quad \mathbf{6-4}$$

Concerning the interface shear strength τ_y , for $\rho = 1.7 \text{ nm}^2$, an interface shear strength of 6.3 GPa is obtained. This is seven times larger than the value of 0.9 GPa obtained for CNT bundles without cross-linking. The equation for τ is slightly below the value found in [13] ($\tau_y \cong 3 \rho \text{ GPa nm}^2$), which contrasts with the finding on modulus above. The reason for this becomes clear from examining figure 6-3 (c) and other similar cases, from which it is observed that while original cross-links may be quite complex and initially stiffer than those in [13], re-bonds after failure tend to be chain-like, resembling the cross-links involving a single interstitial in [13]. In addition, unlike [13], there are some direct bonds between CNTs in the system shown above, which as noted above do not reform once broken and thus do not contribute to the sliding stress. The results shown above provide further evidence to that in [13] that a friction-like sliding stress emerges at the atomistic scale, thus conforming to the standard constant sliding stress used in the majority of models to predict composite performance. An important issue in composite behaviour is toughness, which is dominated by the energy dissipated by frictional sliding during fibre pull-out. The energy dissipated due to “friction” generated by breaking and re-forming of interstitial-mediated inter-tube bonds can be computed as the work done during pull-out, corresponding to the area under the applied force vs. displacement curve. Typically, the pull-out work is converted into a fracture toughness by division by the composite cross-sectional area; here the “composite” cross-sectional area is taken to be the area of the circle enclosing the 7-tube bundle. For a density of $\rho = 1.46 \text{ nm}^2$, a toughness of $\sim 2.8 \text{ Jm}^{-2}$ is obtained for just 1 nm of pull out. Such a value far exceeds the

work done by weak van der Waals bonding between perfect nanotubes (0.2 J m^{-2} for 1 nm of pull out for the simulations shown above).

6.3 Tensile Properties of Irradiated Specimens

The trade-off for the greatly enhanced shear properties illustrated above is a reduced tensile strength due to irradiation-produced defects. For the tensile tests, the tensile stress was defined as the tensile force divided by the cross-sectional area of the CNT bundle ($\sim 15 \text{ nm}^2$), which was computed as seven times the area of a single CNT, as given in equation 6-5,

$$A = 7\pi \left[\left(r + \frac{t}{2} \right)^2 - \left(r - \frac{t}{2} \right)^2 \right] \quad \mathbf{6-5}$$

where r is the CNT radius and $t = 0.335 \text{ nm}$ is the graphitic layer thickness. The strain was calculated by dividing the change in length by the original length of the CNT bundle.

Figure 6-6 (a) shows the tensile stress versus strain for the bundles irradiated with energies of 100 eV/ion (for all random trajectories); the curves from other irradiation energies (not shown here) are similar in form. For comparison, the result for pristine (unirradiated) bundle is also shown. For the pristine case, the Young's modulus, tensile strength and maximum strain are 860 GPa, 91 GPa and 17.2% respectively, which is at the low end of theoretical values in the literature for individual CNTs [14, 54, 55]. MD simulations tend to underestimate tensile strength compared to more accurate quantum mechanics calculations [35, 37-39]. However, changes due to irradiation are of interest, not exact theoretical values, so the fact that these values are in the correct range is sufficient.

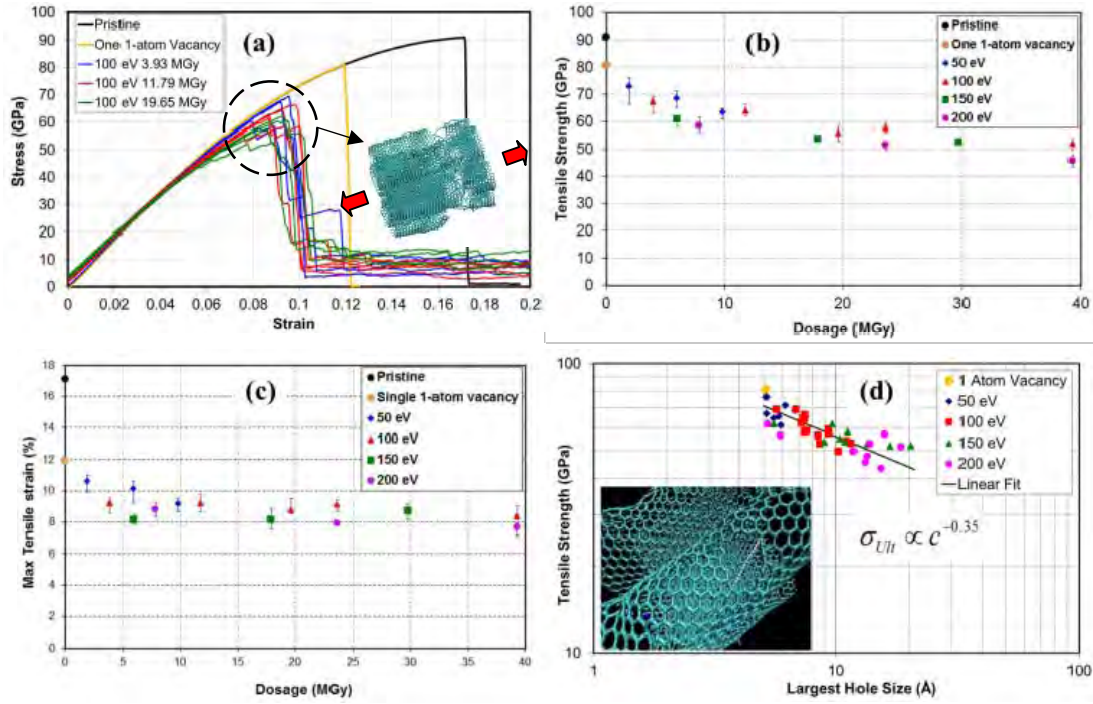


Figure 6-6: Tensile test result on 7-tube bundles, (a) stress versus strain for incident energy of 100 eV, (b) tensile strength, (c) maximum strain and (d) strength vs. maximum hole size

Figure 6-6 (a) shows that carbon atom irradiation causes a significant decrease in stiffness, strength and maximum strain relative to the pristine case. However, while pristine CNTs are the ultimate baseline, their existence in practical macro-scale composites can be considered rare. Thus, a tensile test simulation was performed on a bundle with just one single-atom vacancy in one CNT and from figure 6-6 (a), a tensile strength and tensile strain of 81 GPa and 11.9% respectively can be observed, representing drops of 11% and 31%, respectively from the pristine case. This level of reduction is in line with previous studies on single CNTs with single vacancies [40]. The reduction in tensile properties due to irradiation is shown to be much milder when considered against this less stringent baseline (a single-atom vacancy in one CNT).

Clean planar fracture was exhibited for the pristine bundle, with the stress dropping to zero after failure. The irradiated bundles exhibited a less clean fracture, with crack propagation between CNTs at sites where inter-tube bonds had formed, and the stress did not reduce to zero as bonds still remained between CNTs after failure occurred.

Another feature evident in figure 6-6 (a) is that the irradiated bundles were already under slight tensile load before they were tensile tested, particularly at higher energies. This is because damage and inter-tube linking caused the equilibrium length of the CNT bundle to reduce during irradiation.

Figure 6-6 (b) and (c) provides a statistical analysis of the results from all tensile test simulations for strength and maximum strain respectively. For the maximum dosage considered here (40 MGy), the tensile strength reduces to ~50 GPa and the maximum strain reduces to ~8%, representing 38% and 33% drops respectively from the single 1-atom vacancy case. It is also noticeable that lower energy irradiation produces less of a reduction. In the previous section, it was shown that for the inter-tube link density range $\rho = 0.7\text{--}1.7 \text{ nm}^2$, the shear properties are predictable and improve by an order of magnitude over non-irradiated bundles. Thus a very large benefit is observed, for a relatively small cost. In fact the reduction in tensile strength considered here is greater than would occur in practical CNT-fibre reinforced composites. In macro-scale CNT fibres, individual CNTs would be unlikely to run along the full length of the fibre, and when embedded in a matrix, load would generally be transferred from the matrix to the outer CNTs and then inwards through shear load transfer between CNTs. Highly imperfect bonding to the matrix would exist at the fibre ends, in contrast with the end conditions here. Inter-tube crosslinks (between CNT ends) would facilitate the transfer of load to all CNTs in the fibre, and so would have major beneficial effects on the tensile strength of macro-scale fibres in composites, which would offset the reductions described above. As noted above, many different types of defects [20] post-irradiation were observed, at random locations within the bundle. Under tensile load, the load transfer within the cross-linked, defective CNT bundles is highly complex. However, figure 6-6 (d) shows that there is still a strong correlation between the reduction in tensile strength and the largest hole size in the bundle after irradiation (measured as the largest distance across the hole, as illustrated in the figure), as one would expect for a single CNT. It is observed that $\sigma_{Ult} \propto c^{-m}$ with $m \sim 0.35$, where c is the largest hole size. This is close to the value $m \sim 0.4$ that was observed in [10] for pristine MWCNTs. There is scatter in Figure 6-6 (d) because tensile strength is also affected by other defects found such as Stone–Wales defects and adatoms. For

example, a tensile test simulation was performed with just one adatom on one CNT and found the bundle strength decreases to 85.9 GPa and the maximum strain diminishes to 13.5%, which are reductions from the pristine case of 5.6% and 22% respectively. This is because the bonding at the attachment point changes from sp^2 to sp^3 , with consequent increase of bond length from 1.42 Å to 1.54 Å, which weakens the CNT structure.

In considering an optimal strategy for irradiation then, one should consider the effect on maximum hole size. In [20] it was shown that for the same dosage, irradiation with 100 eV irradiation led to smaller holes than 200 eV irradiation, and this ties in with the tensile strength values seen in Figure 6-6 (b) and (d). An advantage of C ion irradiation is that it provides extra C atoms to the system, which on subsequent annealing have the potential to migrate to vacancy locations, causing healing of the CNT lattice. A further observation related to this issue is that irradiation at very low energy (1 eV/ion) can actually result in filling in or healing of pre-existing holes as irradiation atoms latch onto dangling bonds on the hole perimeter. This process is illustrated in Figure 6-7 (a) and (b). This results in an increase in tensile strength of the bundle with negligible change in pull-out stress – see Figure 6-8 for the beneficial effect of 1250 additional “healing” C atoms deposited at 1 eV/ion energy. Thus a potential strategy would be to apply low energy irradiation after irradiation at the energies needed to produce cross-links. The limitation on this is that as well as filling in holes, the low energy atoms also adsorb as adatoms. As noted above, adatoms reduce tensile strength, though the effect is masked by vacancy defects which have a greater impact on tensile strength. However, if enough adatoms are deposited during low energy irradiation they will eventually line up somewhere in the bundle, perpendicular to the CNT axial direction, forming a crack-like weakening of the structure. The highlighted area in Figure 6-7 (c) shows one such example after 2000 “healing” atoms were applied, and the CNT bundle failed at this location when tensile loading was applied resulting in a reduction in tensile strength (see Figure 6-8 (a)).

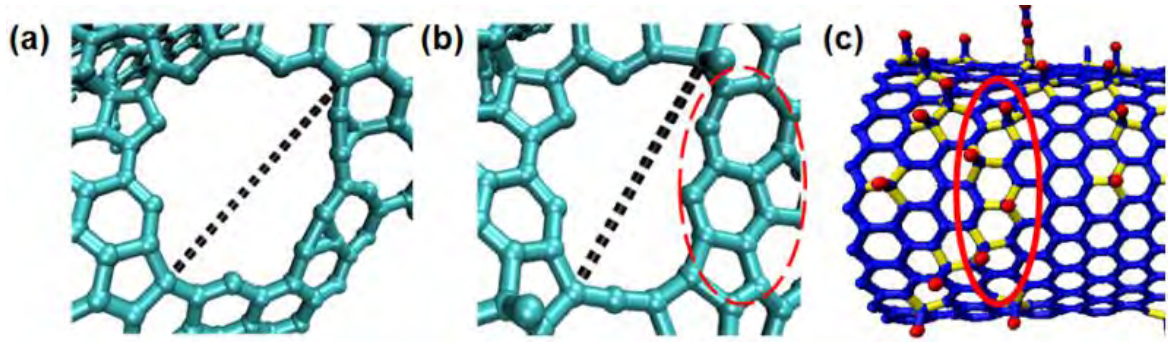


Figure 6-7: Largest hole size for 150 eV, 17.88 MGy, (a) pre-healing, (b) after depositing 3 additional rings of 250 atoms at 1 eV (red dashed ring highlights area where hole healing has taken place), (c) line up of adatoms providing weak point in structure; yellow bonds are ~ 1.54 Å in length, blue bonds are ~ 1.42 Å in length.

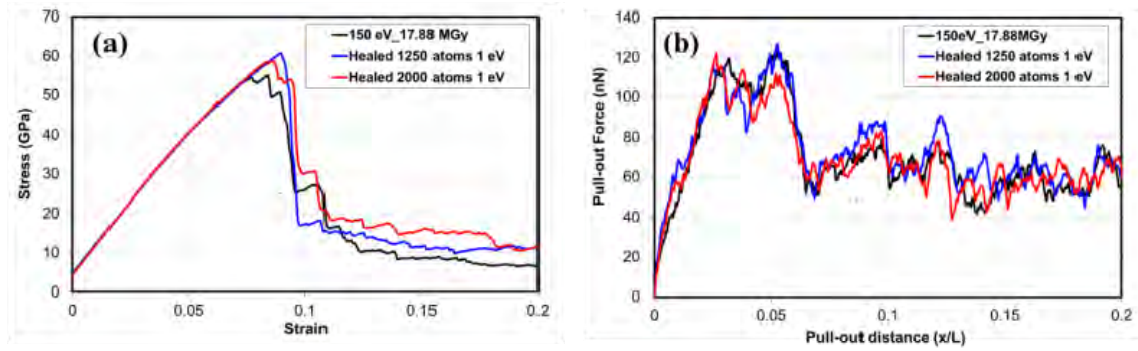


Figure 6-8: Effect of “healing” 1 eV C ion irradiation on (a) tensile strength and (b) pull-out stress

Chapter 7 Conclusions and Recommendations

7.1 Conclusions

Carbon ion irradiation of single wall carbon nanotube bundles, for the purpose of achieving inter-tube cross-links to enhance mechanical performance, has been investigated using classical molecular dynamics. For 7-tube bundles, within the range 100–200 eV/ion, the level of cross-linking is directly proportional to dosage and therefore controllable. Lower energy irradiation produces smaller-sized defects so ~100 eV/ion is the preferred energy level. More than 10 different types of cross-link are formed and a variety of defects are created including single atom and multi-atom vacancies, adatoms, Stone–Wales defects, and 5665 defects. The defect level becomes excessive if either the energy or the fluence is set too high, with amorphisation occurring at the highest level of energy and fluence considered. Extension to larger bundles however is significantly more challenging. In 19-tube bundles, irradiation within the same 100–200 eV/ion range used for 7-tube bundles produces satisfactory cross-linking in the first two layers of CNTs, but almost none with the centre CNT. An energy level of ~500 eV/ion is required to form significant numbers of cross-links with the centre CNT, and at this energy level careful control of fluence is required to avoid excessive damage to the outer layer of CNTs. Larger bundles are likely to prove even more problematic. Thus ion irradiation is likely to be of practical value for improving mechanical properties only for small bundles. However, a scenario whereby small bundles are irradiated prior to twisting into bundles is suggested as a possible future method for producing macroscale cross-linked CNT fibres.

The improvement of the mechanical properties of single wall carbon nanotube bundles has been investigated through carbon ion irradiation using classical molecular

dynamics simulations. These studies were made possible through the use of a recently developed modified REBO potential that introduces an environmental screening coefficient to accurately capture bond breaking and reforming processes. With careful control of irradiation parameters, it is observed that shear and toughness properties are increased by an order of magnitude, while tensile properties are reduced by only 30–40% relative to a bundle with a single defect. In fact, in real CNT fibres containing discontinuous CNT filaments, the increased load transfer between CNTs would result in an *increase* in tensile strength that would significantly offset or even negate such a reduction.

It is shown that the nano-scale interface response resembles that of traditional micro-scale composites: pull-out is characterized by an elastic stretching region at small displacements followed by the onset of debonding, in which inter-tube bonds are broken, and then a drop to a lower sliding stress, in which inter-tube links involving interstitial C atoms are continuously re-formed and broken. In contrast, direct bonds between CNTs, once broken, do not reform and thus do not contribute to the sliding stress. For energy absorption during pull-out, it is thus desirable to have C interstitials at CNT interfaces, which makes C ion irradiation an attractive option over irradiation by electrons or other types of ions, since extra C atoms are added to the system. Another advantage of adding C atoms to the system is that they may migrate on annealing to partially heal vacancies caused by irradiation.

Within a certain range of cross-link density, the interface shear modulus, shear stress at onset of debonding, and frictional sliding stress after debonding are all linearly related to cross-link density making controlled design of fibre shear properties feasible. Despite the variety of defects formed, the tensile strength of irradiated bundles depends strongly on one parameter, largest hole size in the bundle. A possible post-irradiation treatment with very low energy irradiation is proposed for healing such holes and therefore partially restoring tensile strength. The relationships found here between cross-link/defect density and mechanical properties should hold for larger bundles than considered here, although as noted above the irradiation strategies for achieving such cross-link densities will be more complex.

7.2 Recommendations for Future Work

The following ideas for future work are recommended:

- i. A key finding from the present work is that C atom irradiation of CNT bundles larger than 19 tubes is problematic since penetrating to the innermost tube requires either excessive energy or dosage, which destroys the outer CNTs in the bundle. One idea to explore is based on the fact that irradiation creates adatoms on the CNT walls, which during pullout, were shown here to mediate the spontaneous formation of inter-tube cross-links. Based on this finding, a possible route to micron-scale CNT fibres is postulated through the drawing of CNTs from a CNT forest, and twisting into a yarn. Several groups are working on this technique at present [5, 7]. The idea arising from the present work is to irradiate the small CNT bundles as they are being drawn off the forest, before they are twisted into a yarn. The resulting adatoms from the irradiation should spontaneously form cross-links when the small bundles are brought into close proximity through the twisting process. A postdoctoral fellow within our group is now investigating the theoretical feasibility of this idea by performing irradiation simulations of several adjacent small bundles of CNTs and perform twisting simulations in order to create CNT yarns. Tensile tests are being performed for these irradiated CNT yarns and cross-links and defects are being analysed.
- ii. The interaction of CNTs with the matrix (e.g. ceramic or polymer) is a critical issue in creating improved CNT-reinforced composites, which has not been addressed in this work. The presence of defects and adatoms on the CNT surface from irradiation should improve the potential for covalent bonding with the matrix, and this could be investigated in future.
- iii. It would be helpful to perform some quantum mechanical simulations to help validate some of the work performed here. The author is not familiar with

such methods, but for example, perhaps the one atom impacts with a small section of a CNT wall could be simulated to verify the formation of adatoms, and displacement of atoms from the CNT wall.

- iv. CNT bundles are likely in practice to contain MWCNTs, so the study could be extended to identify suitable dosages and energies for such situations. However, the computation time will increase substantially, and based on the findings for the 19-tube bundles here, it seems likely that it will be difficult to penetrate to the inner wall of MWCNTs with large number of walls, without destroying the outer walls.

Bibliography:

- [1] Iijima, S., (1991), 'Helical Microtubules of Graphitic Carbon'. *Nature*, 354(6348): p. 56-58.
- [2] Lau, K.T. and Hui, D., (2002) 'The revolutionary creation of new advanced materials - carbon nanotube composites', *Composites Part B-Engineering*, 33(4): p. 263-277.
- [3] Neocleus, S., Pattison, S.W., Moisala Mata, A.M., Windle, A.H., Eder, D., (2011) 'Hierarchical Carbon Nanotube-Inorganic Hybrid Structures Involving CNT Arrays and CNT Fibers '. *Functional Materials Letters*, 4(1): p. 83-89.
- [4] Kim, Y.A., Kojima, M., Muramatsu, H., Umemoto, S., Watanabe, W., Yoshida, K., Sato, K., Ikeda, T., Hayashi, T., Endo, M., Terrones, M., Dresselhaus, M. S., (2006) 'In situ Raman study on single- and double-walled carbon nanotubes as a function of lithium insertion', *Small*, 2(5): p. 667-676.
- [5] Ghemes, A., Minami, Y., Muramatsu, J., Okada, M., Mimura, H., Inoue, Y., (2012) 'Fabrication and mechanical properties of carbon nanotube yarns spun from ultra-long multi-walled carbon nanotube arrays'. *Carbon*, 50(12): p. 4579-4587.
- [6] Barber, A.H., Andrews, R., Schadler, S.H., Wagner, H. D., (2005) 'On the tensile strength distribution of multi-walled carbon nanotubes', *Applied Physics Letters*, 87, 203106.
- [7] Park, J. and Lee, K.H., (2012) 'Carbon nanotube yarns', *Korean Journal of Chemical Engineering*, 29(3): p. 277-287.
- [8] Brenner, D.W., (1990) 'Empirical Potential for Hydrocarbons for Use in Simulating the Chemical Vapor- Deposition of Diamond Films', *Physical Review B*, 42(15): p. 9458-9471.
- [9] Byrne, E.M., Letertre, A., McCarthy, M.A., Curtin, W.A., Xia, Z., (2010) 'Optimizing load transfer in multiwall nanotubes through interwall coupling: Theory and simulation', *Acta Materialia*, 58(19): p. 6324-6333.

- [10] Byrne, E.M., McCarthy, M.A., Curtin, W.A., Xia, Z., (2009) 'Multiwall Nanotubes Can Be Stronger than Single Wall Nanotubes and Implications for Nanocomposite Design', *Physical Review Letters*, 103(4).
- [11] Fonseca, A.F., Borders, T., Baughman, R.H., Cho, K., (2010) 'Load transfer between cross-linked walls of a carbon nanotube', *Physical Review B*, 81(4).
- [12] Li, L., Curtin, W.A., Xia, Z., Yang, Y.Q., (2009) 'Molecular Dynamics Simulations of Interfacial Sliding in Carbon-Nanotube/Diamond Nanocomposites', *Journal of the American Ceramic Society*, 92(10): p. 2331-2336.
- [13] Pavia, F. and Curtin, W.A., (2011) 'Interfacial sliding in carbon nanotube/diamond matrix composites', *Acta Materialia*, 59(17): p. 6700-6709.
- [14] Peng, B., Locascio, M., Zapol, P., Li, S., Mielke, S.L., Schatz, G.C., Espinosa, H.D., (2008) 'Measurements of near-ultimate strength for multi-walled carbon nanotubes and irradiation-induced crosslinking improvements', *Nature Nanotechnology*, 3(10): p. 626-631.
- [15] Pregler, S.K. and Sinnott, S.B., (2006) 'Molecular dynamics simulations of electron and ion beam irradiation of multiwalled carbon nanotubes: The effects on failure by inner tube sliding', *Physical Review B*, 73(22).
- [16] Cornwell, C.F. and Welch, C.R., (2011) 'Very-high-strength (60-GPa) carbon nanotube fibre design based on molecular dynamics simulations', *Journal of Chemical Physics*, 134 (20).
- [17] Federizzi, R.L., Moura, C.S., Amaral, L., (2006) 'Polymerization of carbon nanotubes through self-irradiation', *Journal of Physical Chemistry B*, 110(46): p. 23215-23220.
- [18] Kis, A., Csanyi, G., Salvétat, J.P., Lee, T.-N., Couteau, E., Kulik, A.J., Benoit, W., Brugger, J., Forro, L., (2004) 'Reinforcement of single-walled carbon nanotube bundles by inter-tube bridging', *Nature Materials*, 3(3): p. 153-157.
- [19] Ni, B., Andrews, R., Jacques, D., Qian, D., Wijesundara, M.B.J., Choi, Y.S., Muthu, B.J., Sinnott, S.B., (2001) 'A combined computational and experimental study of

- ion-beam modification of carbon nanotube bundles', *Journal of Physical Chemistry B*, 105(51): p. 12719-12725.
- [20] O'Brien, N.P., McCarthy, M.A., Curtin, W.A., (2013) 'Improved inter-tube coupling in CNT bundles through carbon ion irradiation', *Carbon*, 51: p. 173-184.
- [21] Xia, Z.H., P.R. Guduru, Curtin, W.A., (2007) 'Enhancing mechanical properties of multiwall carbon nanotubes via sp(3) inter-wall bridging', *Physical Review Letters*, 98(24).
- [22] Sammalkorpi, M., Krashenninnikov, A.V., Kuronen, A., Nordlund, K., Kaski, K., (2005) 'Irradiation-induced stiffening of carbon nanotube bundles', *Nuclear Instruments & Methods in Physics Research Section B-Beam Interactions with Materials and Atoms*, 228: p. 142-145.
- [23] Xu, Z.J., Zhang, W., Zhu, Z.Y., Huai, P., (2009) 'Molecular dynamics study of damage production in single-walled carbon nanotubes irradiated by various ion species' *Nanotechnology*, 20(12)
- [24] Majure, D.L., Haskins, R.W., Lee, N.J., Ebeling, R.M., Maier, R.S., Marsh, C.P., Bednar, A.J., Kirgan, R.A., Welch, C.R., Cornwell, C. F., (2008) 'Large-Scale Atomic/Molecular Massively Parallel Simulator (LAMMPS) Simulations of the Effects of Chirality and Diameter on the Pullout Force in a Carbon Nanotube Bundle', *DoD HPCMP Users Group Conference., IEEE Computer Society, Los Alamitos, CA: Seattle, WA.* p. 201-207.
- [25] Brenner, D.W., Shenderova, O.A., Harrison, J.A., Stuart, S.J., Ni, B., Sinnott, S.B., (2002) 'A second-generation reactive empirical bond order (REBO) potential energy expression for hydrocarbons', *Journal of Physics-Condensed Matter*, 14(4): p. 783-802.
- [26] Cornwell, C.F., Welch, C.R., Majure, D., Haskins, R., Lee, N.J., Ebeling, R., Maier, R., Marsh, C., Bednar, A., Kirgan, R., (2008) 'Critical Carbon Nanotube Length in Fibres', *DoD HPCMP Users Group Conference, Seattle, WA: IEEE Computer Society, Los Alamitos, CA.*

- [27] Baskes, M.I., J.E. Angelo, Bisson, C.L., (1994) 'Atomistic Calculations of Composite Interfaces', *Modelling and Simulation in Materials Science and Engineering*, 2(3A): p. 505-518.
- [28] Salvétat, J.P., Briggs, G.A.D., Bonard, J.M., Bacsá, R.R., Kulik, A.J., Stockli, T., Burnham, N.A., Forro, L., (1999) 'Elastic and shear moduli of single-walled carbon nanotube ropes', *Physical Review Letters*, 82(5): p. 944-947.
- [29] Krashennnikov, A.V., Banhart, F., Li, J.X., Foster, A.S., Nieminen, R.M., (2005) 'Stability of carbon nanotubes under electron irradiation: Role of tube diameter and chirality', *Physical Review B*, 72 (12).
- [30] Salonen, E., A.V. Krashennnikov, Nordlund, K., (2002) 'Ion-irradiation-induced defects in bundles of carbon nanotubes', *Nuclear Instruments & Methods in Physics Research Section B-Beam Interactions with Materials and Atoms*, 193: p. 603-608.
- [31] Ni, B. and Sinnott, S.B., (2000) 'Chemical functionalization of carbon nanotubes through energetic radical collisions', *Physical Review B*, 61(24): p. 16343-16346.
- [32] Terrones, M., Terrones, H., Banhart, F., Charlier, J.-C., Ajayan, P.M., (2000) 'Coalescence of Single-Walled Carbon Nanotubes', *Science*, 288(5469): p. 1226-1229.
- [33] Sun, L.T., Gong, J.L., Wang, Z.X., Zhu, D.Z., Hu, J.G., Lu, R.R., Zhu, Z.Y., (2005) 'Irradiation-induced phase transformations in carbon nanostructures', *Nuclear Instruments & Methods in Physics Research Section B-Beam Interactions with Materials and Atoms*, 228: p. 26-30.
- [34] Jager, H.U. and Albe, K., (2000) 'Molecular-dynamics simulations of steady-state growth of ion-deposited tetrahedral amorphous carbon films', *Journal of Applied Physics*, 88(2): p. 1129-1135.
- [35] Pastewka, L., Moser, S., Moseler, M., (2010) 'Atomistic Insights into the Running-in, Lubrication, and Failure of Hydrogenated Diamond-Like Carbon Coatings', *Tribology Letters*, 39(1): p. 49-61.
- [36] Schittenhelm, H., Geohegan, D.B., Jellison, G.E., Puretzky, A.A., Lance, M.J., Britt, P.F., (2002) 'Synthesis and characterization of single-wall carbon nanotube-

- amorphous diamond thin-film composites', *Applied Physics Letters*, 81(11): p. 2097-2099.
- [37] Hirai, Y., Nishimaki, S., Mori, H., Kimoto, Y., Akita, S., Nakayama, Y., Tanaka, Y., (2003) 'Molecular dynamics studies on mechanical properties of carbon nanotubes with pinhole defects', *Japanese Journal of Applied Physics Part 1- Regular Papers Short Notes & Review Papers*, 42(6B): p. 4120-4123.
 - [38] Shenderova, O.A., Brenner, D.W., Omeltchenko, A., Su, X., Yang, L.H., (2000) 'Atomistic modelling of the fracture of polycrystalline diamond', *Physical Review B*, 61(6): p. 3877-3888.
 - [39] Yakobson, B.I., Campbell, M.P., Brabec, C.J., Bernholc, J., (1997) 'High strain rate fracture and C-chain unravelling in carbon nanotubes', *Computational Materials Science*, 8(4): p. 341-348.
 - [40] Belytschko, T., Xiao, S.P., Schatz, G.C., Ruoff, R.S., (2002) 'Atomistic simulations of nanotube fracture', *Physical Review B*, 65(23).
 - [41] Zhang, M., Atkinson, K.R., Baughman, R.H., (2004) 'Multifunctional carbon nanotube yarns by downsizing an ancient technology', *Science*, 306(5700): p. 1358-1361.
 - [42] Zhang, S.L., Mielke, S.L., Khare, R., Troya, D., Ruoff, R.S., Schatz, G.C., Belytschko, T., (2005) 'Mechanics of defects in carbon nanotubes: Atomistic and multiscale simulations', *Physical Review B*, 71(11).
 - [43] Pastewka, L., Pou, P., Perez, R., Gumbsch, P., Moseler, M., (2008) 'Describing bond-breaking processes by reactive potentials: Importance of an environment-dependent interaction range', *Physical Review B*, 78(16).
 - [44] Sorescu, M., Grabias, A., Tarabasanu-Mihaila, D., Diamandescu, L., (2003) 'Bulk versus surface effects in magnetic thin films obtained by pulsed laser deposition', *Applied Surface Science*, 217(1-4): p. 233-238.
 - [45] Pomoell, J.A.V., Krashennnikov, A.V., Nordlund, K., Keinonen, J., (2004) 'Ion ranges and irradiation-induced defects in multi-walled carbon nanotubes', *Journal of Applied Physics*, 96(5): p. 2864-2871.

- [46] Pregler, S.K., Jeong, B.-W., Sinnott, S.B., (2008) 'Ar beam modification of nanotube based composites using molecular dynamics simulations', *Composites Science and Technology*, 68(9): p. 2049-2055.
- [47] Krasheninnikov, A.V. and Nordlund, K., (2010) 'Ion and electron irradiation-induced effects in nanostructured materials', *Journal of Applied Physics*, 107(7).
- [48] Plimpton, S., (1995) 'Fast Parallel Algorithms for Short-Range Molecular-Dynamics', *Journal of Computational Physics*, 117(1): p. 1-19.
- [49] Banhart, F., Li, J.X., Krasheninnikov, A.V., (2005) 'Carbon nanotubes under electron irradiation: Stability of the tubes and their action as pipes for atom transport', *Physical Review B*, 71(24).
- [50] Tolvanen, A., Kotakoski, J., Krasheninnikov, A.V., Nordlund, K., (2007) 'Relative abundance of single and double vacancies in irradiated single-walled carbon nanotubes', *Applied Physics Letters*, 91(17).
- [51] Tersoff, J., (1988) 'Empirical Interatomic Potential for Carbon with Applications to Amorphous-Carbon', *Physical Review Letters*, 61(25): p. 2879-2882.
- [52] Filleter, T., Bernal, R., Li, S., Espinosa, H.D., (2011) 'Ultrahigh Strength and Stiffness in Cross-Linked Hierarchical Carbon Nanotube Bundles', *Advanced Materials*, 23(25): p. 2855-+.
- [53] Sears, K., Skourtis, C., Atkinson, K., Finn, N., Humphries W., (2010) 'Focused ion beam milling of carbon nanotube yarns to study the relationship between structure and strength'. *Carbon*, 48(15): p. 4450-4456.
- [54] Mielke, S.L., Troya, D., Zhang, S., Li, J.-L., Xiao, S., Car, R., Ruoff, R.S., Schatz, G.C., Belytschko T., (2004) 'The role of vacancy defects and holes in the fracture of carbon nanotubes', *Chemical Physics Letters*, 390(4-6): p. 413-420.
- [55] Ogata, S. and Shibutani, Y., (2003) 'Ideal tensile strength and band gap of single-walled carbon nanotubes', *Physical Review B*, 68(16).
- [56] Thostenson, E.T., Ren, Z., Chou, T.-W., (2001) 'Advances in the science and technology of carbon nanotubes and their composites', *Composites Science and Technology*, 61, 1899-1912.

- [57] Haile, J.M., (1997) '*Molecular dynamics simulation: Elementary methods*', 1st edition, U.S.A.: John Wiley and Sons, Inc.
- [58] An Shen, G., (2006) *Effect of interfaces on the thermal, mechanical and chemical characteristics of carbon nanotubes*, unpublished thesis (PhD), The Florida State University.
- [59] Sinnott, S.B., Hu, Y., Jang, I. (2003) 'Modification of carbon nanotube-polystyrene matrix composites through poly-atomic ion beam deposition: predictions from molecular dynamics simulations', *Composites science and technology*, 63, 1663-1669.
- [60] Odegard, G. M., Pipes, R. B., Hubert, P. (2004) 'Comparison of two models of SWCN polymer composites', *Composites Science and Technology*, 64, 1011-1020.
- [61] Akita, S. and Nakiyama, Y. (2003) 'Extraction of inner shell from multiwall carbon nanotubes for scanning probe microscope tip', *The Japan Society of Applied Physics*, 42, 3933-3936.
- [62] O'Brien, N.P., McCarthy, M.A., Curtin, W.A., (2013) 'A theoretical quantification of the possible improvement in the mechanical properties of carbon nanotube bundles by carbon ion irradiation', *Carbon*, 53: p. 346-356.
- [63] Xia, Z., Curtin, W.A., (2004) 'Pullout forces and friction in multiwall carbon nanotubes', *Physical Review B*, 69, 233408.
- [64] Clark, J., (2000) *Bonding in ethene – sp² hybridisation* [online image] available: <http://www.chemguide.co.uk/basicorg/bonding/ethene.html> [accessed 02 March 2014].
- [65] Clark, J., (2000) *Bonding in methane – sp³ hybridisation* [online image] available: <http://www.chemguide.co.uk/basicorg/bonding/methane.html> [accessed 02 March 2014].

APPENDICES

APPENDIX A

**Detailed Schematics and Snapshots
of Bond Breaking Behaviour for
Different Types of Inter-tube Bond**

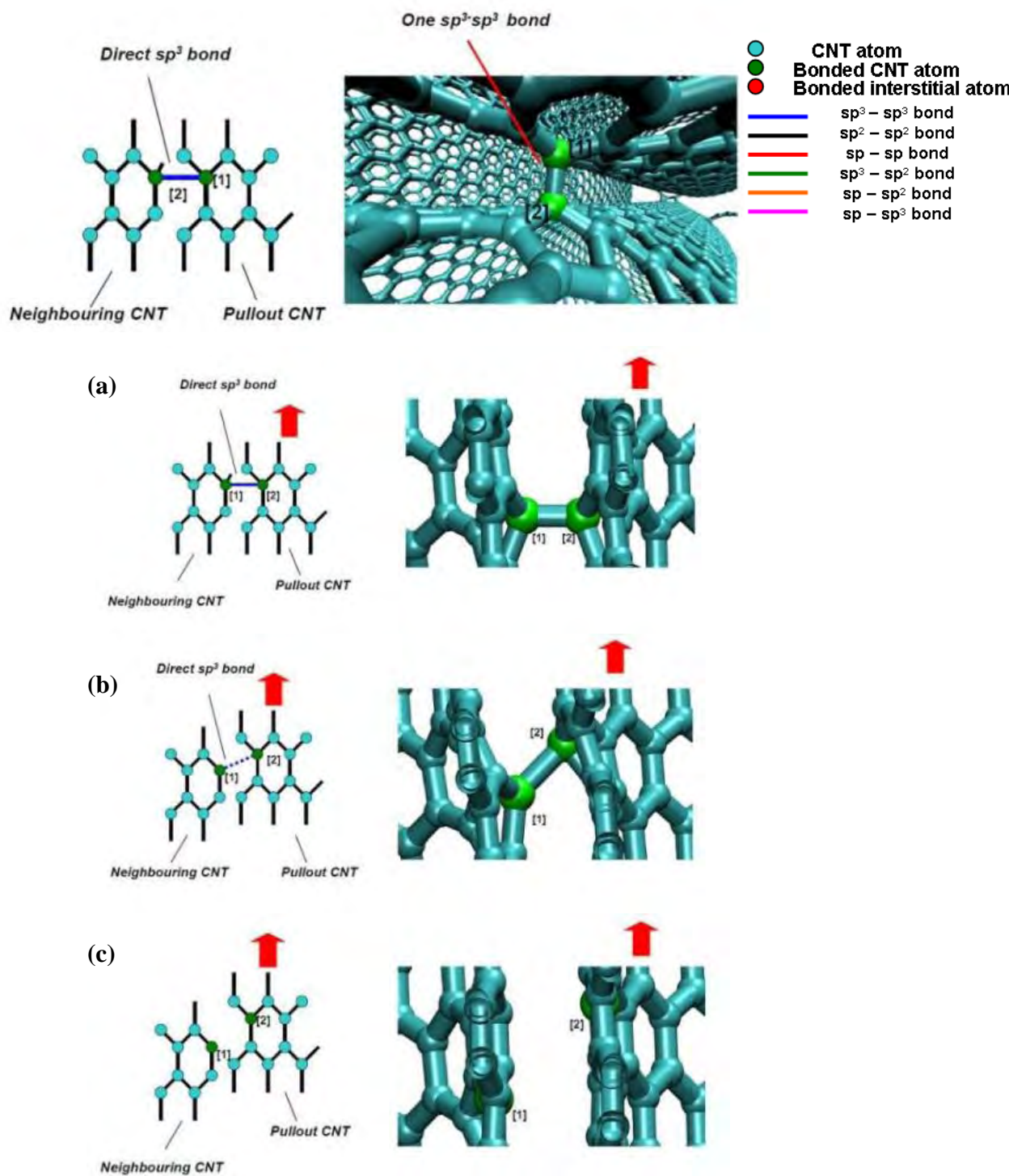


Figure A-1: Schematics and snapshots of bond breaking behaviour for a direct sp^3 - sp^3 inter-tube bond.

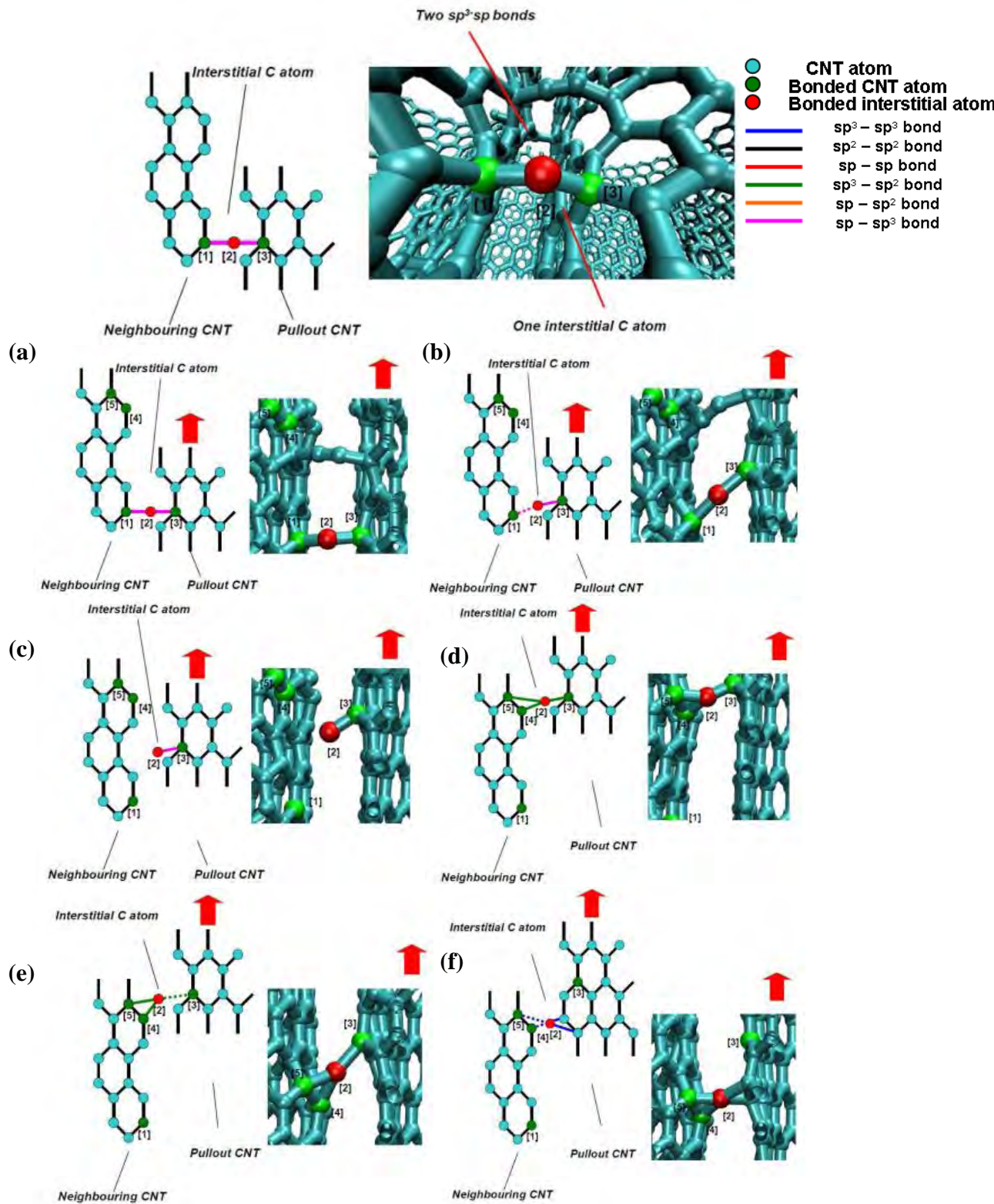


Figure A-2: Schematics and snapshots of bond breaking and re-forming behaviour for an inter-tube bond involving two sp^3-sp bonds and one interstitial atom.

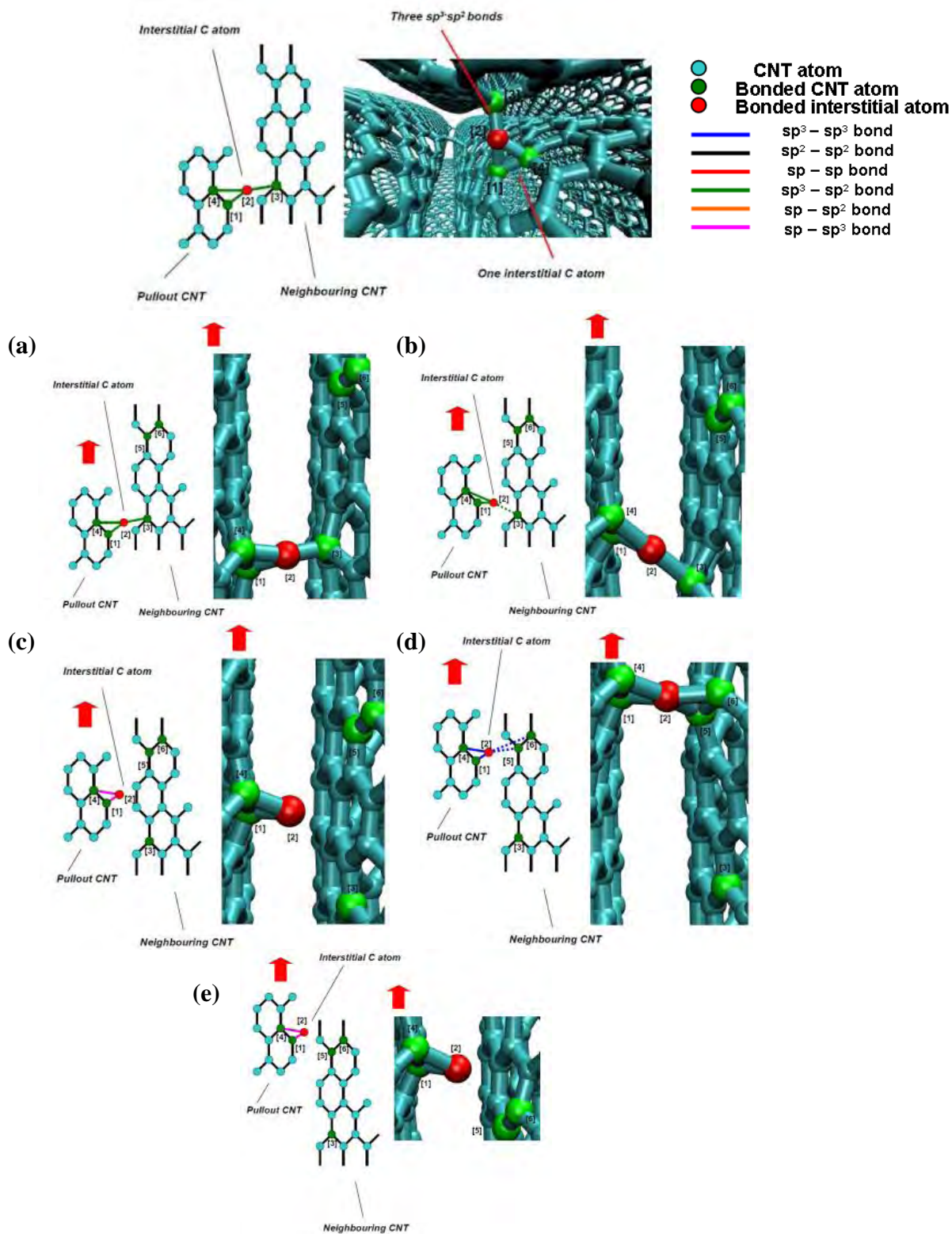


Figure A-3: Schematics and snapshots of bond breaking and re-forming behaviour for an inter-tube bond involving three sp^3-sp^2 bonds and one interstitial atom

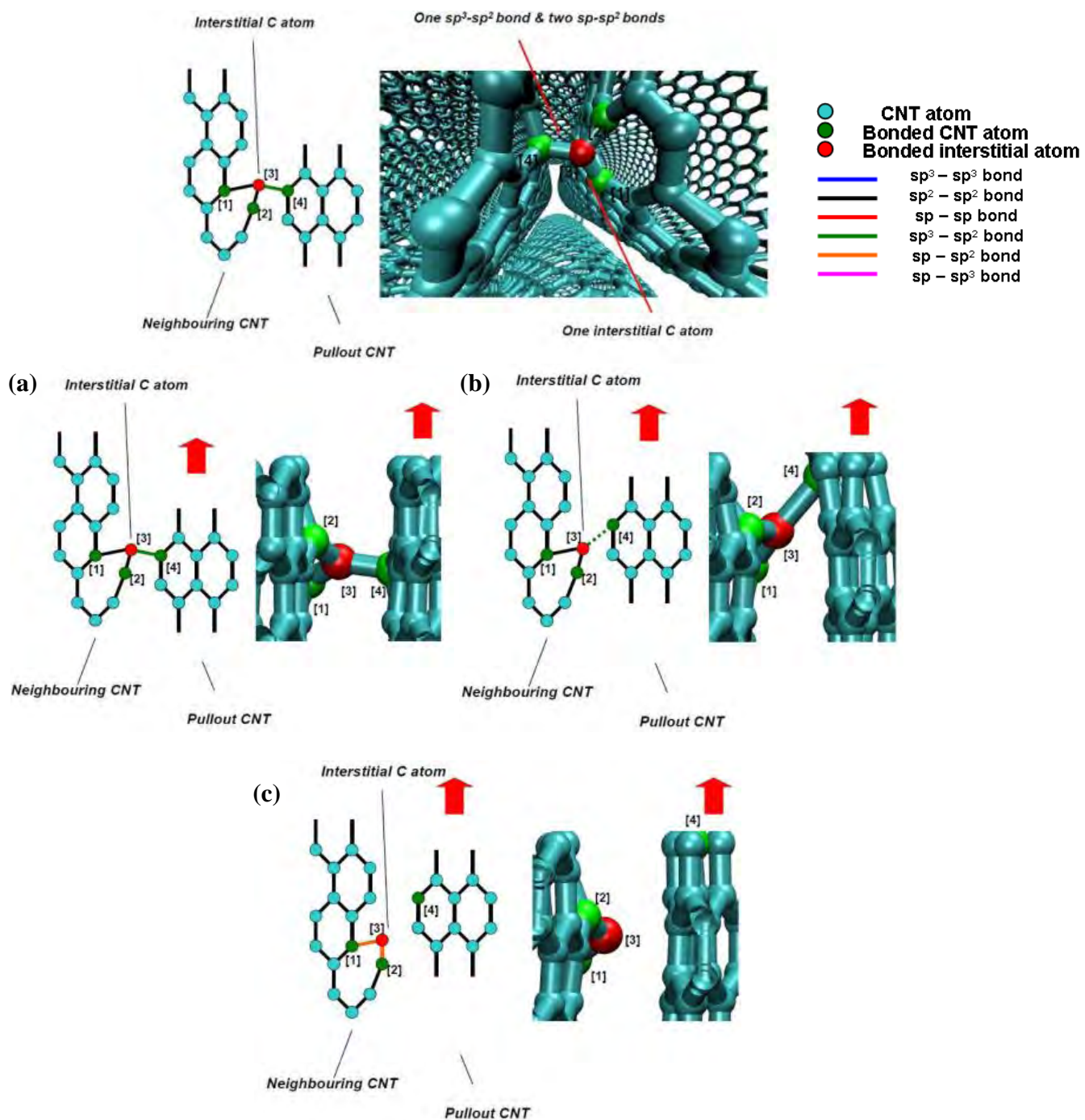


Figure A-4: Schematics and snapshots of bond breaking and re-forming behaviour for an inter-tube bond involving one sp^3 - sp^2 and two sp^2 - sp^2 inter-tube bonds, and one interstitial atom

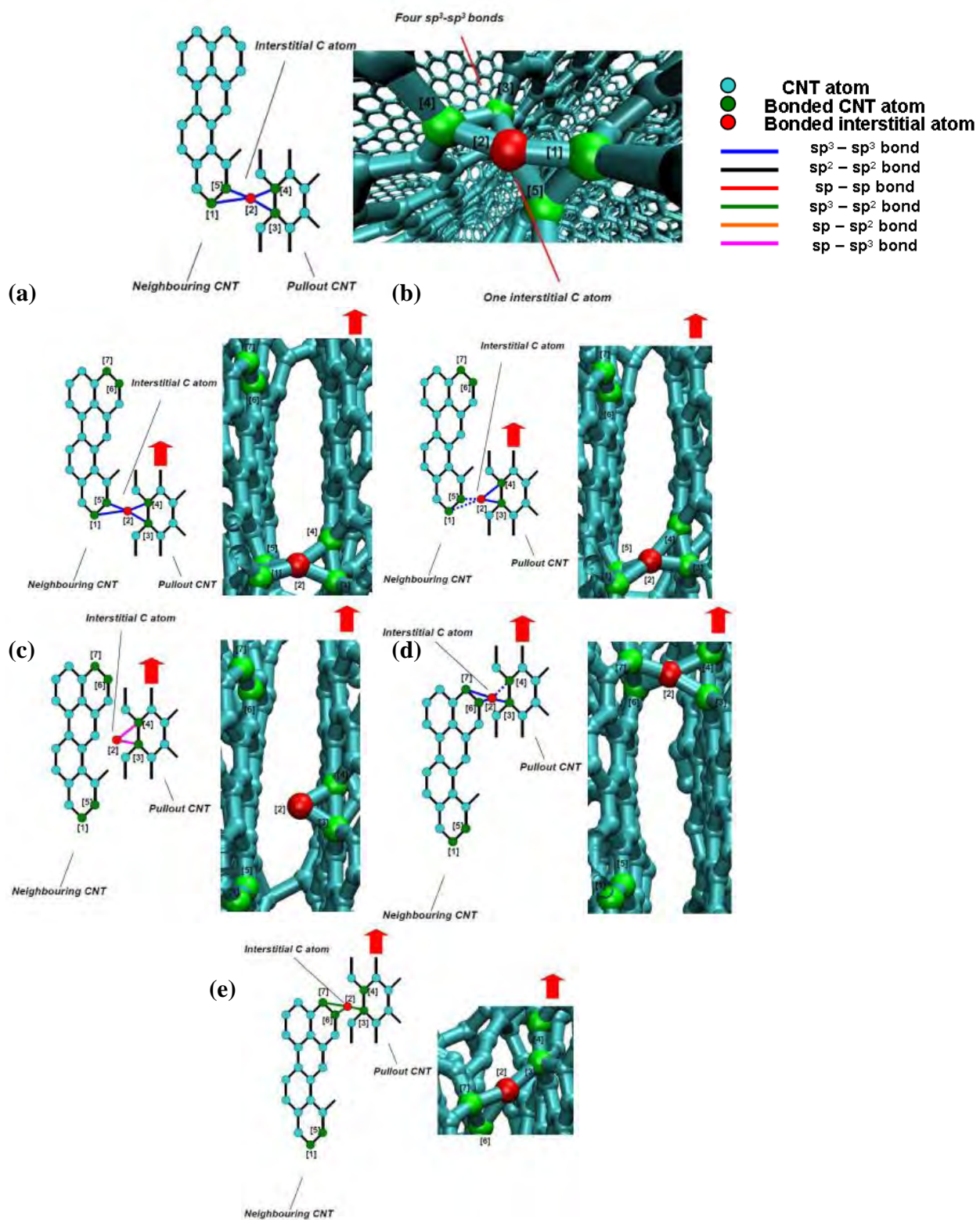


Figure A-5: Schematics and snapshots of bond breaking and re-forming behaviour for an inter-tube bond involving four sp^3 - sp^3 inter-tube bonds and one interstitial atom

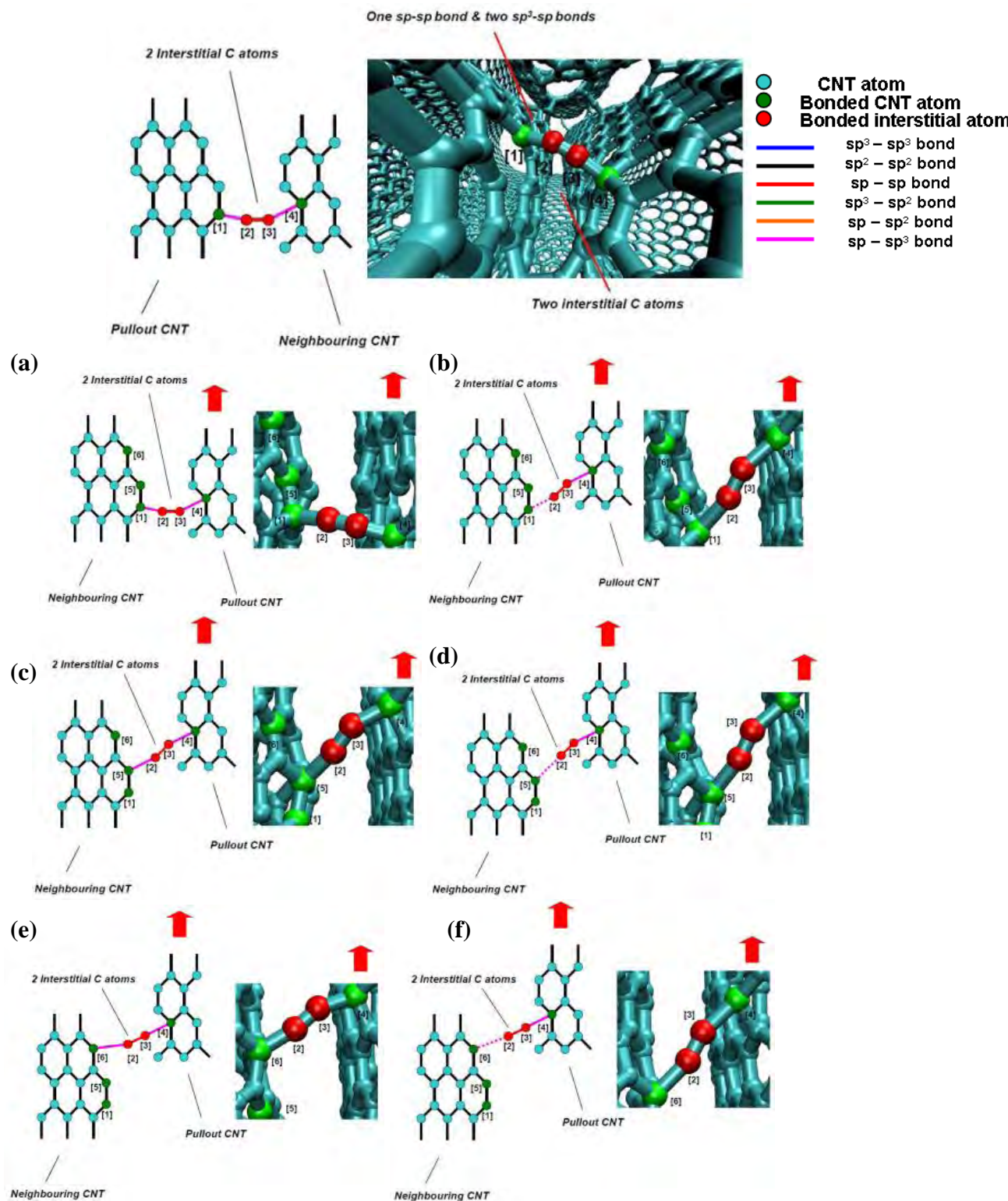


Figure A-6: Schematics and snapshots of bond breaking and re-forming behaviour for an inter-tube bond involving one sp-sp and two sp³-sp inter-tube bonds, and two interstitial atoms

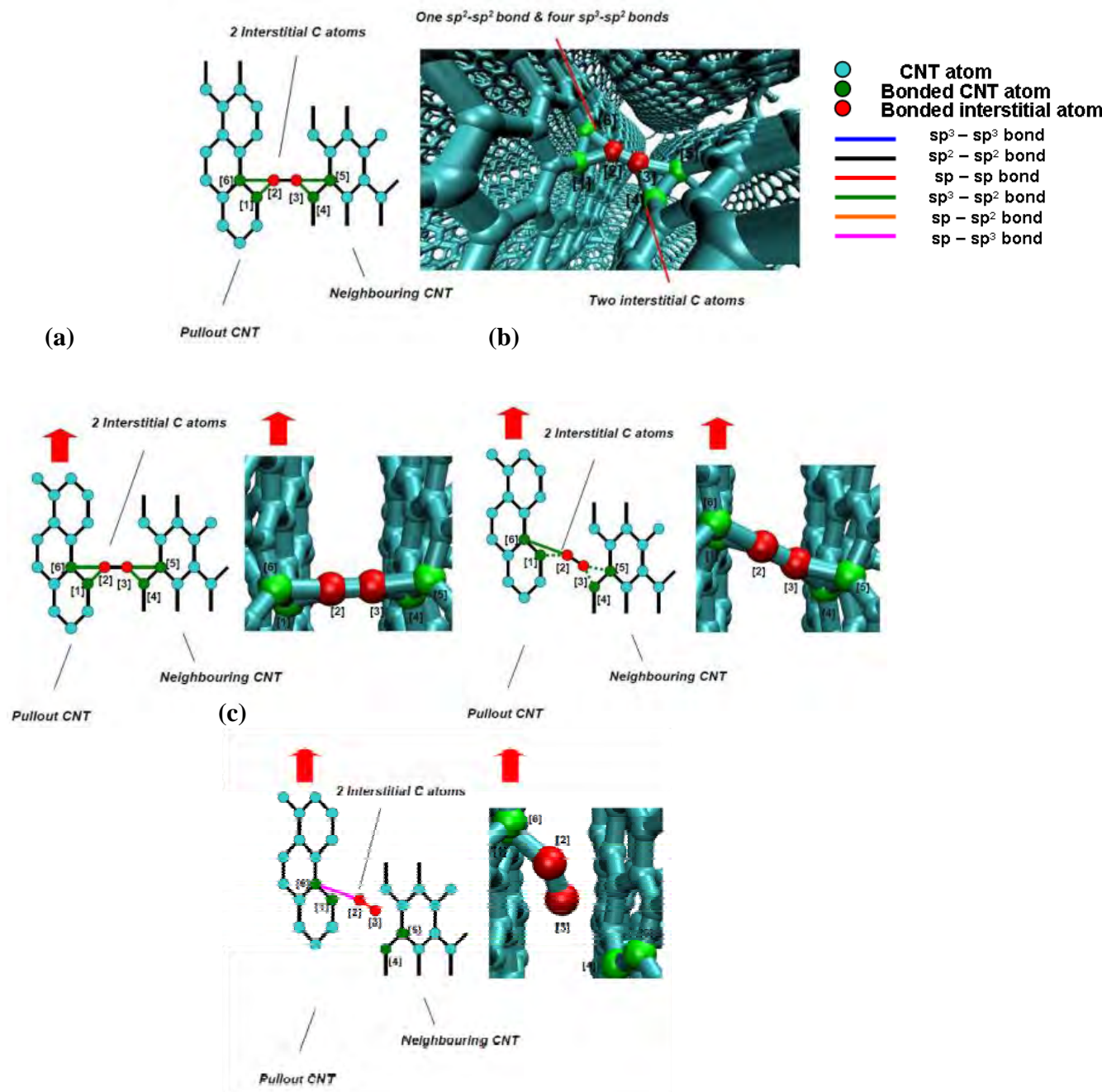


Figure A-7: Schematics and snapshots of bond breaking and re-forming behaviour for an inter-tube bond involving one sp^2-sp^2 and four sp^3-sp^2 inter-tube bonds, and two interstitial atoms

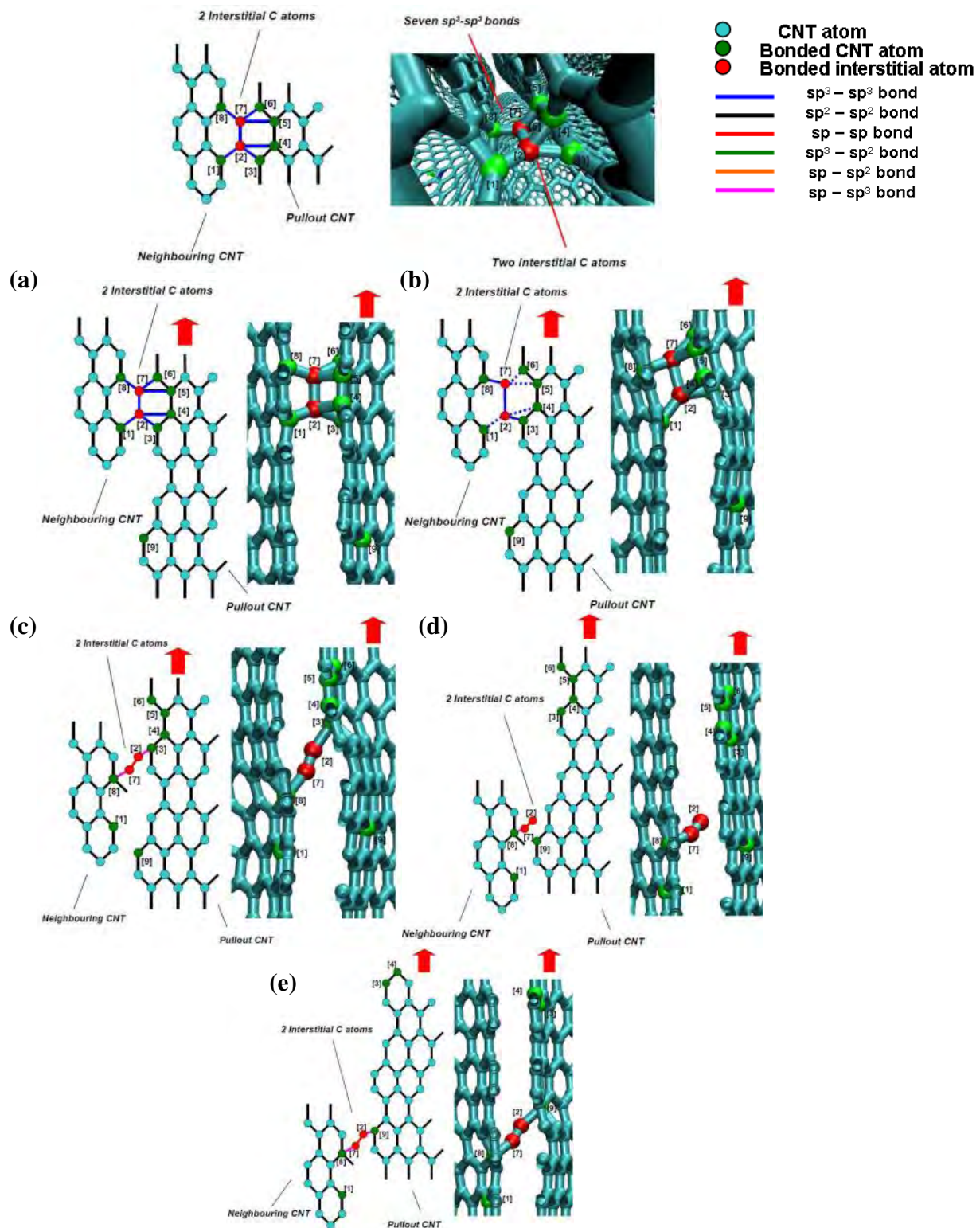


Figure A-8: Schematics and snapshots of bond breaking and re-forming behaviour for an inter-tube bond involving seven sp^3-sp^3 inter-tube bonds, and two interstitial atoms

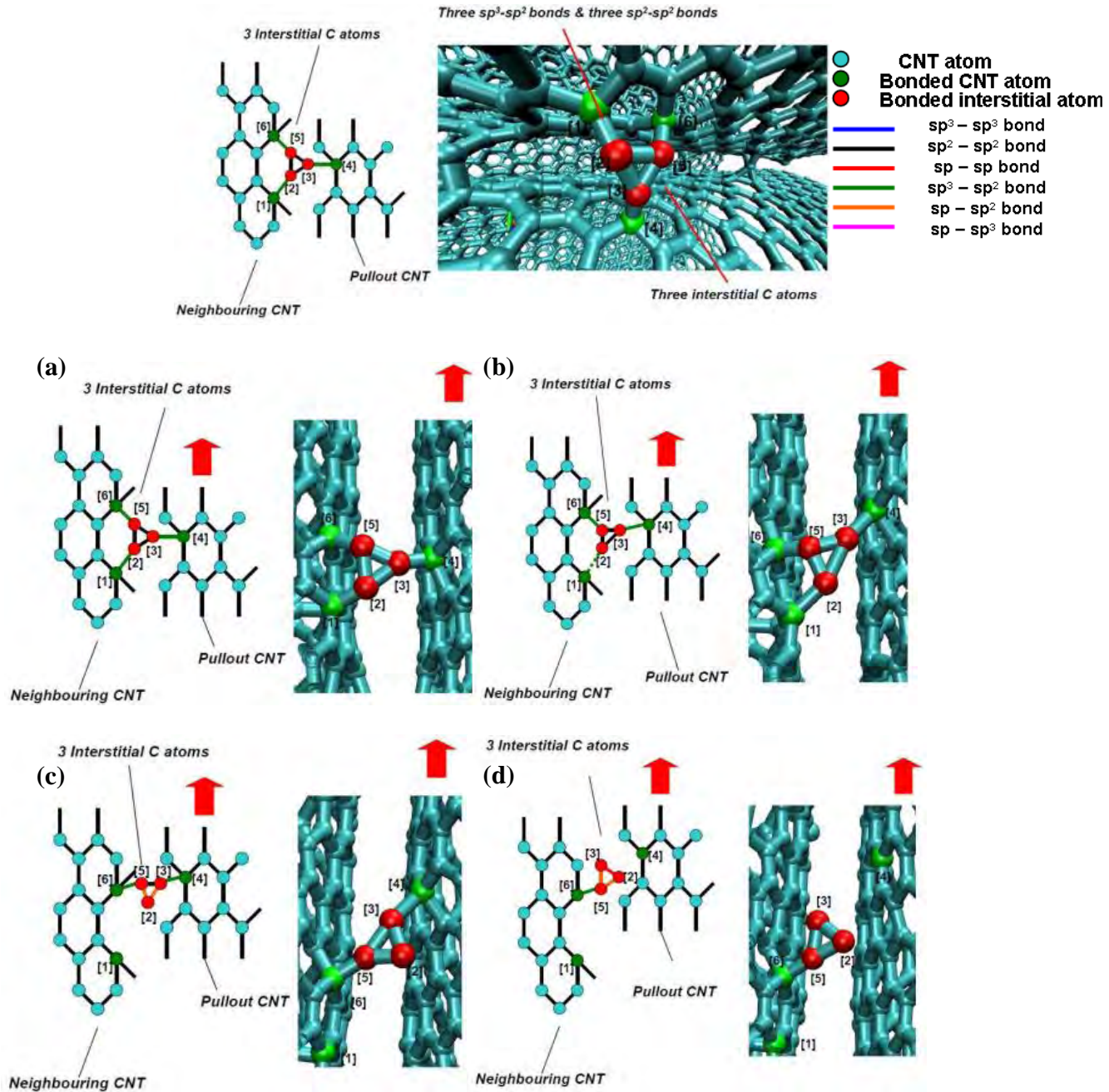


Figure A-9: Schematics and snapshots of bond breaking and re-forming behaviour for an inter-tube bond involving three sp^3-sp^2 and three sp^2-sp^2 inter-tube bonds, and three interstitial atoms

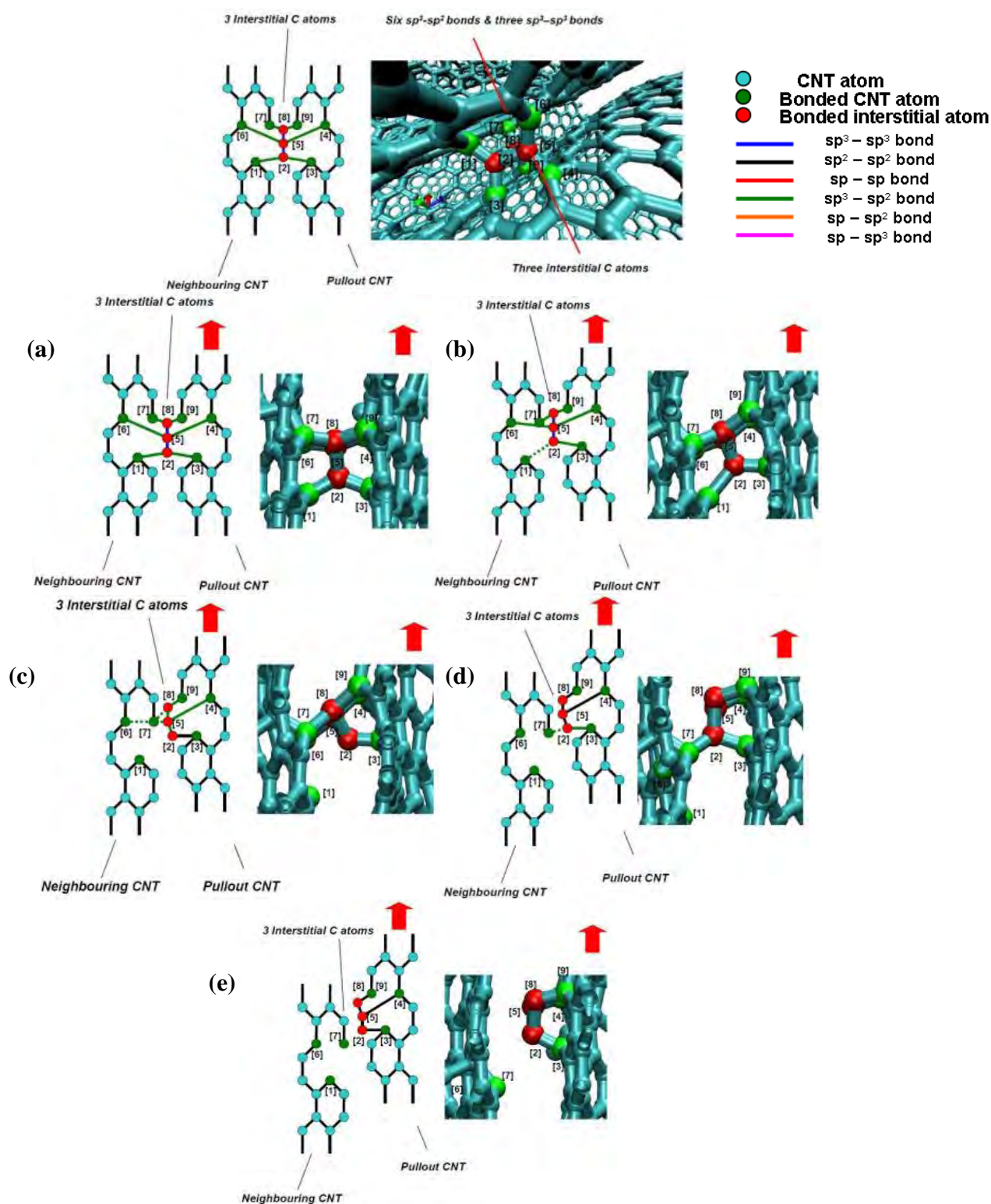


Figure A-10: Schematics and snapshots of bond breaking and re-forming behaviour for an inter-tube bond involving six sp^2 - sp^2 and three sp^3 - sp^3 inter-tube bonds, and three interstitial atoms

APPENDIX B

**O'Brien, N.P., M. A., McCarthy, W. A., Curtin, 2013,
Improved Inter-tube Coupling in CNT Bundles
Through Carbon Ion Irradiation, Carbon, 51, 173-184.**

APPENDIX C

O'Brien, N.P., M. A. McCarthy, W. A. Curtin, 2013, A Theoretical Quantification of the Possible Improvement in the Mechanical Properties of Carbon Nanotube Bundles by Carbon Ion Irradiation, Carbon, 53, 346-356.